NTNU

Norwegian University of
Science and Technology

Patient specific numerical simulation of flow in the human upper airways

Maria Rolstad Jordal

Master of Energy and Environmental Engineering
Submission date: June 2016
Supervisor: Bernhard Müller, EPT
Co-supervisor: Sigrid Kaarstad Dahl, SINTEF
Sverre Gullikstad Johnsen, SINTEF

Norwegian University of Science and Technology
Department of Energy and Process Engineering

NTNU

Norwegian University
of Science and Technology

Department of Energy
and Process Engineering

EPT-M-2016-65

MASTER THESIS

for

Student
Maria Rolstad Jordal
Spring 2016

Patient specific numerical simulation of flow in the human upper airways

Pasient-spesifikk numerisk simulering av strømning i de øvre luftveier

Background and objective

Snoring is caused by the soft parts of the upper airways collapsing and preventing the air from flowing freely. In some cases snoring is so severe that medical attention is required. The most severe, obstructive sleep apnea syndrome (OSAS), affects 2-4 % of the population. A variety of treatment options exists, but today there are no available methods for predicting the outcome of the treatment. This project will be part of a larger project: *Modeling of obstructive sleep apnea by fluid-structure interaction in the upper airways*, which is a collaboration project between NTNU, SINTEF and St.Olavs Hospital and funded by the Research Council of Norway. The primary objective is to demonstrate the potential of a new patient-specific clinical tool based on mathematical models in predicting the response to OSAS treatment.

The objective of the master project is to simulate flow in the upper airways of one OSAS patient before and after surgical intervention in the nasal cavity. The computational models will be based on CT data from the patient, taken prior to surgery and three months after surgery, respectively. The selected patient will be a patient who has demonstrated a significant effect on the apnea-hypopnea index (AHI) due to the surgical intervention.
A patient specific CFD study, using the software tool ANSYS Fluent, will be conducted to assess the effect of the surgical intervention on the flow in the upper airways. The study will be limited to inspirational flow, at constant pressure drop from inlet (nostril) to outlet (larynx). Computed results will be compared to available measured data.

The following tasks are to be considered:

1. Generate patient specific 3-dimensional models of the upper airways before and after surgical intervention, based on CT data.
2. Grid generation, and refinement/convergence studies.
3. Numerical simulation of inhaling flow in the patient's upper airways using ANSYS FLUENT before and after surgery.
4. Qualitative comparison of flow in the upper airways before and after surgery, based on CFD modelling results.
5. Comparison of selected computed results with measured data.

-- " --

Within 14 days of receiving the written text on the master thesis, the candidate shall submit a research plan for his project to the department.

When the thesis is evaluated, emphasis is put on processing of the results, and that they are presented in tabular and/or graphic form in a clear manner, and that they are analyzed carefully.

The thesis should be formulated as a research report with summary both in English and Norwegian, conclusion, literature references, table of contents etc. During the preparation of the text, the candidate should make an effort to produce a well-structured and easily readable report. In order to ease the evaluation of the thesis, it is important that the cross-references are correct. In the making of the report, strong emphasis should be placed on both a thorough discussion of the results and an orderly presentation.

The candidate is requested to initiate and keep close contact with his/her academic supervisor(s) throughout the working period. The candidate must follow the rules and regulations of NTNU as well as passive directions given by the Department of Energy and Process Engineering.

Risk assessment of the candidate's work shall be carried out according to the department's procedures. The risk assessment must be documented and included as part of the final report. Events related to the candidate's work adversely affecting the health, safety or security, must be documented and included as part of the final report. If the documentation on risk assessment represents a large number of pages, the full version is to be submitted electronically to the supervisor and an excerpt is included in the report.

Pursuant to "Regulations concerning the supplementary provisions to the technology study program/Master of Science" at NTNU §20, the Department reserves the permission to utilize all the results and data for teaching and research purposes as well as in future publications.

The final report is to be submitted digitally in DAIM. An executive summary of the thesis including title, student's name, supervisor's name, year, department name, and NTNU's logo and name, shall be submitted to the department as a separate pdf file. Based on an agreement with the supervisor, the final report and other material and documents may be given to the supervisor in digital format.

☐ Work to be done in lab (Water power lab, Fluids engineering lab, Thermal engineering lab)
☐ Field work

Department of Energy and Process Engineering, 13. January 2016

Olav Bolland
Department Head

Bernhard Müller
Supervisor

Sigrid K. Dahl
Sigrid Kaarstad Dahl
~~Johnsen~~
Co-Supervisor

Sverre Gullikstad JOHNSEN
Co-Supervisor

Abstract

In this master thesis, a patient specific computational fluid dynamics (CFD) study has been done on the air flow in the human upper airways before and after surgical intervention. The patient studied is a 67 years old man who went from having moderate obstructive sleep apnea syndrome (OSAS), to close to none after intranasal surgery. The apnea-hypopnea index (AHI) was reduced from 23 to 5.7 as a result of the surgery.

From post- and pre-operatively computed tomography (CT) of the patient, a geometry of the human upper airways was generated by segmentation in ITK-SNAP 3.4.0 [1]. The paranasal sinuses were excluded, and the geometry was verified by a clinician. The model was further post-processed to eliminate digitalization artefacts. Because of a difference in the head positioning of the patient during pre- and post-operative CT, the pharynx and larynx looked rather different. To have two comparable models, the two geometries were combined so that the only difference before and after surgery is the nasal cavity.

Computational grids were generated in ANSYS Meshing [2], and a grid refinement study was done. The final grid consists of 3 mill. polyhedra grid cells. The flow was simulated as laminar at a flow rate of 250 ml/s (slow breathing) in ANSYS Fluent 16.2 [2]. Other assumptions includes steady state, incompressible flow, rigid walls, no slip at the wall and atmospheric pressure at the inlets.

The CFD results were post-processed in ANSYS CFD-post [2]. After surgery, the flow was found to be more evenly distributed between the two nasal cavities and the flow pattern slightly changed. An increase in the pressure drop over the nasal cavity could be seen. For verification, the nasal resistance was compared with measured results from rhinomanometry and rhinoresistometry. The correspondence for the right nasal cavity was good post-operative, but remarkably lower for the other measures.

The high reduction in AHI measured clinically is not as clearly observed in the CFD results. The increase of flow in the left nasal may indicate that the patient has changed from mostly oral to nasal breathing after surgery. Because of the obstruction in the nose pre-operatively it is likely that the patient breathed mostly through his mouth, causing a backward movement of the tongue and a closing of the pharyngeal airway. Changing to nasal breathing as a result of the surgery would increase the pharyngeal volume and explain the great improvement in AHI. This hypothesis is not verified, but supported by clinicians. Further work is needed to gain more confidence in the results.

Sammendrag

I denne masteroppgaven er det utført en pasient-spesifikk numerisk studie av strømningen i de øvre luftveiene for å studere effekten av et kirurgisk inngrep i nesen. Pasienten valgt for denne studien er en mann på 67 år som hadde moderat obstruktiv søvn-apne syndrom (OSAS) før operasjon. Som følge av operasjonen, ble Apnea-hypopnea indeksen (AHI)redusert fra 23 til 5.7.

Ut i fra pre- og post-operative CT bilder av pasienten ble det laget en geometri. Dette ble gjort med segmenteringsverktøyet ITK-SNAP 3.4.0 [1]. For å sikre at modellen er anatomisk korrekt, har modellen blitt laget i samråd med klinikere. Geometrien ble etterbehandlet for å redusere eventuelle feilkilder som resultat av digitaliseringen. En vesentlig forskjell i pasientens hodestilling i de pre- og post-operative CT bildene førte til at pharynx og larynx så svært ulike ut i de to modellene. For å kunne studere det kirurgiske inngrepets effekt på strømningen ble de to modellene kombinert slik at den eneste forskjellen er nesekaviteten. I ANSYS Meshing [2] ble det laget et grid for å utføre numeriske strømningsberegninger. Dette bestod av omtrent 3 millioner polyheder celler. Strømningen ble simulert som laminær med en volumstrøm på 250 ml/s (rolig pust) i ANSYS Fluent [2]. Andre antakelser inkluderer stasjonær og inkompressibel strømning, faste vegger, og atmosfærisk trykk ved innløpene.

Resultatene fra simuleringene ble videre behandlet i ANSYS CFD-post [2]. Før operasjon var det en betydelig forskjell mellom hvor mye luft som strømmet gjennom høyre og venstre nesekavitet. Denne forskjellen var redusert etter operasjon. Uventet nok, økte trykkforskjellen over nesekaviteten betydelig etter operasjon. Resistansen i nesekaviteten regnet ut fra simuleringene ble sammenlignet med kliniske målinger. De beregnede resistansene var betydelig lavere, med unntak av resistansen i den høyre nesekaviteten etter operasjon, som stemte relativt bra overens med de målte verdiene.

Den betydelige reduksjonen i AHI målt under søvnstudiet var ikke like lett å observere fra de numeriske beregningene. Basert på observasjonen om en jevnere strømning i venstre og høyre nesekavitet, kan det tenkes at pasientens pustemønster har endret seg. Muligens var obstruksjonen i nesen før operasjon så betydelig at pasienten pustet mye med munnen mens han sov. Ved munnpusting endrer kjeven stilling, og tungen faller bak mot pharynx. Dette øker sjangsen for apne. Dersom kirurgien førte til at det ble enklere å puste med nesen, og at pasienten derfor hovedsaklig puster med nesen når han sover, kan dette forklare den store endringen i AHI. Dette er dog ikke blitt bekreftet, men hypotesen anses som en mulighet også av klinikere. Videre arbeid er nøvendig for å bekrefte/avkrefte hypotesen.

Preface

This master thesis is a part of a larger research project; "Modeling of Obstructive Sleep Apnea by Fluid-Structure Interaction in the Upper Airways", which is a collaboration project between the Norwegian University of Science and Technology (NTNU), SINTEF and St. Olav University Hospital. It is funded by NTNU and the Research Council of Norway [3, 4]. The aim of this project is "to demonstrate the potential of a new patient-specific clinical tool based on mathematical models in predicting the response to Obstructive Sleep Apnea Syndrome (OSAS) treatment" [4]. The main project is subdivided into four work packages (WP); Clinical Research (WP1), Soft Tissue Modelling (WP2), Mathematical Modelling of Fluid-Structure Interaction (WP3) and Computation Fluid Dynamics (CFD) Modelling for Prediction of Success of obstructive sleep apnea syndrome (OSAS) Surgery (WP4). This master thesis is contributing to WP4.

At St. Olav University Hospital in Trondheim, Norway, intranasal surgery is being performed on patients with OSAS, but only one third of the patients experience improvement in OSAS after surgery. It is not known why there is such a low success rate after surgery, and why some patients improve and others do not [5]. By studying the geometry and flow patterns of the upper airways before and after surgery, the impact of intranasal surgery on the airflow in the upper airway might become clearer.

The main objective of the thesis is "to simulate the flow in the upper airways of one OSAS patient before and after surgical intervention in the nasal cavity". The thesis is organized as follows; First an introductory chapter covering the background from both the field of medicine and fluid dynamics. In chapter two, a review of the relevant literature will be presented. Chapter three explains the methodology on how to utilize computed tomography (CT) images as a basis for creating model geometries wherein fluid dynamics simulations can be run. In chapter four, the simulated results will be presented and compared with selected clinical measurements. The results, methodology and challenges will be further discussed in chapter five.

Finally conclusion and further work will be presented in chapter five and six. The master thesis is a continuation of the project work "Geometry Retrieval from CT and MRI of the Human Upper Airways" fall 2015 by the same author [6], and will include part of the same introductory chapter and some of the same methodology for the geometry retrieval.

The results from this work will be presented at the 22nd Congress of the European Society of Biomechanics in July 2016 as part of an oral session on Respiratory Biomechanics [7]. The conference abstract can be found in Appendix I.

I would like to thank my supervisor prof. Bernhard Müller (NTNU) and my two co-supervisors dr. Sigrid Kaarstad Dahl (SINTEF MK) and dr. Sverre Gullikstad Johnsen (SINTEF MK) for guidance and motivation throughout the entire process. Your insight and knowledge have been valuable and inspirational. I would also like to thank Mads Henrik Moxness (Aleris) and prof. Ståle Nordgård (NTNU) for good discussion and insightful information from the field of medicine. In addition, I would like to thank dr. Kjell Arne Kvistad (St.Olavs Hospital) for helping me out with the segmentation procedure from CT, and Else Bartnes (St. Olav Hospital) for explaining and providing the clinical measurements.

Contents

Abstract i

Sammendrag iii

Preface v

Abbreviations x

List of Figures xi

1. Introduction 3

1.1 Anatomy of the Human Upper Airways 4

1.1.1 Definition of the Anatomical Planes and Directions 6

1.1.2 The Nose, Nasal Cavity and Sinuses 6

1.1.3 Pharynx 7

1.1.4 Larynx 7

1.2 Obstructive Sleep Apnea Syndrome 8

1.2.1 Characteristics 8

1.2.2 Biologic Basis 8

1.2.3 Risk factors for OSAS 9

1.2.4 Complications and Associations 9

1.2.5 Available Treatments 10

1.3 Medical Imaging 11

1.3.1 CT 11

1.3.2 MRI 12

1.4 Geometry Retrieval 13

1.5 Computational Fluid Dynamics 13

1.5.1 Governing Equations 13

1.5.2 Computational Grid 14

2. Literature Review **16**
2.1 History of OSAS . . . 16
2.2 Previous Modelling Work . . . 17
2.2.1 Modelling of the Airflow in the Nasal Cavity . . . 17
2.2.3 Predicting Surgery Outcome for Alleviation of OSAS . . . 19

3.Method **21**
3.1 Geometry Retrieval . . . 21
3.1.1 Data Acquisition . . . 23
3.1.2 Segmentation . . . 23
3.1.3 Post-processing of the Surface Mesh . . . 31
3.1.4 Editing the Geometry . . . 34
3.2 Grid Generation . . . 37
3.2.1 Grid Convergence Test . . . 37
3.2.2 Final Grid . . . 38
3.3 Numerical Simulation . . . 38
3.3.1 The Commercial Solver ANSYS Fluent . . . 39
3.3.2 Assumptions . . . 39
3.4 Clinical Measurements . . . 40
3.4.1 Procedure of the Measurements . . . 40
3.4.2 Acoustic Rhinometry . . . 40
3.4.3 Rhinorestometry and Rhinomanometry . . . 41
3.4.4 Peak Nasal Inspiratory Flow . . . 41

4. Results **42**
4.1 Geometry . . . 42
4.1.1 Geometry Information . . . 42
4.1.2 Comparison of the Pre- and Post-operative Geometry . . . 43
4.2 Grid Generation . . . 47
4.2.1 Grid Convergence Test . . . 47
4.2.2 Final Grid . . . 51
4.3 CFD Results . . . 53
4.3.1 Velocity . . . 53
4.3.2 Vorticity . . . 55
4.3.3 Pressure . . . 56
4.3.4 Wall Shear Stress . . . 59
4.3.5 Comparison of CFD Results and Measured Data . . . 60

5. Discussion **62**
5.1 Is the Procedure Repeatable? 62
5.1.1 CT and the Effect of the Nasal Cycle 62
5.1.2 The Segmentation Procedure 65
5.2 Comparison of CFD and Measured Results 65
5.2.1 Can the AHI Improvement be Seen in the CFD Results? 65
5.2.2 Comparison with Rhinometric measurements 66

6. Conclusion **71**

7. Further Work **73**

A Appendix **74**
I. Conference Abstract accepted to ESB2016 75
II. Measurement from Acoustic Rhinometry, pre-operative 76
III. Measurement from Acoustic Rhinometry, post-operative 1 77
IV. Measurement from Acoustic Rhinometry, post-operative 2 78

Abbreviations

AHI	Apnea Hypopnea Index
AR	Acoustic Rhinometry
CFD	Computational Fluid Dynamics
CPAP	Continious Positive Airway Pressure
CPU	Central Processing Unit
CT	Computed Tomography
HU	Hounsfield Units
MAD	Mandibular Advancment Device
MRI	Magnetic Resonance Imaging
OHS	Obesity Hypoventilation Syndrome
OSAS	Obstructive Sleep Apnea Syndrome
PNIF	Peak Nasal Inspiratory Flow
RANS	Reynold Averaged Navier Stokes
RITR	Right Inferior Turbinate Reduction
RMM	Rhinomanometry
RRM	Rhinoresistometry
SIMPLE	Semi-implicit Method for Pressure Linked Equations

List of Figures

1 Schematic of the respiratory system [8] 4
2 Schematic view of the upper respiratory tract, coronal (left) and sagittal (right) plane [9]. 5
3 The anatomical planes and position definition [10]. 6
4 Non-obstructed (left) and obstructed airway (right) [11]. 9
5 Representation of pixel (2D) and voxel (3D) [10]. 12
6 Flow chart representation of the work flow for geometry retrieval. . . 22
7 The DICOM files as they appear in ITK-SNAP 3.4.0. Active Contour Segmentation is marked with a blue square. 24
8 ITK-SNAP window with a selected Region of Interested. 26
9 ITK-SNAP window at step number one of segmentation; Pre-segmentation. 27
10 ITK-SNAP window at step number two of segmentation; Initialization. 27
11 ITK-SNAP window at step number three of segmentation; Evolution. 28
12 ITK-SNAP window showing the result of the automatic segmentation. 29
13 Pre-operative CT of patient number 12 from the ITK-SNAP window showing coronal (a) and sagittal (b) views of the nasal cavity and paranasal sinuses. The figures illustrate what parts of the air-filled spaces and channels that are included in the segmented volume. The maxillary sinuses(MS), ethmoid sinuses and cells (ES), frontal sinus (FS) and spenoidal sinuses (SS) are all marked on the figure. The sinus ostiums are the thin channels connecting the segmented volume (red) and the paranasal sinuses, and those have been left out of the segmented volume. Note that the marker (blue cross) are placed at the same locations in both (a) and (b). 31
14 The effect of the Laplacian Smoothing filter on the pre-operatively nasal cavity seen from the left. The original geometry extracted from ITK-SNAP is seen in (a), and (b) shows the same geometry after the smoothing process. 33

15 (a) and (b) show the different head position of patient number 12 in the pre- and post-surgical CT recordings, respectively. 34
16 The final post-operative model before the boolean operation were added to combine all four parts to one single geometry. 37
17 The original pre-operative geometry, after mesh reduction and with smoothing, respectively. Viewed from the right side. 43
18 The pre- and post-operative nasal cavity after smoothing seen from the left side. 43
19 The pre- and post-operative nasal cavity after smoothing seen from below. 44
20 The pre- and post-operative nasal cavity after smoothing seen from the right. 45
21 The pre- and post-operative model seen from the front. 46
22 The final pre- and post-operative model seen from the left. 47
23 Location and numbering of cross-sections. 48
24 Area-averaged velocity plotted at cross-sections marked in Fig. 23 for three tetrahedra grids. 49
25 Area-averaged pressure plotted at cross-sections marked in Fig. 23 for three tetrahedra grids. 49
26 Area-averaged velocity plotted at cross-sections marked in Fig. 23 for four polyhedra grids. 50
27 Area-averaged pressure plotted at cross-sections marked in Fig. 23 for four polyhedra grids. 50
28 View of the pre(left)- and post(right)-operative grid. Parts of cross-sections from the nasal cavity, and from the nasopharynx and below. 52
29 View of the transition zones of the post-operative model. The volume that is combining the pre-and post-operative parts is seen to the left, and the transition to the extended outlet to the right. 52
30 Contour plot of the velocity across a sagittal cut plane at the middle of pharynx and larynx, and the left nasal cavity. The pre-operative results to the left, and the post-operative on the right. 53
31 Contour plot of the velocity magnitude across coronal cross sections in the nasal cavity pre-operative (left) and post-operative (right). The models are viewed from the right side. 54
32 Velocity streamlines in the left nasal cavity pre- and post-operative, respectively. 55

33 Velocity streamlines in the right nasal cavity pre- and post-operative, respectively. 55
34 Vorticity regions in the pre(left)- and post-operative(right) models . . 56
35 Contour plots of the pressure distribution at the wall in the nasal cavity pre(left)- and post(right)-operative. The nasal cavity is viewed from the left. 57
36 Contour plots of the pressure distribution at the wall in the nasal cavity pre(left)- and post(right)-operative. The nasal cavity is viewed from the right. 57
37 Contour plots of the pressure distribution at the wall in the pharynx pre(left)- and post(right)-operative. 58
38 Plot of the area-averaged pressure at the cross-sections in Fig.23 pre- and post-operatively. 58
39 Wall shear on the pre- and post-operative model seen from the left. . 59
40 Wall shear at the posterior pharynx, pre-operative(left) and post-operative(right). 60

41 Coronal CT view of the nasal cavity pre(left)- and post(right)-operative 63
42 The figure shows two different CT axial views of Patient 12 taken pre-operative. No remarkable difference in the cross-sectional areas of the left- and right nasal cavity in the middle of the nose are observed. . 64
43 Placement of cross-sectional planes along the path of the soundwave suggested by Terheyden et al. [12]. 68

1. Introduction

The objective of this master thesis is to simulate the flow in the upper airways of one obstructive sleep apnea syndrome (OSAS) patient before and after intranasal surgery. The computational models will be created from computer tomography (CT) images.

To be able to do the Computational Fluid Dynamics (CFD) modelling in Work Package (WP) 4 "Modeling for Prediction of Success of OSAS Surgery" [13] of the research project "Modeling of Obstructive Sleep Apnea by Fluid-Structure Interaction in the Upper Airways" [3, 4], the first step is to obtain a geometry of the human upper airway. CT of the patients were obtained in WP1 "Clinical Research" of [3, 4], and a method for creating a geometry from CT datasets was developed in the project work "Geometry Retrieval from CT and MRI of the Human Upper Airways" [6] fall 2015. This master thesis is a continuation of that project work, and will in addition to geometry retrieval also include grid generation, flow modelling and a comparison with measured data.

Some theoretical background is necessary to understand the purpose of the study and be able to create a model. In chapter 1.1, the anatomy of the upper airways is presented. The physiology of OSAS is further being explained in chapter 1.2. Risk factors, treatment and complications associated with OSAS will also be explained in the same chapter. In chapter 1.3, the physics behind the medical images and the data they contain is explained. Chapter 1.5 includes a brief introduction to geometry retrieval. Finally, in chapter 1.6, an introduction to CFD and grid generations is given. Parts of chapter 1 can also be found in [6].

1.1 Anatomy of the Human Upper Airways

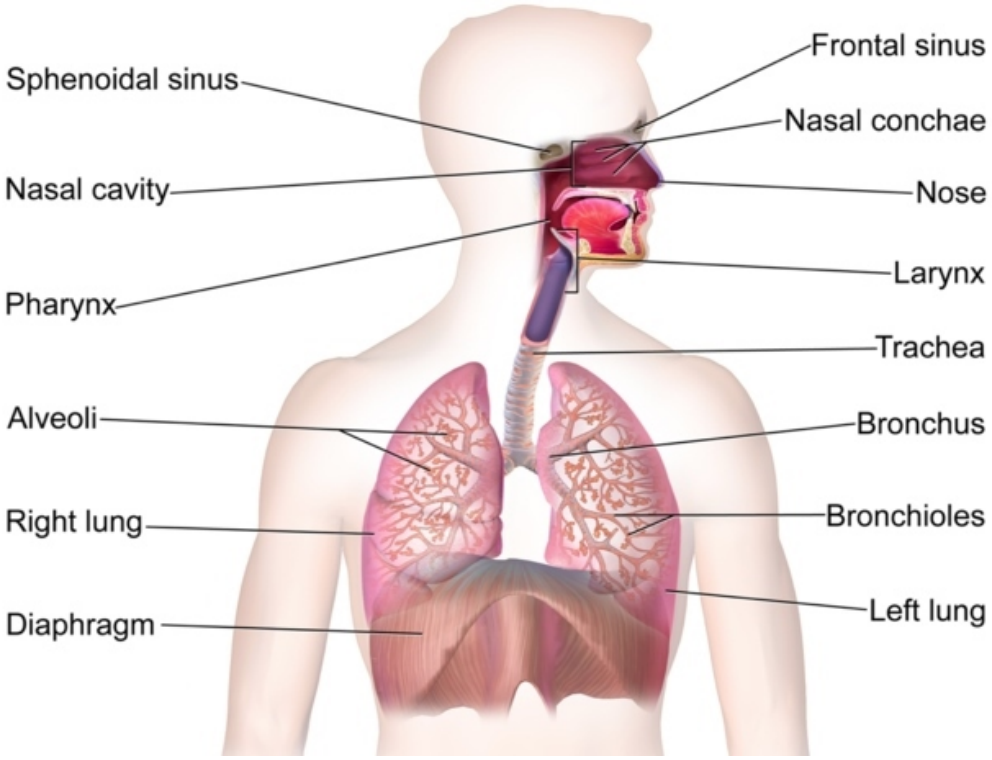

Figure 1: Schematic of the respiratory system [8]

.

The main function of the human respiratory system is to exchange the oxygen inhaled from air with carbon dioxide in the blood. The respiratory system can be divided into the upper- and lower respiratory tract where the lower airway includes organs within the chest cavity, while the upper airway includes the organs outside of it. The dividing of the respiratory system is also based on its functions. Air is first inhaled through the nose and mouth and gets warmed, humidified and filtered in the upper respiratory system. As the air enters the lower respiratory system, the gas exchange takes place in the alveoli (Fig. 1). After the gas exchange, the air, that is now containing carbon dioxide, will be exhaled through the upper respiratory system. This exchange happens on every inhalation and exhalation. Other main functions of the respiratory system are sound production, smell and control of body pH-levels [10].

For the case of OSAS, only the upper respiratory system is of interest. A more detailed description of the anatomy will be presented in the following subsections.

The human upper airways begin at the nose and end at the beginning of trachea (Fig. 1). The upper airway consists of the main components; the nose and nasal cavity, the mouth and oral cavity, the pharynx and the larynx (Fig. 2). Study of the airflow for OSAS patients with nasal obstructions will be done when the mouth is closed, hence the physiology of the mouth will not be explained further in this section.

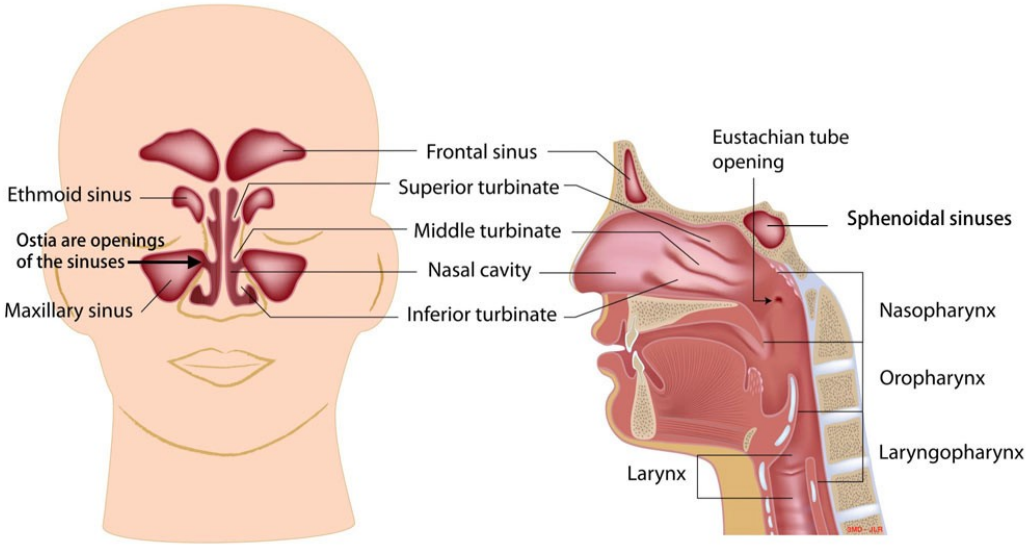

Figure 2: Schematic view of the upper respiratory tract, coronal (left) and sagittal (right) plane [9].

1.1.1 Definition of the Anatomical Planes and Directions

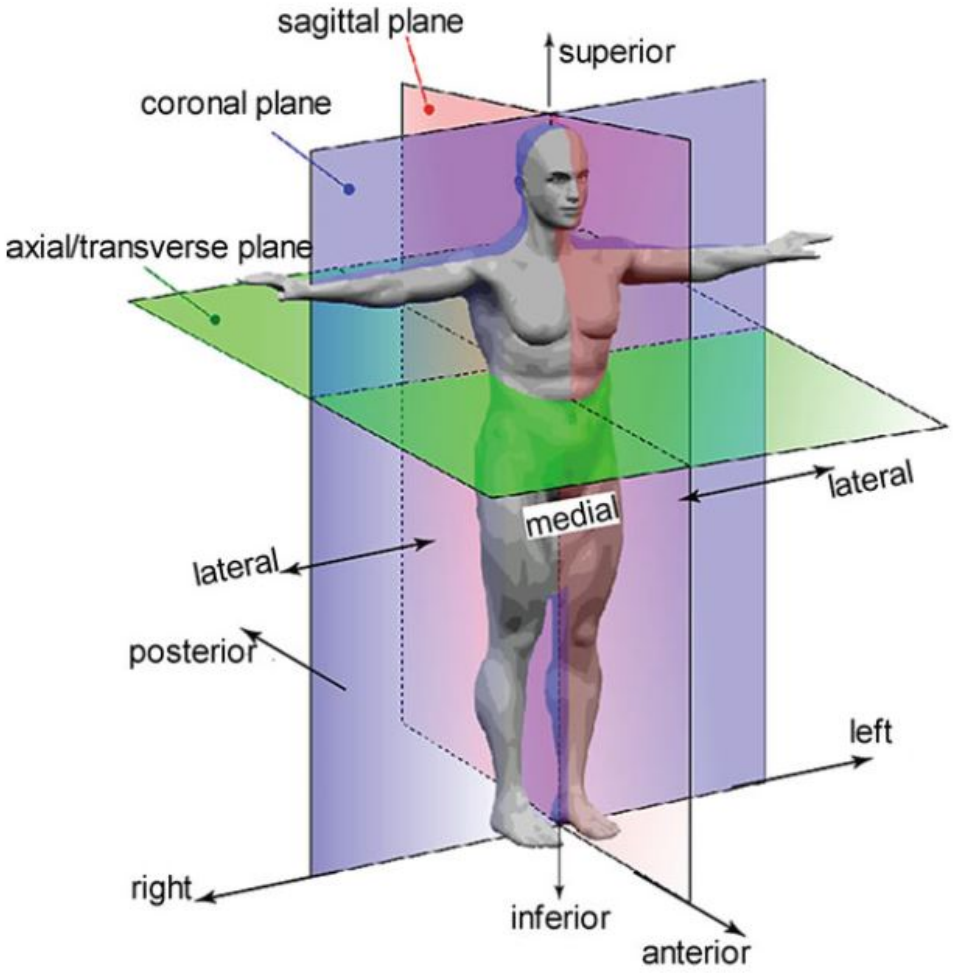

Figure 3: The anatomical planes and position definition [10].

Fig. 3 shows the definitions of the anatomical planes and directions. These definitions will be used throughout the report.

1.1.2 The Nose, Nasal Cavity and Sinuses

The first part of the upper respiratory tract is the nose which is both air inlet and outlet for inhalation and exhalation, respectively.

Air enters the nares (also called nostrils) and flows into the two nasal cavities. Breathing can be affected of the nasal cycle, which is a phenomena observed in about 80% of the normal individuals. During each nasal cycle, one of the nasal passages is dominant causing the airflow through the nasal cavities to be asymmetrical. Each nasal cycle last from 30 minutes to 6 hours [10]. The nasal cavities are

separated by nasal septum cartilage. The nasal septum is in most cases straight, but a deviated septum is common and often caused by some external trauma [14]. In each of the nasal cavities there are three (rarely four) turbinates/conchaes; the inferior, middle and superior turbinate. These are scroll-like projections from the lateral nose wall that regulate, humidify, filter, pressurize, elevate and streamline the air [15]. The nasal cavity is connected to the paranasal sinuses by small channels. The paranasal sinuses are air-filled spaces and consist of four pairs of sinuses; the frontal, sphenoid, ethmoid and maxillary sinuses (Fig. 2). The functions of the paranasal sinuses is speculative, but they do add resonance to the voice and decrease the weight of the skull [14].

1.1.3 Pharynx

The pharynx is a tube like structure that extends from the cranial base to the level of the sixth cervical vertebra and consists partly of collapsible walls [14]. As both food and air pass through the pharynx, it is part of both the digestive and the respiratory system.

The pharynx can be divided into three subdivisons; the nasopharynx, oropharynx and laryngopharynx (sometimes referred to as the hypopharynx) as shown in Fig. 2. The nasopharynx is located above the soft palate and behind the posterior nares. The soft palate faces upward during swallowing, preventing food and air to enter the nasopharynx. Inferior of the soft palate and posterior to the mouth is the oropharynx. This goes all the way down to the hyoid bone which also marks the upper boundary of the epiglottis. Both food and air pass through the oropharynx and are later separated by the epiglottis in the laryngopharynx. The laryngopharynx is located between the hyoid bone and at the junction where the airway splits into the trachea and oesophagus, and becomes continuous with the oesophagus [14].

1.1.4 Larynx

The larynx (also known as the voice box) is an air passage and serves as a sphincter that transmits air from the oropharynx to the trachea (see Fig. 2) and creates sound for speech [14].

1.2 Obstructive Sleep Apnea Syndrome

1.2.1 Characteristics

Obstructive sleep apnea syndrome (OSAS) is characterized by an obstruction in the upper airway preventing the air from flowing freely, causing apneas (pauses in breath) and hypopneas(shallow breathing) during sleep and a lack of sleep quality. The most prevalent symptoms are daytime sleepiness, snoring and unrefreshing sleep [16].

The severity of OSAS is characterized by the number of apnea/hypopnea events per hour during sleep, which defines the apnea-hypopnea index (AHI). To count as an event, the apnea/hypopnea must exceed 10 seconds. An AHI less than five is considered normal, between 5 and 15 is considered as mild OSAS, between 15 and 30 is moderate OSAS and above 30 is defined as severe OSAS [17]. The Epworth Sleepiness Scale (ESS) is another method used to assess the severity of OSAS. On the ESS, the patient reports the likelihood from 0-3 of falling asleep during eight everyday scenarios [16], hence it is less accurate as it is not measurable.

1.2.2 Biologic Basis

The basis of OSAS is a narrowing and closing of the airway. This usually happens in the oropharynx where the airway is naturally narrow, preventing the air from flowing freely to the lower respiratory tract. As a result of this, the gas exchange in the alveoli does not function properly and the patient experiences hypoxaemia(low concentration of oxygen in the blood) and hypercapnia(high concentration of carbon-dioxide in the blood). The only way to establish airway patency again is arousal from sleep [18].

A narrow airway can be caused by an increased volume in the soft palate or tongue, parapharyngeal fat pads or the lateral walls surrounding the pharynx. During sleep, the muscles are less active and a collapse in the oropharynx can occur as shown in Figure 4. The sleep position of the patient is also of interest. The pharynx has no fixed rigid support, and all the collapsible walls, the soft-palate and tongue move posterior when sleeping on the back because of gravity. Because of this, changing sleeping position can have an effect on the volume of the pharynx [19].

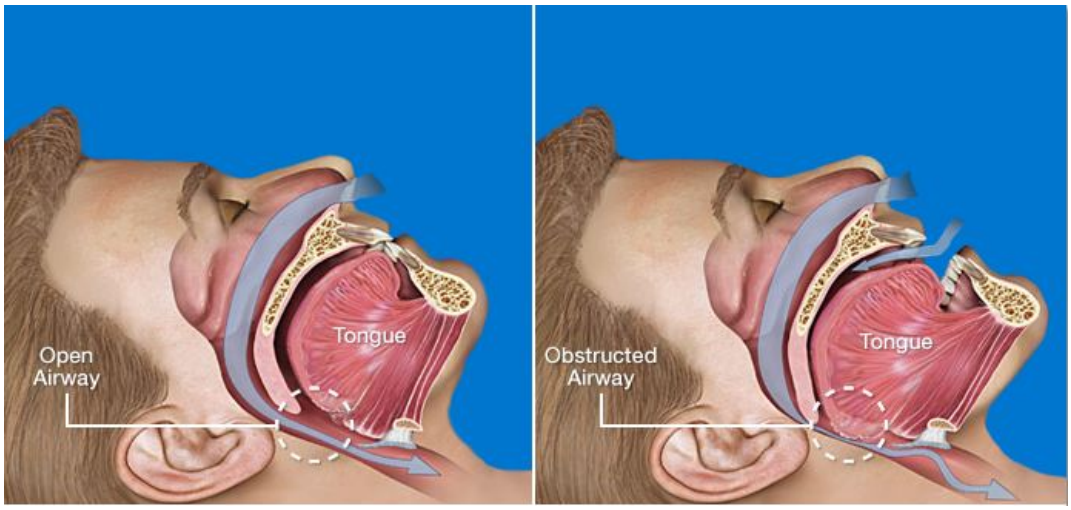

Figure 4: Non-obstructed (left) and obstructed airway (right) [11].

Another cause of obstruction can be observed further up in the nasal cavity where a deviated septum and/or enlargement of the turbinates prevent the air from flowing and causing an airway flow resistance. The low airway pressure also causes the pharyngeal airway to collapse.

1.2.3 Risk factors for OSAS

It is estimated that approximately 2% of middle aged women and 4% of middle aged men suffer from OSAS. OSAS can be caused by different types of obstructions, and there are therefore several different risk factors. One of the most common risk factors are obesity [16]. The following predisposing factors are pointed out by the American Academy of Sleep Medicine [17]; obesity (particularly in the upper body), male gender, craniofacial abnormalities, increased pharyngeal soft tissue, nasal obstruction and familial history.

1.2.4 Complications and Associations

The poor quality of sleep caused by OSAS leads to a series of other health issues such as increased risk of cardiovascular diseases, diabetes and depression [16]. Subjects with untreated OSAS also have daily struggles because of the excessive daytime sleepiness. They are in worst case unable to work as they are not able to stay awake and/or function properly during the work day. The unemployment is an economic burden on the society and a burden for the subject itself. OSAS patients are also more likely to have work accidents and get into driving accidents because of their

lessened ability to keep focused. Healthcare costs are also higher for OSAS patients, but these costs are however reduced when they are treated with success [20].

1.2.5 Available Treatments

Today there exist several treatments for OSAS. However, the response to them differs between the patients based on where and what the obstruction is.

One of the first treatments for OSAS was tracheostomy where a tube is inserted into the trachea through the neck. This creates an airway outlet and avoids the problem with obstructions further up in the airway. Tracheostomy is a very effective and successful method, but is only used in special cases or if the patient does not respond to any of the other available treatments. Reasons for avoiding this treatment include inability to swim, unsightly appearance, frequent coughing up of mucous, formation of granulation tissue, aspiration, pneumonia and vocal cord paralysis [21].

Other surgical approaches for OSAS can also be performed to open up the airway depending on what causes the obstructions. Intranasal surgeries such as straightening of the septum or decrease of the turbinates or tissue removal from the soft palate, uvula, tonsils, adenoids or tongue will increase the airway volume. Often, a combination of surgeries is needed for alleviation of OSAS. Surgery to change craniofacial structures can also be performed, but are more complex than the above mentioned surgeries [22].

Continuous Positive Airway Pressure (CPAP) is the standard treatment to OSAS as most patients respond well to this treatment and it does not involve surgery. With CPAP treatment a mask is placed either over the nose, in the nares or over both nose and mouth and a steady stream of positive pressurized air is provided through the mask. The CPAP prevents the pharyngeal airway from collapsing during sleep and therefore reduces the apneas remarkably and daytime sleepiness is reduced/non-apparent. Some patients do however find it impractical to use the mask every night and prefer surgery instead [16]. Another non-surgical treatment is Mandibular Advancement Devices (MAD) such as mandibular advancement splints protrude the lower jaw during sleep, and increases the volume of the pharynx. This prevents upper airways collapse [23].

OSAS can be a result of obesity, and studies have shown that OSAS is more prevalent in the obese and overweight part of the population. Losing weight will in some

cases alleviate OSAS as the fat around the pharynx will decrease with the the weight loss and allow the air to flow freely in the pharynx [16].

1.3 Medical Imaging

Medical imaging is a non-invasive technique which can provide a visualization of the interior of the body. There are several types of medical imaging, but only CT and MRI will be considered in this report.

1.3.1 CT

A CT scanner emits X-rays into the body, and creates a picture based on how the photons in the X-rays are absorbed or redirected from the structures they pass through in the body. The degree to which an X-ray beam is reduced by the structure is called attenuation, and the grayscale image represents this in Hounsfield units (HU). HU is defined by

$$HU = 1000 \cdot \frac{\mu_P - \mu_W}{\mu_W} \tag{1}$$

where μ_P and μ_W are the mean X-ray attenuation coefficients of the tissue in the pixel and water, respectively [10]. On the Hounsfield units scale, air defines the lower limit at -1024 HU, water is at 0 HU, and at the upper limit, tooth enamel, is at 3072 HU [10].

The main advantages of CT are the short scanning time (only a few minutes depending on the machine itself) and the representation of the bony structures. The disadvantages are that soft tissue does not show up in detail and that it is not a completely harmless procedure as it exposes the patient to ionizing radiation [10].

CT provides 3D volumetric data from a series of 2D pictures with a specified slice thickness. As seen in Fig. 5, the 2D-slices make up voxels which are 3D-elements defined as the surface area of the pixels extruded between the slices [10].

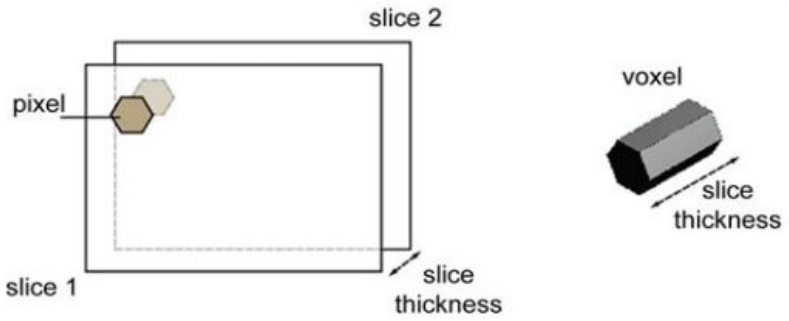

Figure 5: Representation of pixel (2D) and voxel (3D) [10].

1.3.2 MRI

MRI is based upon the fact that the body is largely composed of water and lipid and uses radio waves and magnetic fields to get a distribution map of the hydrogen nucleus/protons in the body [24].

Each hydrogen atom contains a nuclei which has both angular momentum and magnetic moment. The magnitude of these values is fixed, but the directions are random. In an MRI machine, a strong magnetic field (usually 1-3 Tesla) is imposed causing all the protons to align in the same or exact opposite direction with respect to the direction of the magnetic field. A radio frequency pulse is then sent through the body, flipping the spin of the nuclei and when the signal is stopped, the protons will return to their original orientation emitting their own radio signals in the process. It is this radio signal ("echo") that the scanner detects and makes use of. The relaxation time is the time it takes the proton to return to its original state, and both longitudinal (T1) and transverse (T2) relaxation are of interest, as they provide different information for the various tissues [24].

Essentially, MRI gives a proton density map for each slice which all together make up a 3D model of the body of interest. All the different proton densities represent different body parts and are shown as grayscales on the MR image. The lightest colour refers to the lowest density, and pure air is on the other end of the scale and shows up as dark in the images.

The imaging process takes from 20-60 minutes, and the patient has to lay still for the entire time to achieve good quality images. Another disadvantage is that all metal has to be removed from the patient because of the strong magnetic field utilized in the procedure. Hence patients with metal in the body due to e.g. previous surg-

eries cannot undergo MRI. The main advantages of MRI are that it is a completely harmless procedure, the different soft tissues show up detailed, and the images can be taken in coronal, axial and sagittal slices [24].

1.4 Geometry Retrieval

Geometry retrieval from the medical images can be done by segmentation. As the image sets contain information about more than just the upper airway, the region of interest must be separated from the rest. During segmentation, each of the voxels in the images get labelled based on specified characteristics. All the voxels with the same label can then be extracted all together making up a model of an anatomical feature [10].

Segmentation can be done both automatically and manually and there exist several software making the process easier. The commercial software MIMICS [25] is widely used, but there are also several free softwares such as ITK-SNAP [1] and Slicer [26].

1.5 Computational Fluid Dynamics

1.5.1 Governing Equations

Computational Fluid Dynamics (CFD) uses numerical methods to solve the flow governing equations, that is the Navier-Stokes equations for conservation of mass (eq. 2) and momentum (eq. 3).

$$\frac{\partial \rho}{\partial t} + div\rho V = 0 \tag{2}$$

$$\rho \frac{DV}{Dt} = \rho g + \nabla \cdot \tau_{ij} \tag{3}$$

where the viscous stress tensor τ_{ij} is

$$\tau_{ij} = -p\delta_{ij} + \mu\left(\frac{\partial u_i}{\partial x_j} + \frac{\partial u_j}{\partial x_j}\right) + \delta_{ij}\lambda divV \tag{4}$$

If the flow is incompressible, the density ρ is constant, and eq.2 and 3 reduces to eq. 5 and 6

$$divV = 0 \tag{5}$$

$$\rho\frac{DV}{Dt} = \rho g - \nabla p + \mu\nabla^2 V \tag{6}$$

In eq. 2 - 6, V is the velocity vector, g is the acceleration of gravity, p is the pressure, δ_{ij} is the Kronecker delta function, λ is the second viscosity coefficient, μ is the viscosity [27].

When using CFD, the governing equations are solved numerically over control volumes and must be discretized into algebraic form.

1.5.2 Computational Grid

The flow physics can be represented by a set of mathematical equations. Grid generation is in essence dividing the entire geometry into smaller grid cells to be able to solve flow equations over the domain. To simulate the flow field on a geometry, such as the upper airway, these mathematical equations are applied to every grid cell. In order to obtain good and accurate results, the grid is of great importance. The type of grid cells, size of the cells and the grid structure define where, and how many times the equations are solved [10].

1.5.2.1 Grid Characteristics

There are numerous possibilities for grid generation. The grid can either be structured or unstructured. A 3D structured grid is made up of hexahedrons while an unstructured grid is commonly made up of triangles, tetrahedra or polyhedra cells in irregular patterns. An unstructured grid is better in use for irregular geometries such as the upper airway. In addition to triangles and tetrahedra, the unstructured grid can consist of other cell types. Often a hybrid grid (several different cell types) is needed to fit the geometry in the best way [10].

1.5.2.2 Evaluation of grid quality

To ensure that the grid is of good quality, the cell shapes can be evaluated based on a series of measures. The aspect ratio defined the base to height ratio of a cell element. It can be within the range of 0 to 20, where 0 is a perfect element, and 20 refers to an extremely stretched element. Most preferable, the aspect ratio should be within the range of 0.2 and 5 in the interior region of the grid. Near the wall, however, the aspect ratio can be relaxed [10]. The same formation of the element is measured with the maximum corner angle. Skewness is a measure of how skewed the elements are. The ratio is from 0 to 1, and should be within the range of 0

to 0.25 to be considered good. Another indication of the twisting of the element is the warping factor, where 0 indicates no twisting. The Jacobian Ratio indicate placement of the midside node. It ranges from 0 to 1000 for triangles and 0 to 100 for quadrilaterals, where 0 is optimal for both elements. Element quality refers to the quality and volume of the element, and range from 0 to 1 where 1 is a perfect element. The same range applies to the orthogonal quality [28].

The above mentioned ratios can be measured before simulations, but the best way to estimate the grid quality is by seeing how it affects the simulations. A good approach is to start with a coarse grid at first, and then refine the grid until the size of the cells no longer affects the simulations, and grid independence is reached.

2. Literature Review

2.1 History of OSAS

Even though OSAS is a common disease with significant implications for individuals as well as society, it is quite new as a research area as the syndrome itself was not recognized until advances in technology made it possible to measure the symptoms.

The first description of a syndrome similar to OSAS in literature is found in Charles Dickens "The Pickwick Papers" (1836) where an obese (overweight) boy is struggling with daytime sleepiness and heavy snoring. This character gave name to the "Pickwickian Syndrome" which was a term widely used after Burwell et. al. 1956 [29] described the syndrome in their case study of an obese man struggling with daytime sleepiness. The Picwickian Syndrome became known as Obesity Hypoventilation Syndrome (OHS) afterwards. Characteristics of OHS/The Pickwickian Syndrome is similar to those of OSAS as approximately 90% of those with OHS also have OSAS [30], but the subject is always obese when being affected by OHS. In 1966, Gastaut et al. [31] published a paper observing two "Picwickian" patients and documented that the apneas are cyclic. Further they suggested somnolence as either being caused by a primary disturbance of the brain stem centres that regulates wakefulness and sleep, where the disturbance is somehow linked to obesity, or as a result of the low quality of sleep during night. In the same paper, Gastaut et al. [31] also suggested the respiratory disturbances were caused by a mechanism obstructing the upper outlet of the airflow and in particularly a backward movement of the tongue, which today is known to be a common obstruction for patients with OSAS [16, 32].

During the 1960's and 1970's, tracheostomy was the only available treatment, but not a desired one. However, in 1981 Sullivan et al. [33] introduced and documented the effect of CPAP on OSAS patients and revolutionized the treatment of OSAS. After this, OSAS has become a research area of interest, and numerous papers on OSAS and its treatment options have been published.

2.2 Previous Modelling Work

The respiratory system have always been of interest and studied, but was for ages only a field of medicine. With the help of new technology, the respiratory system is now also considered an engineering problem. A review of previous work will be given in the following sections.

2.2.1 Modelling of the Airflow in the Nasal Cavity

The first experimental models were made from casts obtained from plastic imprints of human cadavers. These had the advantage of being anatomically correct, but the small size and complex geometry of the nasal cavity made it difficult to study the flow in detail. As CT and MRI technology improved, making enlarged models based on the medical images made it possible to study the flow in detail.

Schreck at al. [34] made a three times enlarged model from MRI, and located two distinct vortices in the nasal cavity that seemed to be almost independent of flow rate. The largest were located in the upper exterior nose, and a smaller one in the lower exterior nose. The nasal resistance, describing the ease of flow through the nasal cavities, was found to increase significantly with only a small reduction in the cross sectional areas. The resistance measured for inspiratory and expiratory flow was similar, and the findings indicated that the resistance is insensitive to the inlet conditions. These studies were the first to relate the resistance to both flow rate and geometry. From the same studies, the onset of turbulence was found to be at a flow rate of 200 ml/s. A fully developed turbulence was not reached until a flow rate of 500 ml/s.

Hahn et al. [35] made a twenty times enlarged model of the left nasal cavity from CT scan to study the flow in detail. Steady flow was used. They found characteristic flow patterns for flow rates ranging from 1100 to 180 ml/s. From experiments, they found that 50% of the inhaled air flew through the combined middle and inferior turbinates, and only 14% through the olfactory region. The highest flow rates were found to be turbulent, while flow rates of less than 200 ml/s was disturbed laminar. The results of Hahn et. al. was later used for validation of results from numerical simulations by Keyhani et al. [36]. They were the first to do numerical simulations on an anatomically correct model of the nasal cavity - previously only simplified model airways and the anterior part of the nose had been studied with flow simulations.

From the same CT scan that was used by Hahn, a three-dimensional reconstruction of the left nasal cavity was made. Simulations were done assuming laminar flow at flow rates between 125 and 200 ml/s as suggested by Hahn and Schreck. The flow was modelled as quasi-steady with an inlet velocity field perpendicular to the naris. The numerical and experimental results showed good agreement and confirmed the laminar approximation. The results also agreed with previous experimental studies where the highest velocities occurred along the nasal floor, lowest in the olfactory region and the main path was between the inferior and middle turbinates and the septum.

Experimental and numerical simulations on models from same CT were also done by Croce et al. [37], but with both nasal cavities modelled. The experiments was done with flow rates up to 1500 ml/s, and the numerical simulations with flow rates upto 353 ml/s. The flow was simulated as laminar for all flow rates. The experiments and numerical simulations corresponded well for flow rates up to 250 ml/s. Croce hypothesized that the decreasing correspondence for higher flow rates indicated that turbulent effects dominated, and that the laminar model was not valid for the higher flow rates. This transition to turbulence was at a slightly lower flow rate than the limit previously suggested for turbulence. Croces model are however more detailed as it was based off higher resolution CT than used before, and previous models might therefore be smoother which could allow for the laminar model to be used for higher flow rates. For all flow rates, similar flow patterns to those simulated before were found; maximum velocities in the nasal valve, and the main part of the flow goes between the inferior and middle turbinates. Another main result from the flow simulations was that the anterior part of the nose predominates in nasal resistance. 92% of the pressure drop was generated between the nostril and the ostium, and 48% of the pressure drop was already reached in the nasal valve region.

When studying the nasal airflow, a common assumption have been to use a truncated inflow either at the nostrils, or with an extended pipe from the nostrils. A more natural environment to model would be to include the flow outside the face. This does however increase the size of the model and the computational time. Taylor et al. [38] studied the effect the inflow geometry had on the flow. From CT image datasets, two geometrical models (A and B) were segmented, and silicone models were made from these. The silicone models were then scanned with CT, which new computer models were made from. This procedure ensured that the replicas and computer models were identical. Numerical simulations were done with three different inflow configurations; a flat velocity profile at the nostril, a flat and parabolic profile at the

entrance to a convergent pipe inflow to the nose and pressure boundary conditions including the external face. For subject A, the inflow conditions had a negligible effect on pressure drop, and some small variations were found for subject B. The greatest variation between the inflows were found at the olfactory region. Based on this, the flow is relatively insensitive to the inflow conditions.

2.2.3 Predicting Surgery Outcome for Alleviation of OSAS

One of the motivations for investigating the flow in the nasal cavity is to be able to predict the outcome of surgery. CFD can possibly provide a non-invasive and cost-efficient guidance to medical personnel on what surgery procedure to choose.

DeBacker et al. [39] examined whether or not the treatment outcome of mandibular advancement device (MAD) could be predicted by CFD and functional imaging. Ten subjects with heavy snoring and OSAS were treated with patient-specific MAD. The subjects underwent three sleep studies; one without MAD, one after using the MAD for four months and one split night with and without the MAD. For each patient, two sets of CT were obtained after the split night - with and without the MAD. From these CT scans the geometry of the upper airway was reconstructed. The flow was simulated in both geometries. The airway volume, resistance and the angle of the mandible were calculated in both cases. From this, the outcome of the treatment was successfully predicted. The AHI was best correlated with the resistance, but a good correlation between AHI both the angle of the mandible and the upper airway volume was also found. From the clinical tests, the treatment was successful for seven patients, and both successful and unsuccessful treatments were predicted by examining the changes in the airway volume and resistance. The study shows great potential for predicting the outcome of MAD treatment using CFD and CT.

A similar study correlating reduction in airway resistance with AHI after a widening of the pharyngeal airway was done by Fan et al. [40]. The widening of the airway was however more extensive as they studied the pharyngeal airflow of an OSAS patient before and after a surgical procedure increasing the length of the lower jaw bone. From CT of the patient both pre- and post-operatively, two models of the pharyngeal airway was constructed. CFD simulations of the flow showed that the airway resistance had decreased by 40% which reduced the collapsibility of the pharyngeal airway.

Rhee et al. [41] did a case-study to evaluate weather or not virtual surgery can predict the outcome of surgery. A patient with nasal obstructions underwent septoplasty and right inferior turbinate (RITR) reduction. The surgery procedure was decided based on clinical representation. Pre-and post-operative models were made from CT scan image data of the patient using Mimics. The pre-surgery model was then altered by the surgeon in Mimics to reproduce the surgery. This was done by making three models that represented three different surgery approaches; septoplasty only, RITR only, and a combination of both (the actual surgery). The governing flow equations were solved for all models (pre-operative, post-operative and the three virtual surgeries) with a flow rate of 15.7 l/min. The results from the simulations included nasal resistance, airflow allocation and regional airflow distribution within the nasal cavity. A comparison of the results for virtual surgery showed only minor differences between septoplasty alone and septoplasty with RITR. This indicates that septoplasty alone would based on CFD results been enough to improve the airflow, and that the patient could have had a smaller surgery if CFD had have been part of the surgery planning.

Later, Mylavarapu et al. [42] did a case-study with virtual surgery to see if it is possible to plan human upper airway surgery using CFD. A man with sub-glottis stenosis was the subject for the study. From CT scans an airway model of the pharynx and larynx was reconstructed using MIMICS. Four types of virtual surgeries were performed on the model to enlarge the constricted area. Inspirational and expirational flow for all four surgery cases, and for the pre-operative condition was modelled. The flow field was solved with the turbulent model RANS k-ω SST and a flow rate of 20 l/min. Velocity, pressure, wall shear and airway resistance for all five cases were compared to find the optimal surgical solution. Based on the virtual surgeries, a less invasive surgery was suggested and performed on the patient. A considerable improvement in breathing was found for the patient in the clinical follow-up. Although this is only one case-study, it shows great potential for using CFD as a tool for planning surgery in addition to the existing clinical assessments.

3.Method

The physical changes in the upper airway after nasal surgery are well documented for all the patients in the research project as they undergo CT and MRI both before, and three months after, surgery. To model the flow, the first step is to create a geometry of the upper airways from the CT datasets through segmentation. The choice of CT over MRI is explained in [6], but is overall based on better resolution and easier segmentation when using CT. The raw geometry file must then be post-processed and converted to a solid which a computational grid can be generated from. Patient specific flow patterns can then be studied by solving the governing equations over the entire computational domain using realistic boundary conditions. A grid convergence study is necessary to ensure a grid independent solution. For validation of the results, clinical measurements have been compared to the CFD-results.

3.1 Geometry Retrieval

From the medical images, the body scanned can be viewed as a volume. It is however not possible to get only a selected body part on the images, but the entire upper body - including the upper airway - is visible. The only part of interest for this project is the upper airway, and that part must therefore be retrieved and separated from the body surrounding it. The raw geometry file must then be post-processed for further work. A flow-chart representation of the process can be seen in Fig.6, and the procedure will be explained in detail in the following subsections.

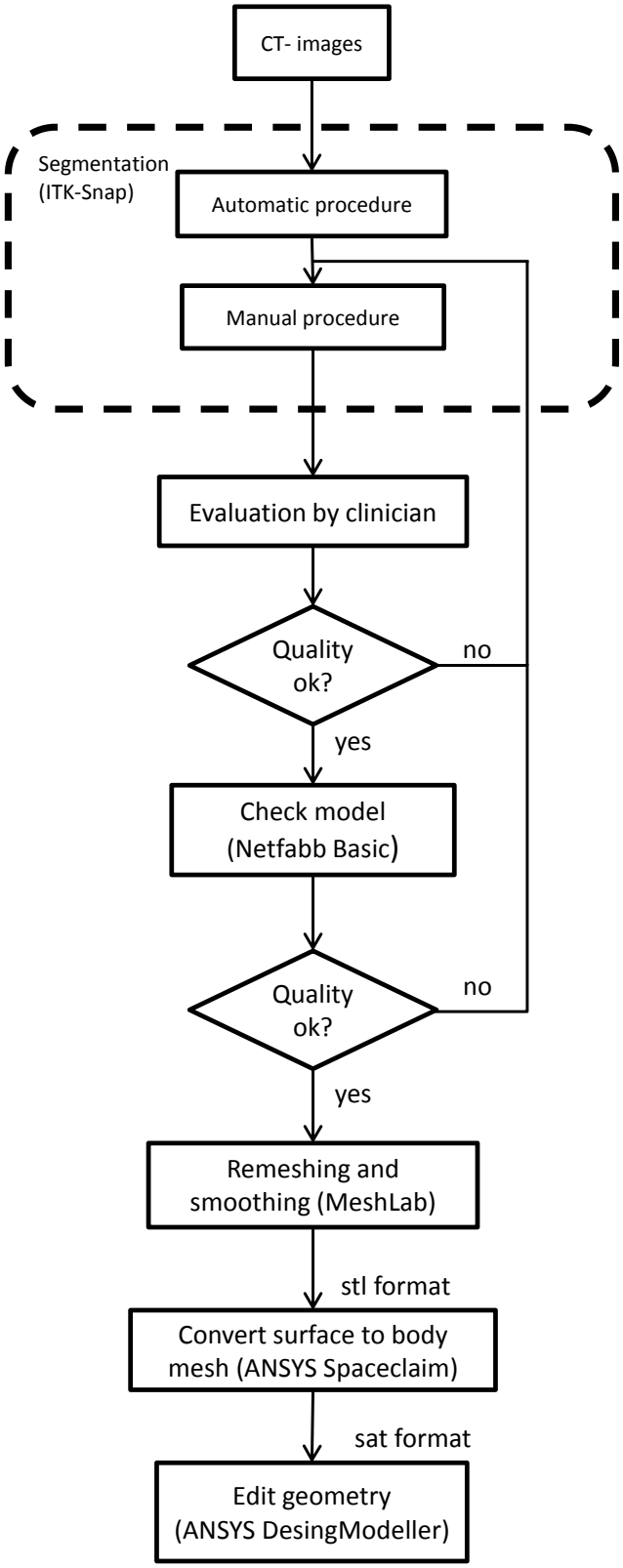

Figure 6: Flow chart representation of the work flow for geometry retrieval.

3.1.1 Data Acquisition

The CT images were provided by the radiologic department at St. Olav Hospital, Trondheim University Hospital. The CT was done with a Siemens Sensation 64 in the transverse plane. The pre-operative scan provided 342 slices with a slice thickness of 1.0 mm, and the post-operative CT scan provided a total of 423 slices with a slice thickness of 1.5 mm, All of the 2D CT images consisted of 512x512 pixels. The volume of each voxel was 0.167 mm^3 pre-operative, and 0.423 mm^3 post-operative.

3.1.1.1 Patient data

To study the effect of intranasal surgery for alleviation of OSAS, three cases with different surgical outcome will be studied in the research project [4]; a patient who improved in AHI after surgery, a patient who had no change in AHI after surgery, and a patient who got a higher AHI after surgery.

The patient chosen for this particular study is a man born in 1948 with a BMI of 28. He underwent intranasal surgery at St. Olav Hospital in the fall of 2015 for alleviation of OSAS. The patient had a narrow nasal passage on his left side obstructing the airflow, and had surgery to increase the volume of this passage. As a result of intranasal surgery, his AHI was reduced from 23 to 5.7, indicating that his OSAS was reduced from moderate to close to none (section 1.2.1). He has been selected because he had the largest improvement in AHI of all patient that had underwent surgery at the time of selection.

3.1.2 Segmentation

Through the segmentation procedure the bounding geometry is defined. The air filled spaces in the nasal cavity, pharynx and larynx is extracted, but the paranasal sinuses are excluded from the model. Due to the patients mouth being closed, and the tongue filling up most of the oral cavity, the oral cavity is not taking part of the current upper airways geometry.

3.1.2.1 Setup in ITK-SNAP

To perform the segmentation the freeware ITK-SNAP 3.4.0 [1] was used to make a 3D model of the upper airways from both pre- and post-operative CT data. There

exist several softwares, but ITK-SNAP has been chosen for this project work as it is free and has been given good credits [1,43]. ITK-SNAP is user friendly and includes only the main functions needed for segmentation of anatomical structures.

The DICOM (Digital Imaging and Communications in Medicine) files obtained from CT-scans were imported to ITK-SNAP as DICOM image series and appear as in Fig. 7.

Figure 7: The DICOM files as they appear in ITK-SNAP 3.4.0. Active Contour Segmentation is marked with a blue square.

.

In ITK-SNAP, the DICOM files are viewed clockwise as three 2D image series in the transverse, sagittal and coronal plane (Fig. 7). The fourth window shows the segmented volume, but as nothing is segmented in Fig. 7, this window is left empty. The cursor (blue cross) is positioned at the same voxel in all four windows, and the x,y,z coordinates are viewed in the menu on the left. These coordinates correspond to the CT slice that are viewed and the same numbers can also be seen under each of the image sets.

For segmentation of the upper airways, both automatic and manual segmentation are needed. Automatic segmentation uses built in algorithms while manual segmentation is to manually select the voxels that are going to be a part of the segmented volume. Most of the pharynx and larynx can be segmented automatically, but the complex structures of the nasal cavity require manual segmentation.

3.1.2.2 Automatic Segmentation

The automatic segmentation was performed with the Active Contour Segmentation with thresholding as the method. When thresholding, a HU-range is chosen, and all connected voxels within this range become part of the segmented volume. Air defines the lower limit of the HU-scale at -1024, hence only an upper value of HU has to be set. The segmentation of the upper airways from CT is based upon the greyscale value (see section 1.4.1). Air defines the lower limit of the HU-scale, but there are however no set rules as to what the upper limit should be. Upper HU-values such as -300 [44] , -400 [39],-460 to -470 [45] and -587 [43] have been used in previous work. All reporting good results. For this segmentation, -300 as the upper HU-value has been chosen. This upper limit is based upon trial and error [6]. The semi-automatic segmentation procedure with thresholding goes as follows:

1. Choose Active Contour ("snake mode") Segmentation, see Fig. 7 where the Snake Mode button is marked with a blue square in the upper left corner.
2. Select region of interest.

   Once snake mode is activated, a region of interest has to be selected. This can be done by manually adjusting the red boxes that appear in the three main windows (Fig. 8). These boxes can be adjusted in all anatomical planes, and define the region and CT slices that will be affected by the segmentation. The size of the box can also be seen in the toolbar on the left side. The user has to define segmentation label and the label that is to be painted over in the toolbar in the lower left corner. In Fig. 8, the active label is simply named label 1 with the color red. Once the desired region of interest is selected, one can proceed to the next step by clicking the "Segment 3D" button.

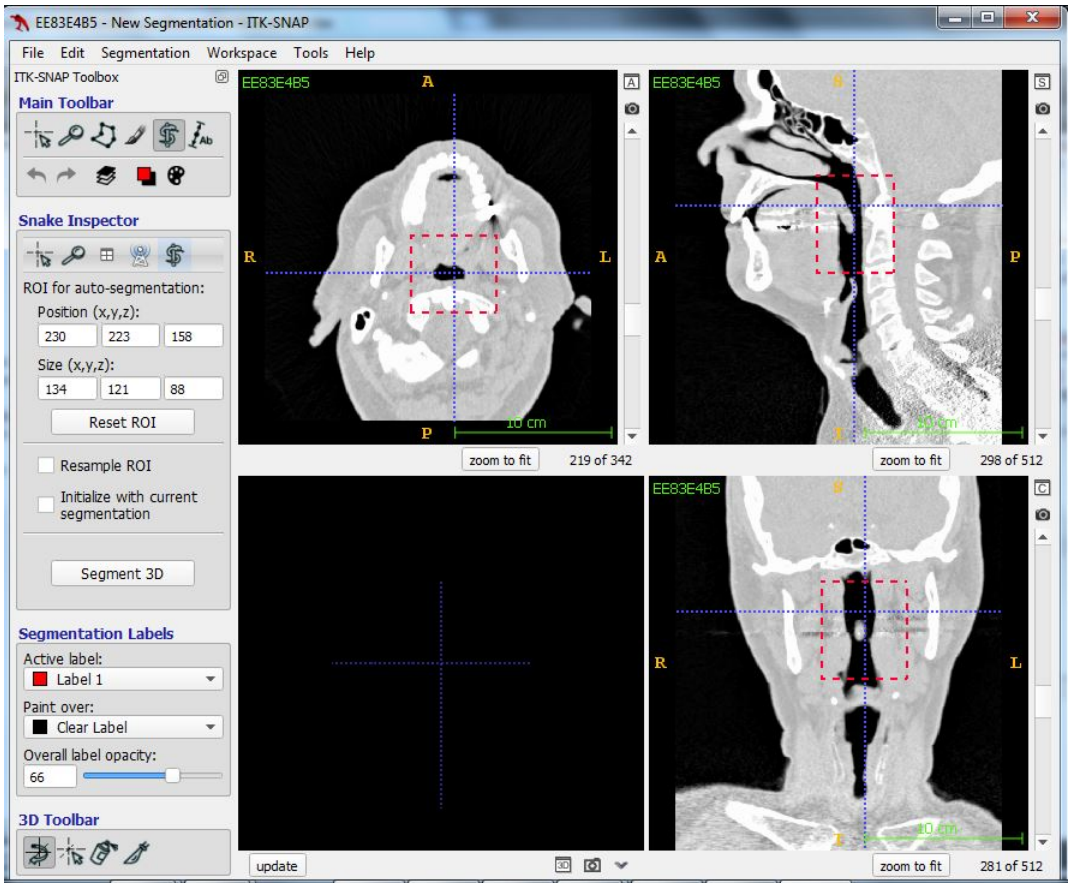

Figure 8: ITK-SNAP window with a selected Region of Interested.

3. Choose thresholding value with no lower limit, and an upper limit of -300 HU.

   The first step of the segmentation is presegmentation. The window is similar to the main window (Fig. 7), but only the slices that makes up the region of interest are visible here (Fig. 9). In this step, one of the following segmentation modes must be selected; thresholding, edge attraction, clustering or classification. In Fig. 9, thresholding is chosen with no lower limit and, an upper limit of -300 HU . The settings apply to the speed function and the result can be seen in the speed images, where all voxels above -300 HU are blue.

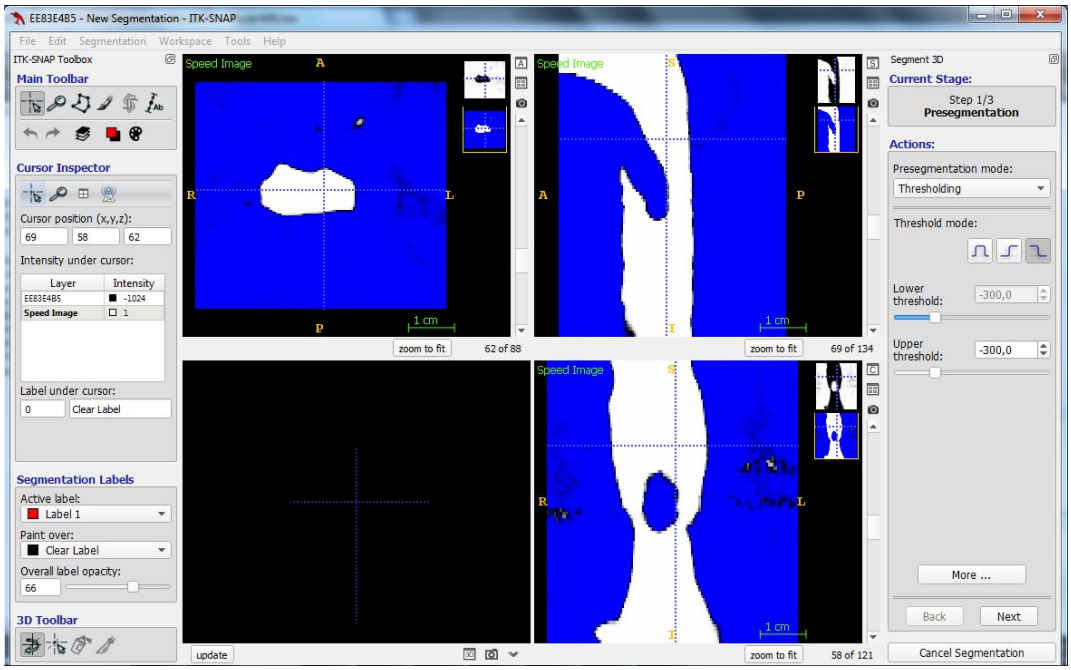

Figure 9: ITK-SNAP window at step number one of segmentation; Presegmentation.

4. Place one or more seeds.

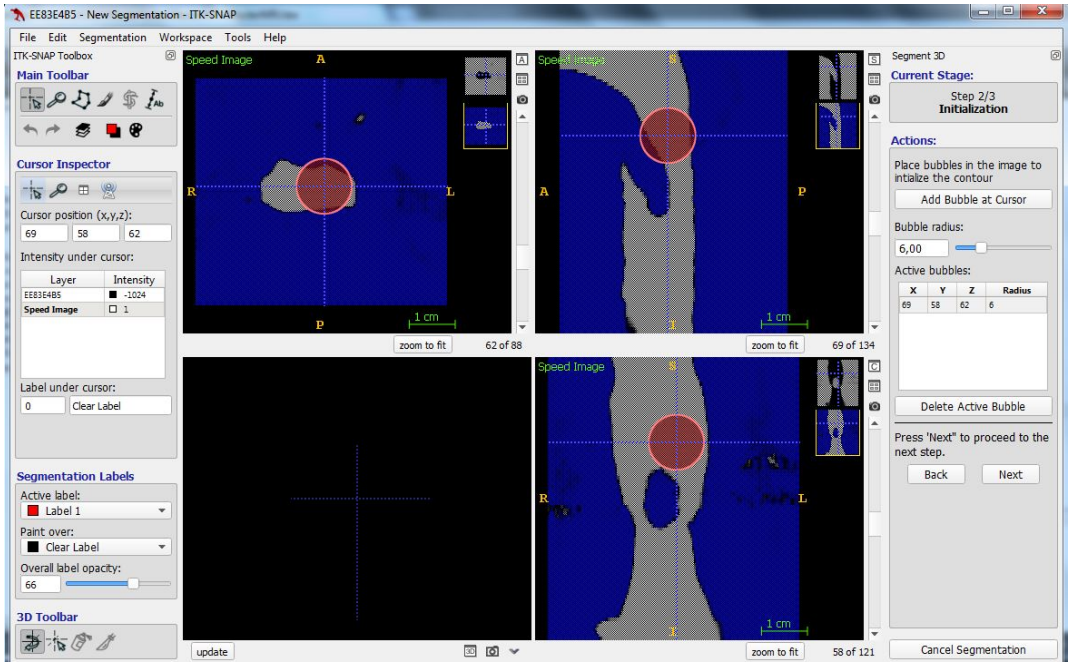

Figure 10: ITK-SNAP window at step number two of segmentation; Initialization.

The second step is initialization where one or more seeds must be placed at the geometry for them to grow into the parts that are going to be

segmented. The seed is shown as a red circle in Fig. 10. The seed must be placed at least partly on the white area, but grows both inward and outward and will adjust if it is partly placed outside the part of interest. Placing several seeds will make the segmentation go faster.

5. Choose timestep and stop the procedure after as many iterations as needed.

   The next step of the segmentation is evolution where the seed grows into all the voxels within the selected thresholding range as a snake, see Fig. 11. This will go on for as many timesteps and iterations as chosen by the user. In this project, about 800 iterations were used with a timestep of 5. This was based on how long it took for the seed to grow into the geometry.

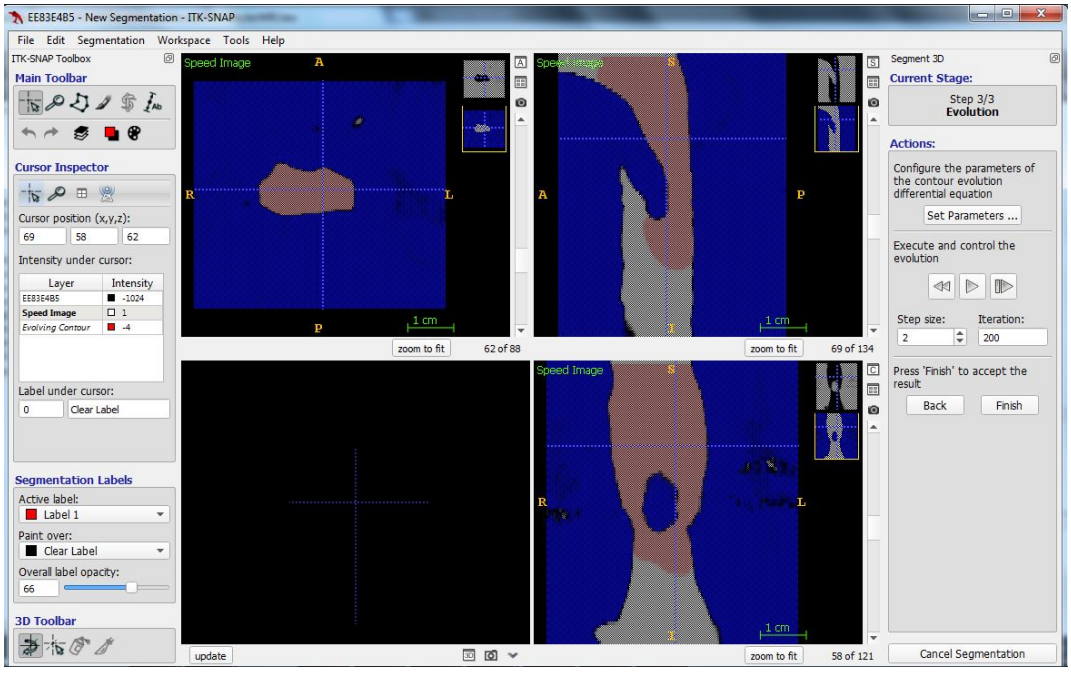

Figure 11: ITK-SNAP window at step number three of segmentation; Evolution.

6. View result

   The result of the segmentation can be seen in Fig. 12, marked as red (label 1). In the lower left corner, a 3D representation of the segmented volume is shown. Note that only the slices that were in the region of interested have been segmented.

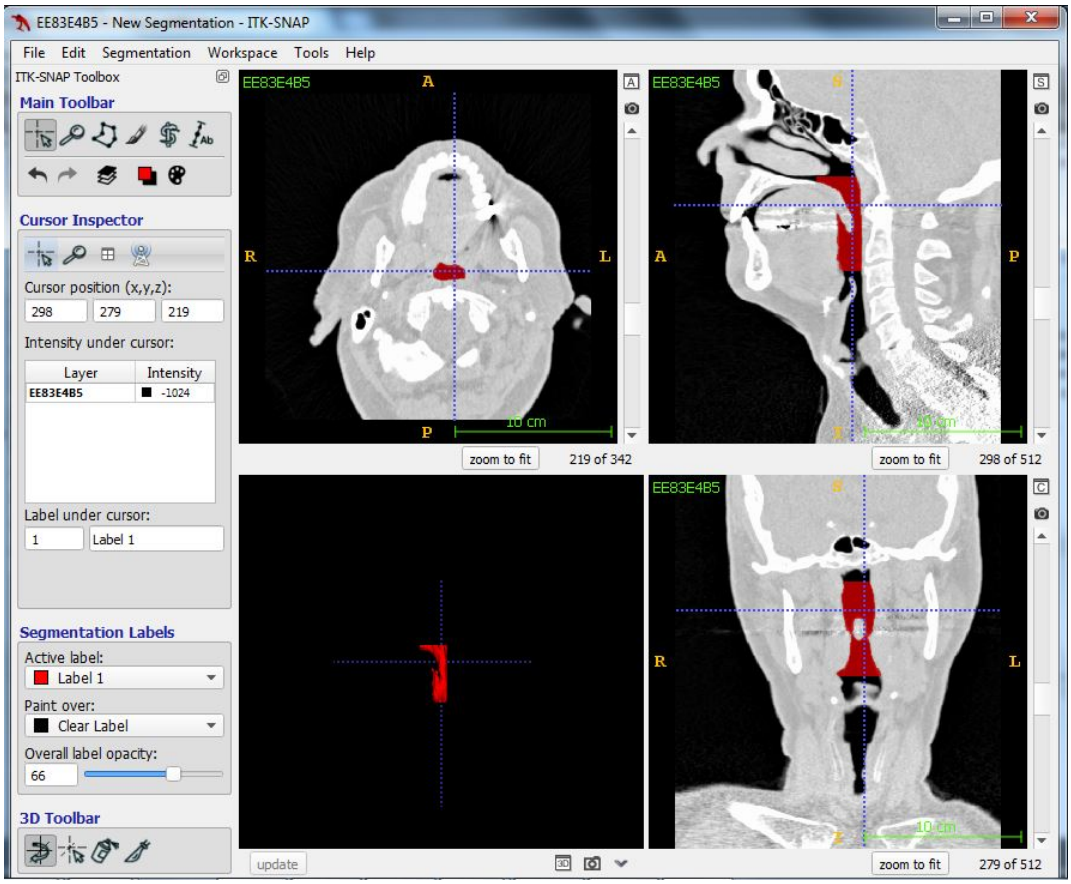

Figure 12: ITK-SNAP window showing the result of the automatic segmentation.

The automatic segmentation procedure was repeated with different regions of interest to segment out the upper airway. This procedure is applicable to most of the pharynx and larynx, with manually segmentation only needed to overlook and fill in missing spots. For the nasal cavity however, most of the segmentation must be done manually.

3.1.2.3 Manual Segmentation

Manual segmentation is more time consuming, but necessary in order to capture the complex geometry of the nasal cavity. The automatic segmentation tends to either include too much or too little of the volume in the nasal cavity, depending on the chosen HU-range. The CT datasets only include sliced images, and the grayscale values of the volume in between the slices are approximated. As there are small volumes, and small differences in the cartilage and mucosa in the nasal cavities, some geometrical features may not show up on the CT. This makes segmentation more challenging, and requires manual work. In addition - leaving out the paranasal

sinuses must be done manually as there are no anatomical boundaries there.

The procedure for manual segmentation was to go through the slices in all planes (coronoal, axial and sagittal) and manually select the voxels that were to be included in the segmented volume. In general, this included most of the volume in the middle of the nasal cavity. This is done by selecting the paint brush mode in the main toolbar. There are three different brush styles; Round brush, square brush or adaptive brush. The square and round brush simply adds a circle or square to the segmented volume, while the adaptive brush does not have any given geometry, and adapts to the geometry based on the settings applied. The adaptive brush was chosen and three different brush options were available; 3D, isotropic and cursor chases brush. For the segmentation, adaptive brush with 3D isotropic segmentation was chosen. These settings provides a semi-automatic segmentation where the voxels that have similar HU-value are segmented. With a very small brush sizem all voxels within in the brush gets segmented.

The choice of excluding all of the paranasal sinuses have been made based on conversation with both an ear-nose-throat surgeon (M. Moxness) and a radiologist (Dr. Kvistad). The paranasal sinuses are air filled spaces that do not affect the flow pattern in the nasal cavity remarkably, and they are excluded for simplicity of the model. All the paranasal sinuses are connected to the nasal cavity by smaller channels (sinus ostium). After conversation with Dr. Kvistad, the bounding geometry excluded all the sinus ostiums and some smaller air filled gaps. As the geometry is extracted from 2D slices in three planes, it is not always clear to see where these borders should be, and it is therefore important to make this decisions together with clinicians. It is especially important to make the same choices and try to leave out the same channels and air filled gaps on the pre- and post-operative models for them to be comparable.

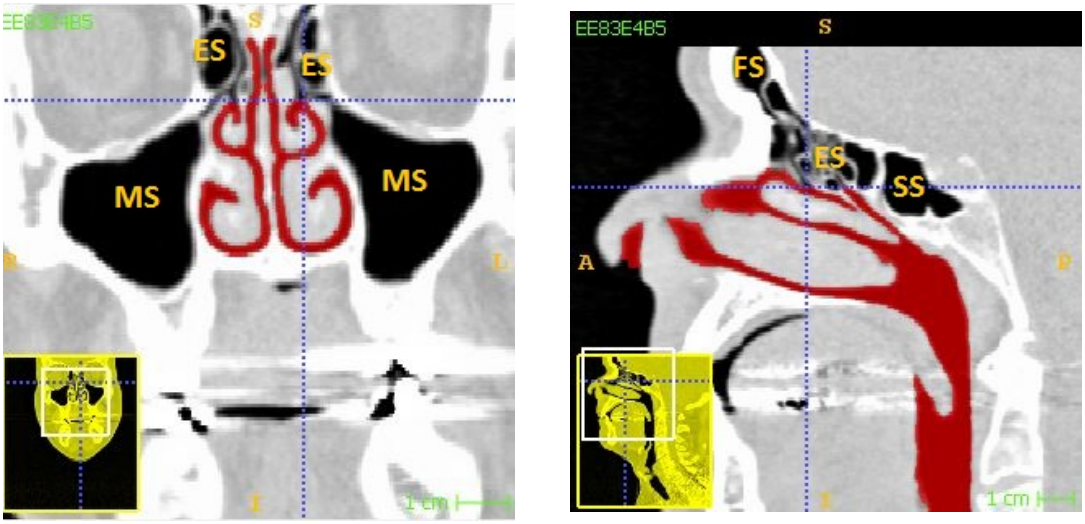

(a) (b)

Figure 13: Pre-operative CT of patient number 12 from the ITK-SNAP window showing coronal (a) and sagittal (b) views of the nasal cavity and paranasal sinuses. The figures illustrate what parts of the air-filled spaces and channels that are included in the segmented volume. The maxillary sinuses(MS), ethmoid sinuses and cells (ES), frontal sinus (FS) and spenoidal sinuses (SS) are all marked on the figure. The sinus ostiums are the thin channels connecting the segmented volume (red) and the paranasal sinuses, and those have been left out of the segmented volume. Note that the marker (blue cross) are placed at the same locations in both (a) and (b).

To ensure well-defined inlets for the flow computations, the nostrils were segmented manually. The nostrils enters the open air, and automatic segmentation would have selected more air than intended as the air space outside the nose was left out of the segmentation process. The inlets were further adjusted in ANSYS DesignModeler [2] for the surface to become even.

3.1.3 Post-processing of the Surface Mesh

The stereolithography (.stl) file extracted from ITK-SNAP is a surface mesh made up of surface triangles. Some post-processing of the model is needed to ensure a good quality geometry.

3.1.3.1 Checking the geometry

The surface mesh generated in ITK-Snap was imported to netfabb basic [46] for a quality check. Netfabb is made especially for 3D-printing, and has several tools for analysing surface meshes and improving them for printing. A check was done to identify possible holes in the geometry. The check was done by importing the .stl file into netfabb and running a "standard analysis". From this analysis, one of

the results was the number of holes in the geometry. If any holes are detected, the repair tool can be used to close those by choosing "Close holes". However, the repair tool may not always be the best solution, and one should go back a step to manual segmentation and close the hole in ITK-SNAP. The main advantage of netfabb is to identify holes that can otherwise be hard to see.

3.1.3.2 Mesh Reduction

From ITK-SNAP a great amount of triangles was generated, and simplifying the mesh through mesh reduction reduces the file size and makes it easier to work with in the following post-processing steps. The mesh reduction was done in MeshLab64bit v1.3.3 [47] with Quadric Edge Collapse Decimation. In addition to the default settings, "Preserve Topology" was checked, and the target number of faces was set to 100 000.

3.1.3.3 Smoothing of the mesh

As a result of the model being generated from a number of slices, the surface mesh is generated with segmentation from each slice, but the gaps from the different slices gives a stairstep-like geometry at the edges. This can be seen in Fig.14a, especially on the lower side and upper side of the nasal cavity. As this is an effect of slice thickness and the digitalization process, and do not mimic the reality, it is necessary to smooth the model. The smoothing of the model was done in MeshLab64bit v1.3.3 by applying the Laplacian Smooth filter with the default settings.

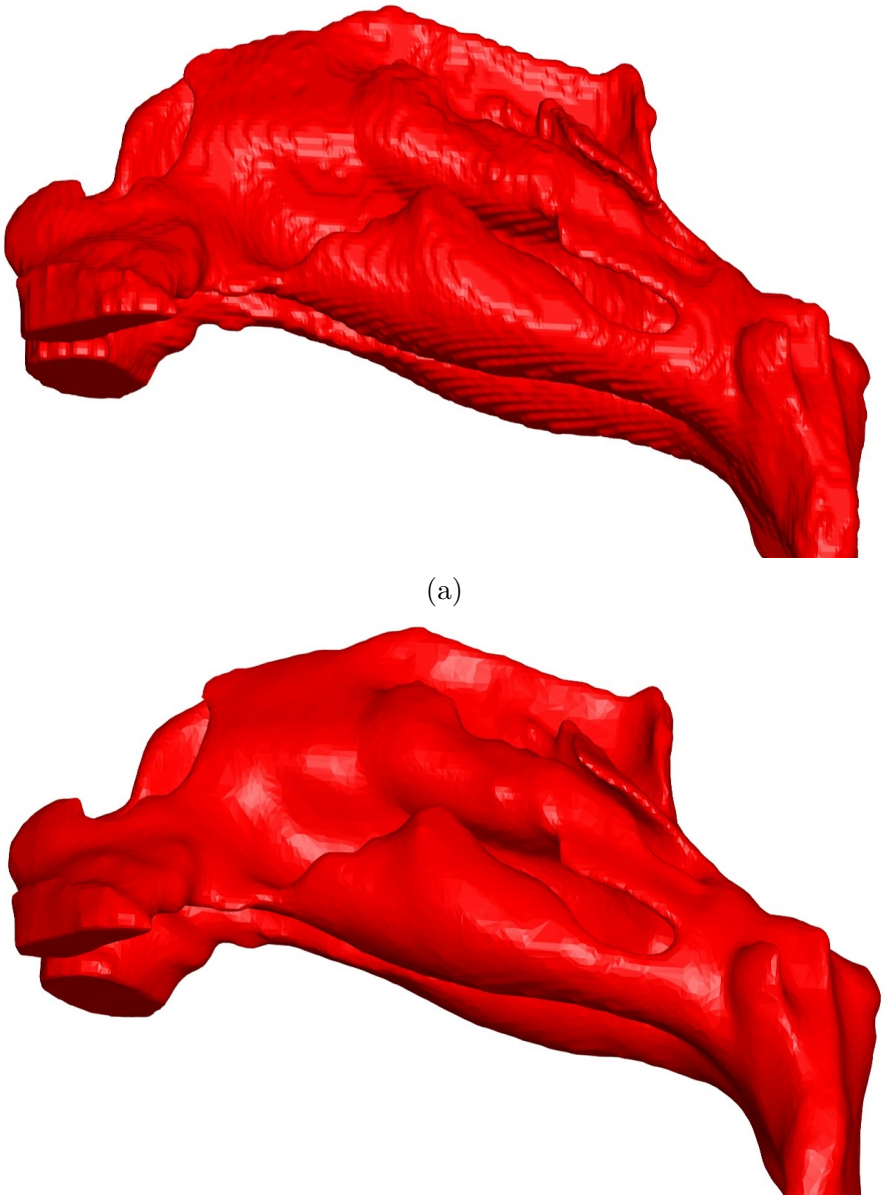

(a)

(b)

Figure 14: The effect of the Laplacian Smoothing filter on the pre-operatively nasal cavity seen from the left. The original geometry extracted from ITK-SNAP is seen in (a), and (b) shows the same geometry after the smoothing process.

3.1.3.4 Conversion from surface mesh to solid body

To be able to generate a grid for flow modelling, the geometry model must be a solid body - not just a surface mesh. To convert the .stl file to a solid body, the .stl files was imported to ANSYS Spaceclaim [2] where they were converted to a solid and exported as a Standard ACIS Text file(.sat) file.

3.1.4 Editing the Geometry

3.1.4.1 Extension of the outlet

From the model generated in ITK-SNAP, the outlet is not normal to the expected flow direction. This is expected to affect the flow, especially by inducing reversed flow (backflow). To avoid this, a new outlet was created. This was done in ANSYS DesignModeler [2] by cutting the geometry at the larynx to create a surface plane normal to the flow direction. The cutplane was made after approximately 2 cm. of the larynx. Further downstream in the larynx is not particularly of interest for the case of OSAS, as this is not an area exposed to collapses. Cutting the outlet here will not leave out information of interest in this case study. After cutting, the surface area of the outlet was extended with the extrude function for the flow to develop.

3.1.4.2 Combining the pre- and post operative model

The head position of the patient was remarkably different in the pre- and post-operative CT recordings as a result of a headrest being used only during the post-operative CT. It can be seen that the angle between the hard palate and the pharynx is greater in the post-operative scan (Fig. 15). There are also differences in the pharynx and larynx as a result of the tilt in the neck.

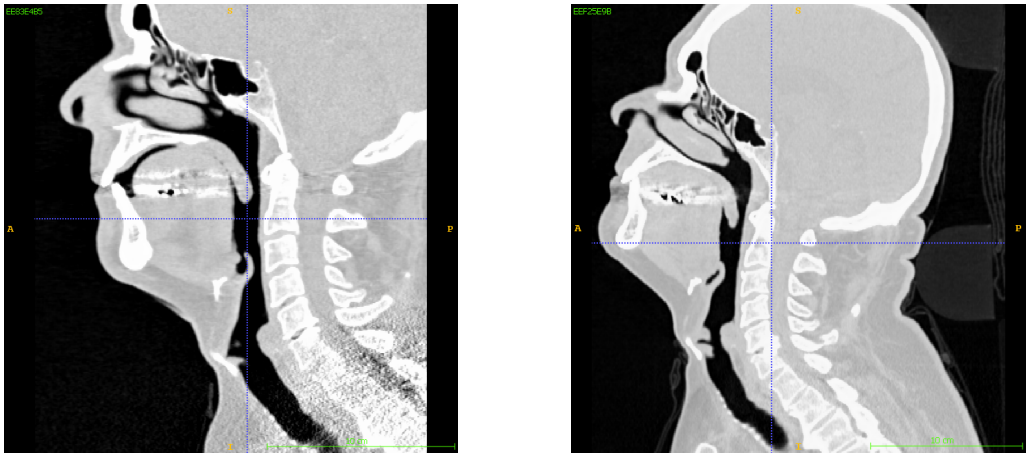

(a) Pre-surgery (b) Post-surgery

Figure 15: (a) and (b) show the different head position of patient number 12 in the pre- and post-surgical CT recordings, respectively.

The head position will cause differences on the pre- and post-operative CFD results which will not be a result of the surgery itself, but the positioning of the patient. As surgery is performed in the anterior of the nasal cavity, it is assumed that this do

not change the geometry of the pharynx and larynx. To avoid any errors from the head-positioning, only the nasal cavity was different on the pre- and post-operative models.

The segmented pre- and post-operative models were combined to make the final post-operative model. The nasal cavity of the post-operative geometry was extracted directly from the post-operative CT, but the pharynx and the larynx of the post-operative model was the exact same as the pre-operative. The final model can be seen in Fig. 16, and the procedure of combining the models was as follows:

1. Both surface meshes were generated in ITK-SNAP through the segmentation procedure described in section 3.1.2. The surfaces meshes were then each reduced and smoothed as described in sections 3.1.3.2 and 3.1.3.3.
2. The two surface meshes from ITK-SNAP were not originally aligned, and had to be aligned in order to combine the models. The alignment was done in Meshlab [47]. Both models were imported into the same project, and aligned by choosing the Align Tool. When using this tool, one of the meshes must be set as basemesh ("Glue Here Mesh"), which the other mesh will be aligned to. The pre-operative mesh was chosen for basemesh. The post-operative mesh was aligned to the pre-operative mesh with "Point Based Glueing", where four identical points was manually selected on the models and the meshes were automatically aligned based on these points. A few more adjustments on the alignment was then done by manually adjusting the post-operative mesh to the pre-operative mesh by the "Manual Rough Glueing" tool.
3. After alignment, both models were imported as .stl files to ANSYS Spaceclaim [2]. From here they were converted to solids (section 3.1.3.4) and exported as .sat files. Both geometries were then imported into ANSYS DesignModeler [2].
4. The post-operative nasal cavity, and the pre-operative pharynx and larynx were combined in ANSYS DesignModeler. This was done by cutting both models at the posterior nasal cavities by creating a plane and slice the models at the plane. The cut had to be made at a point were the geometries were overlapping. The cut was made far back in the nasal cavity were the geometries were expected to be unaffected by surgery. At this location, the shape of the surface area is less complex(compared to the middle region of the nasal cavity), which makes the combination easier. The surface area of the two cut models do not match at the cutting

plane, and a volume was made to combine the two parts without creating a stairstep. This volume was planned to be 3 mm., and the nasal cavity had to be moved 3 mm. forward by the translation tool in order to make space for this. Two surfaces were made - one at each cut section. These two surfaces make up the front and the back of the volume that fills in the gap between the models. The number of edges on the two surfaces do not match as a result of both different CT resolution and different surface area. To make the number of edges equal, all edges was first merged to one by the merge-tool, and then divided into several edges by the split-edge-tool. A total of 128 edges were made on each surface. The two surfaces were then combined with the skin tool, creating a volume of 3 mm.

5. The outlet was modelled as described in section 3.1.4.1. The model is at this step as shown in figure 16.
6. All parts; post-operative nasal cavity, volume to combine the parts, pre-operative pharynx and larynx, and the extended outlet were then combined into one part with the boolean unite feature.

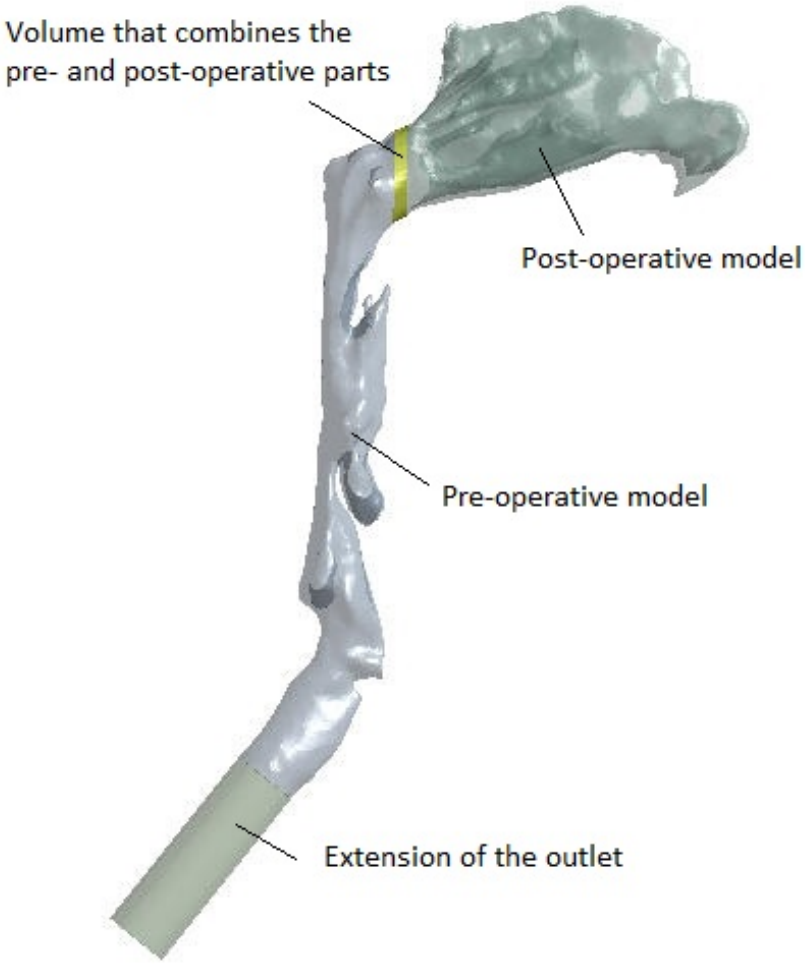

Figure 16: The final post-operative model before the boolean operation were added to combine all four parts to one single geometry.

3.2 Grid Generation

To ensure a good grid quality, and a solution independent of the grid, a refinement study was carried out. Based on these results, a grid could be generated for the final geometry.

3.2.1 Grid Convergence Test

Several grids were generated in ANSYS Meshing 16.2 [2] and went into a grid convergence test to evaluate the grid dependency. The test was carried through for the pre-operative model without the extended outlet. For the pre-operative original geometry three tetrahedral grids were generated; coarse, medium and fine. The size was changed by setting the "Relevance Center" to coarse, medium and fine in AN-

SYS Meshing. Proximity and curvature was chosen for the advanced sizing function. For all other settings, the defaults were used.

Boundary layers were generated on a coarse grid, but no set cell-type for the rest of the grid. The grid generation seems to fail when both inflation layers and tetrahedral as cell type is chosen. Even with no set cell type, the grid is still mostly tetrahedral. The boundary layers were generated by choosing program controlled and the default settings under "inflation" in ANSYS Meshing. This geometry did however have an extended outlet (different than the other grids in the test), but is included in the test to demonstrate the effect of boundary layers. The number of cells are higher, partly due to the extended outlet, but also as a result of the additional boundary layers.

The polyhedral grids were generated by importing the tetrahedral grids made in ANSYS Meshing to ANSYS Fluent, where a built-in-command can change the cell type. This is done by choosing "Convert to poly" with no further options.

The grids were tested by simulation of inspirational flow with 0 Pa at the inlets (nostrils) and -40 Pa at the outlet. Pressure inlets and outlets were chosen as the problem description refers to a "constant pressure drop from inlet to outlet" in both pre- and post-operative models. Simulating with the pressure difference of 40 Pa was chosen as this was a pressure difference approximated to give a mass flow of slow breathing - about 250 ml/s. Calculations of area-average pressure and velocity at different cross sections in ANSYS CFD-Post were used to evaluate the grid.

3.2.2 Final Grid

Based on the results from the grid convergence test, the final grids were made by applying the same settings to the final model. This was first done for the most complex model - the post-operative model - that consisted of the most parts, and was expected to require the most amount of grid cells. The pre-operative grid was then made to approximately match the number of grid cells.

3.3 Numerical Simulation

Simulations were done in ANSYS Fluent 16.2. Because of the large amount of grid cells, the simulations were done on a high performance computer available at NTNU.

With 12 CPUs, this took about 2 days, but the solution was not fully stable. To reach a solution, the flow was solved as transient with a time step of 10e-6 seconds with a maximum of 20 iterations per time step. This went on until the solution was converged with the scaled residuals in the order of e-09 to e-13.

3.3.1 The Commercial Solver ANSYS Fluent

In ANSYS Fluent two solver techniques are available; pressure-based and density-based solver. Even though both solvers can be used for many cases, the pressure-based is the one that has traditionally been used for incompressible flows. The flow simulated is modelled as incompressible, hence the pressure-based solver was chosen. This solver is also default in Fluent. The pressure based solver couples the velocity and pressure and for this SIMPLE (semi-implicit method for pressure-linked equations) was chosen. SIMPLE is default in ANSYS Fluent. For the spatial discretization, the following default settings were used; Gradient: Least square cell based, pressure: second order, momentum: second order upwind. For the transient formulation (when applied), the second order implicit was used to speed up the calculation.

3.3.2 Assumptions

The following assumptions were made when simulating the flow:

- Inspirational flow
- Steady state
- Laminar
- Incompressible
- Air with $\rho = 1.225$ kg/m^3
- Isothermal
- Atmospheric pressure at the inlets (nostrils)
- Velocity outlet (set as velocity inlet with negative velocity) corresponding to a mass flow rate of 250 ml/s
- No-slip at the walls

In the master thesis description, it is said that "the study will be limited to inspirational flow, at constant pressure drop from inlet(nostril) to outlet(larynx)". However, the flow has been simulated with constant flow rate instead. This change is based on the physiology. Humans strives for a given amount of air during sleep that will be sufficient to keep the process of gas exchange in alveoli, and will use as much effort as needed to achieve this. It is therefore more beneficial to study the amount of effort needed to inhale the same amount of air before and after surgery, than to see how much air can be inhaled at a given pressure drop.

The flow is simulated with a laminar model for the entire domain, even though turbulent effects may occur. In the literature, the inspirational flow has been simulated both with laminar and different turbulence models, even for small velocities such as in this case. Most do however agree on the flow being transitional. Swirling and turbulent effects have been observed in the smallest cross-sectional areas in the pharynx. In the majority of the model however, turbulent effects are not dominant with the low air-velocity that is present during sleep.

3.4 Clinical Measurements

3.4.1 Procedure of the Measurements

From St. Olav Hospital, measured data from acoustic rhinometry (AR), rhinomanometry (RMM), rhinorestimetry (RRM) and peak nasal inspiratory flow (PNIF) were available. All tests have been done both pre- and post-operatively, and all includes results before and after decongestion of the nose. The tests were first taken when the nose was at its normal state. After this, the patient were given nasal spray (otrivin), and waited 15 minutes before the tests were taken again. This was to decongest the nose and eliminate the effect of mucosa. The post-operative tests were taken when the patient had a cold (confirmed by Else Bartnes, St.Olavs Hospital), which can have caused some unrealistic results - especially before decongestion of the nose.

3.4.2 Acoustic Rhinometry

Acoustic rhinometry (AR) (RhinoScan, 4.0.5.0, v 3.00.Xj/v 3.0b software) was performed on all patients pre- and post-operatively at St. Olav Hospital to measure the

volume of the nasal cavity. The tests were taken several times, until three measurements were accepted by the software. The three measurements were then averaged. Measurements exists from 1 cm. outside the nose until 12 cm in the nasal cavity. Briefly, AR measures the volume of the nasal cavity by sending in an acoustic pulse and recording the reflection. The cross-sectional areas reported are measured along the path of soundwave. In order to accurately compare the AR with the geometric model, the cross sections should be measured along the path of the sound wave.

3.4.3 Rhinorestometry and Rhinomanometry

Rhinorestometry (RRM) and Rhinomanometry (RMM) measures the resistance in the nose at different flow rates. The resistance, R, is defined as

$$R = \frac{\Delta P}{Q} \tag{7}$$

where Δ P is the pressure difference from the nostrils to the posterior nose/beginning of nasopharynx, and Q is the volumetric flow rate.

The resistances of the left and right nasal cavity are measured individually. This is done by closing one of the nostrils, placing a mask over the nose and mouth, and letting the patient breath in and out at normal pace. This is then registered on the RMM and RRM.

To compare the measured values, the resistance was calculated from the CFD-results. The volumetric flow rate was calculated from the mass flow rates of each of the nostrils, and the pressure drop was defined from the inlets (nostrils) to the posterior nose. The results was compared with the results from RMM and RRM at the same flow rates.

3.4.4 Peak Nasal Inspiratory Flow

The Peak Nasal Inspiratory Flow (PNIF) measures the maximum airflow that the patient is able to breathe. The test is done by the patient closing his mouth, and with a mask covering his nose, breathing in through his nose as much air as quickly as possible. The tests are done until three similar measurements are obtained, and these are then averaged to find the PNIF.

The flow rates from the PNIF measurements were simulated both pre- and post-operatively to examine the pressure difference required to inhale the given flow rates.

4. Results

4.1 Geometry

4.1.1 Geometry Information

The pre-operative geometry retrieved from ITK-SNAP 3.4.0 is a surface mesh consisting of 380 512 surface triangles. The total volume is 66 501.2 mm^3 with a surface area of 32 445 mm^2. After mesh reduction, the surface mesh was reduced to 100 000 surface triangles, with a new volume of 66 494.0 mm^3 and surface area of 32 494 mm^2. The model was then smoothed with the Laplacian smoothing filter. After smoothing, the model consists of 99 996 surface triangles, and the volume and surface area are further reduced to 65 616.1 mm^3 and 30 960.2 mm^2, respectively.

The post-operative surface mesh retrieved from ITK-SNAP 3.4.0 consisted of 260 820 surface triangles. The total volume is 64 725.5 mm^3 with a surface area of 31 457.2 mm^2. The great difference in number of surface triangles between the pre- and post-operative surface mesh (ca. 30%) is a result of the voxel size. The voxel size of the pre-operative model is significantly smaller (half the size) than those in the post-operative model (see section 3.1.1). It is also worth noticing that the post-operative model has a smaller volume and surface area than the pre-operative model. These changes are related to differences in the two models (section 4.1.2). After mesh reduction, the post-operative surface mesh was reduced to 99 999 surface triangles, with a new volume of 64 722.8 mm^3 and surface area of 31 494.3 mm^2. The model was then smoothed with the Laplacian smoothing filter. After smoothing, the model consists of 99 984 surface triangles, and the volume and surface area are further reduced to 63 022.5 mm^3 and 29 369.0 mm^2, respectively.

There are only minor differences between the original geometry and the original with mesh reduction, but the geometry is visibly smoother after the Laplacian smoothing filter has been applied. The results can be seen in Fig. 17 and 14. Both figures are of the pre-operative model, but the result of mesh reduction and smoothing of the

post-operative model is similar to what is shown for the pre-operative model.

Figure 17: The original pre-operative geometry, after mesh reduction and with smoothing, respectively. Viewed from the right side.

4.1.2 Comparison of the Pre- and Post-operative Geometry

4.1.2.1 Nasal Cavity

A distinct difference can be seen between the left- and the right nasal cavity both before and after surgery, in addition to differences between the pre- and post-operative models. The difference between the left side of the nasal cavity before and after surgery can be seen in Fig. 18.

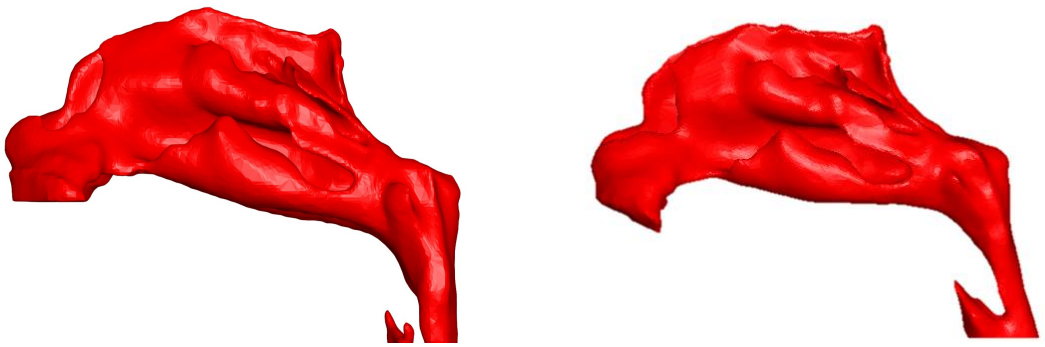

(a) Pre-operative (b) Post-operative

Figure 18: The pre- and post-operative nasal cavity after smoothing seen from the left side.

As seen in Fig. 18, more volume (air) has been added to the post-operative model in the anterior nose as a result of surgery. However, some volume in the same area do also seem to have decreased after surgery - note the sharp bend in the anterior nasal cavity. Differences can also be observed in areas not affected by surgery such as in the posterior and superior nasal cavity. These differences may be a result of differences from CT and/or from the segmentation procedure. A difference in the angle of the inlets are present, and a result of segmentation and the positioning of the patient during CT. A superior view of the nasal cavity (Fig. 19) reveals a difference between the left and right inlet.

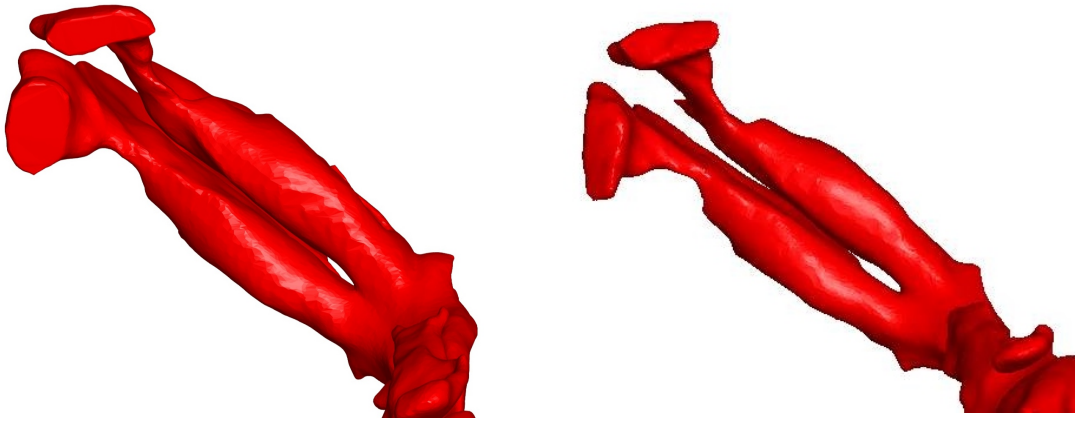

(a) Pre-operative (b) Post-operative

Figure 19: The pre- and post-operative nasal cavity after smoothing seen from below.

The difference between the inlets (nostrils) is present both pre- and post-operatively. The left inlet is remarkably smaller than the right, however more volume is added to the left nasal cavity just right inside the nose were the cross-section was small before surgery.

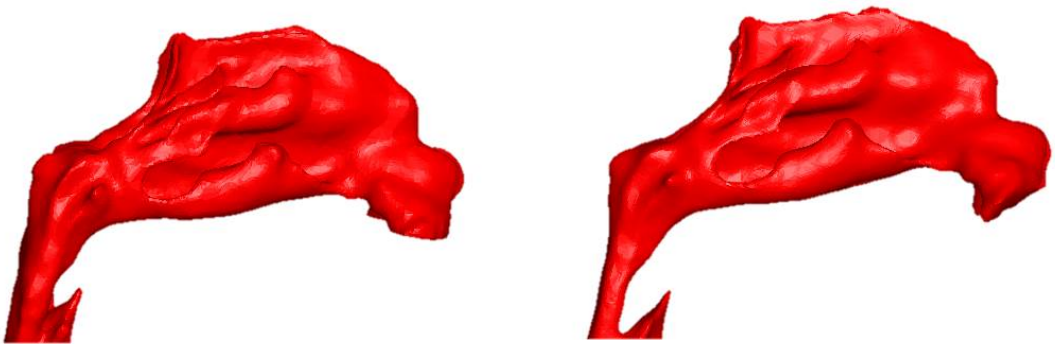

(a) Pre-operative (b) Post-operative

Figure 20: The pre- and post-operative nasal cavity after smoothing seen from the right.

Fig. 20 reveals that changes in the pre- and post-operative models also are present in the right nasal cavity, mostly in the posterior part. These changes are most likely from the segmentation procedure, the positioning of the patient during CT and/or the nasal cycle. This will be discussed further in section 5.

4.1.2.2 Pharynx and larynx

Differences in the pre- and post-operative pharynx and larynx are also present even though these areas are assumed to be unaffected by surgery (Fig. 21).

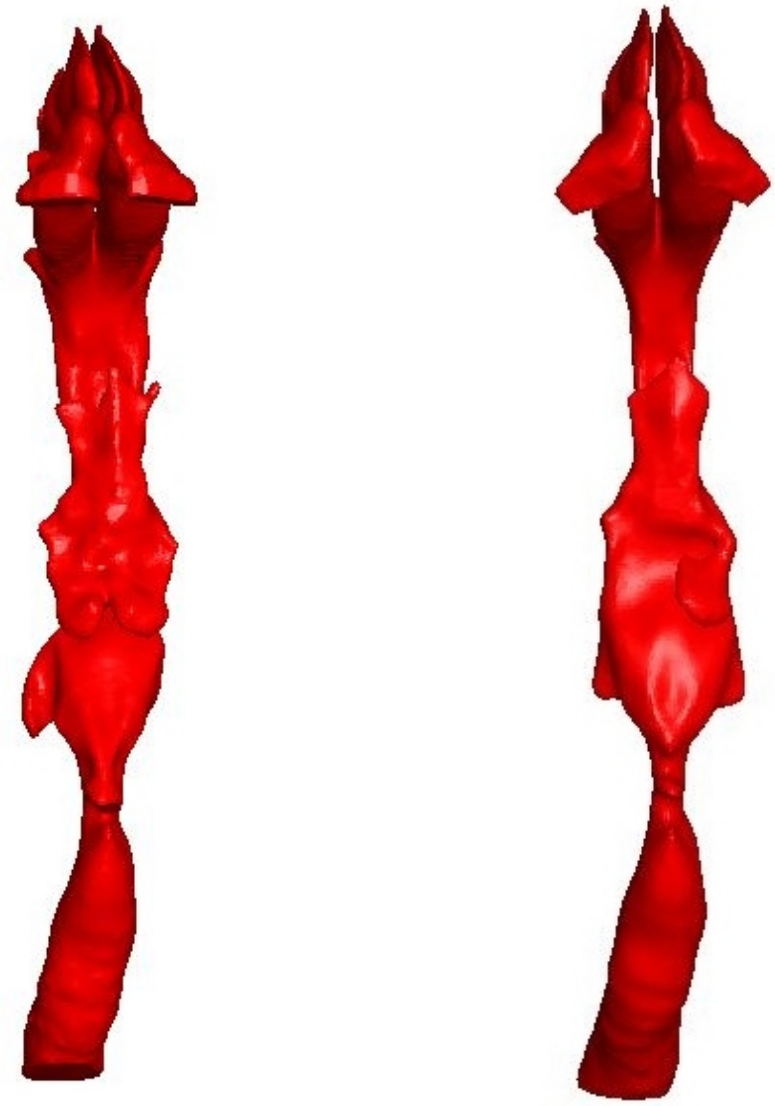

(a) Pre-operative

(b) Post-operative

Figure 21: The pre- and post-operative model seen from the front.

When looking at the models of the pharynx it is important to keep in mind that the walls in the pharynx are not rigid in real life, but quite collapsible. The major part of the differences seen in Fig. 21 are assumed to be a result of the different positioning of the patient during CT as mentioned in section 3.1.4.2. The post-operative (Fig. 21) nasopharynx appear to be smaller, and volume are missing at the epiglottis, causing asymmetry. The volume are also different at the superior larynx where it appear to be asymmetric in the pre-operative model. The shapes are overall different.

4.1.2.3 Final geometry from ANSYS DesignModeler

Both geometries were edited in ANSYS DesignModeler. The outlet of the pre-operative geometry was cut off and extended. The post-operative geometry had great changes. As described in detail in section 3.1.4.2, the pre- and post-operative geometries were combined making a geometry that consisted of the post-operative nasal cavity and the pre-operative pharynx and larynx. This was to eliminate the difference seen in the geometry of the pharynx and larynx in the two models (section 4.1.2.2). The final result can be seen in Fig. 22.

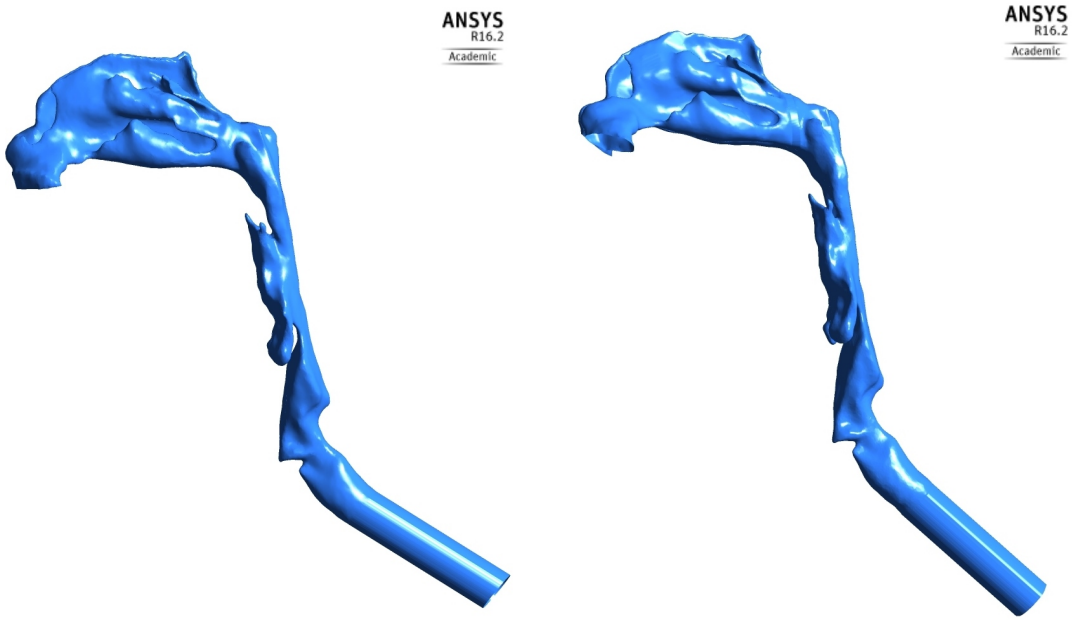

(a) Pre-operative (b) Post-operative

Figure 22: The final pre- and post-operative model seen from the left.

Note that both models now are the same from the nasopharynx and further down. The post-operative nasal cavity is 3 mm. longer than the pre-operative as a volume were added to combine the two parts.

4.2 Grid Generation

4.2.1 Grid Convergence Test

The grid convergence test was carried through for seven different grids as shown in table 1.

Table 1: Grid Convergence

	Type of cells	Number of cells
Fine	Tetrahedral	4 578 136
Fine	Polyhedral	958 613
Medium	Tetrahedral	3 837 189
Medium	Polyhedral	856 460
Coarse	Tetrahedral	2 302 469
Coarse	Polyhedral	545 201
CoarseBL	Polyhedral	2 857 965

Area-averaged pressure and velocity was calculated at the cross-sections marked in Fig. 23 for all grids, and the results can be seen in Fig. 24 to 27.

Figure 23: Location and numbering of cross-sections.

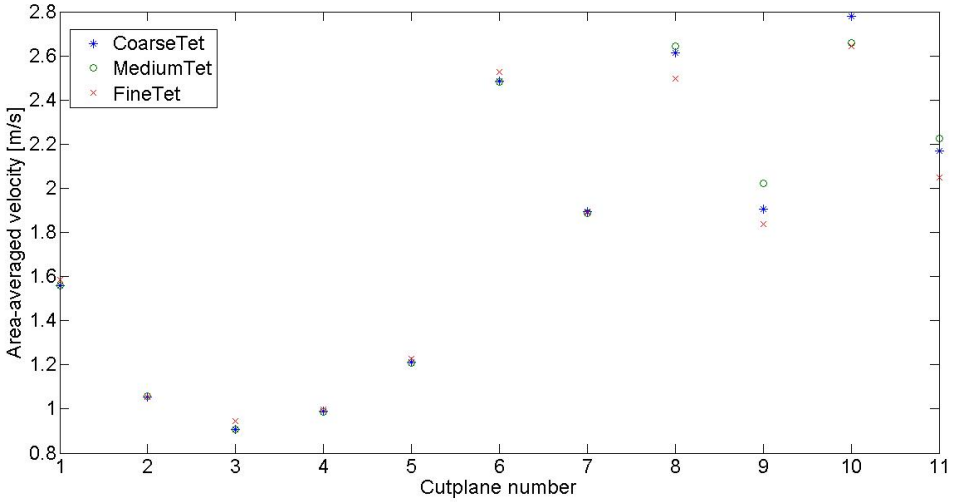

Figure 24: Area-averaged velocity plotted at cross-sections marked in Fig. 23 for three tetrahedra grids.

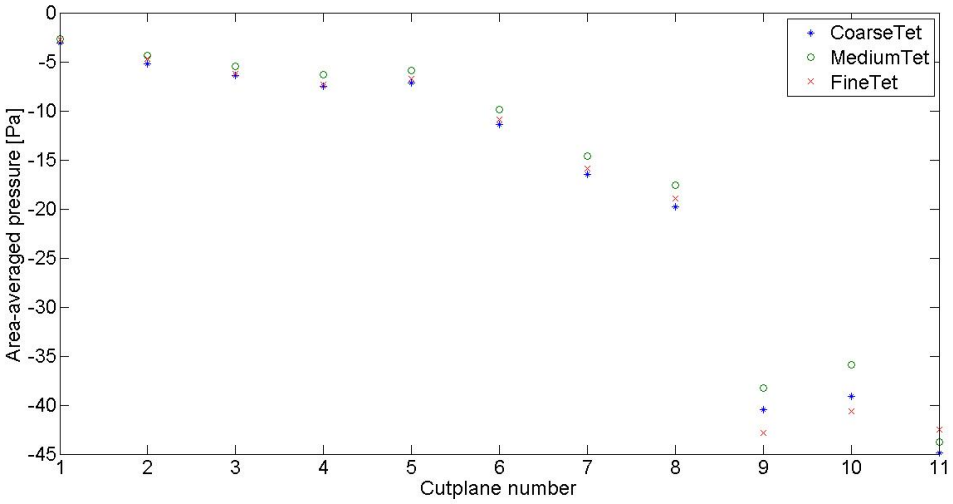

Figure 25: Area-averaged pressure plotted at cross-sections marked in Fig. 23 for three tetrahedra grids.

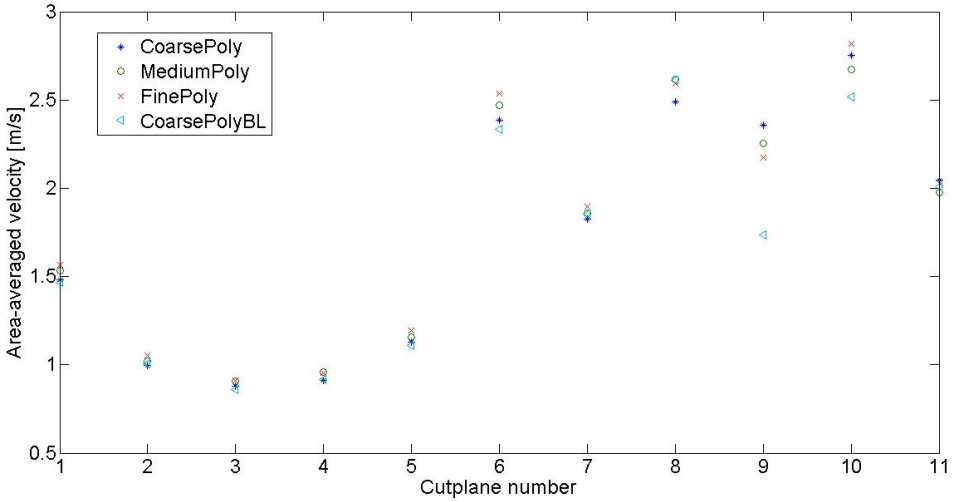

Figure 26: Area-averaged velocity plotted at cross-sections marked in Fig. 23 for four polyhedra grids.

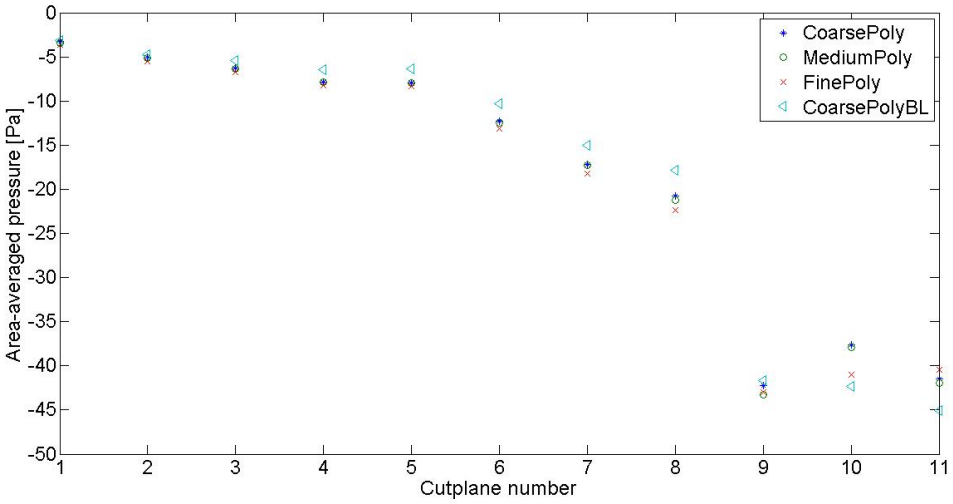

Figure 27: Area-averaged pressure plotted at cross-sections marked in Fig. 23 for four polyhedra grids.

All the grids show the same trend for the pressure- and velocity distribution throughout the geometry, but with slightly different values. The results for the nasal cavity are more or less the same for all grids, but the differences are larger as the flow approaches the larynx. The finest tetrahedra grid has approximately twice as many cells as the finest tetrahedra grid. However, the finest tetrahedra grid has more than eight times as many cells as the coarsest polyhedra grid, and no major changes are seen in the area-averaged pressure and velocity.

The computational time of the tetrahedral grids was significantly longer than for the polyhedra grids, and the tetrahedral grids was therefore discarded. The grid with the boundary layer differ more from the other grids, especially as the larynx is approached, but the outlet of the boundary layer grid is also different. The computational time increased greatly with the boundary layer. The results from coarse, medium and fine polyhedral grid was similar, but the medium size grid was chosen as it is slightly closer to the results from the fine grid. A finer grid was assumed to give a slightly more accurate solution, but with higher computational time.

4.2.2 Final Grid

Based on the grid convergence test, grids were made for both pre- and post-operative models. The time it takes to generate strictly tetrahedral mesh versus the mesh with no set cell type was much higher even though the no set cell type will results in a mesh of almost only tetrahedrals. As the polyhedra mesh was chosen for the simulations, and the fully or mostly tetrahdedra grid would be converted to polyhedra, the grid in ANSYS Meshing was made with no set cell type to save time. The post-operative grid was made with the medium settings which resulted in a grid with 19 783 513 nodes and 3 489 365 polyhedra cells. The pre-operative mesh was then made to approximately match the number of cells, and consists of 17 023 087 nodes and 2 993 762 polyhedra cells. Detail of the grids can be seen in Fig. 28 below.

In Fig.28 it can be seen that the grid in the nasal cavities are similar. At the nasopharynx, the post-operative grid is finer as a result of the additional volume that have been added to get smooth transitions for the different parts. A more detailed view of the transitions can be seen in Fig. 29. A clear difference between the grids on the different parts can be seen, but the transitions are smooth.

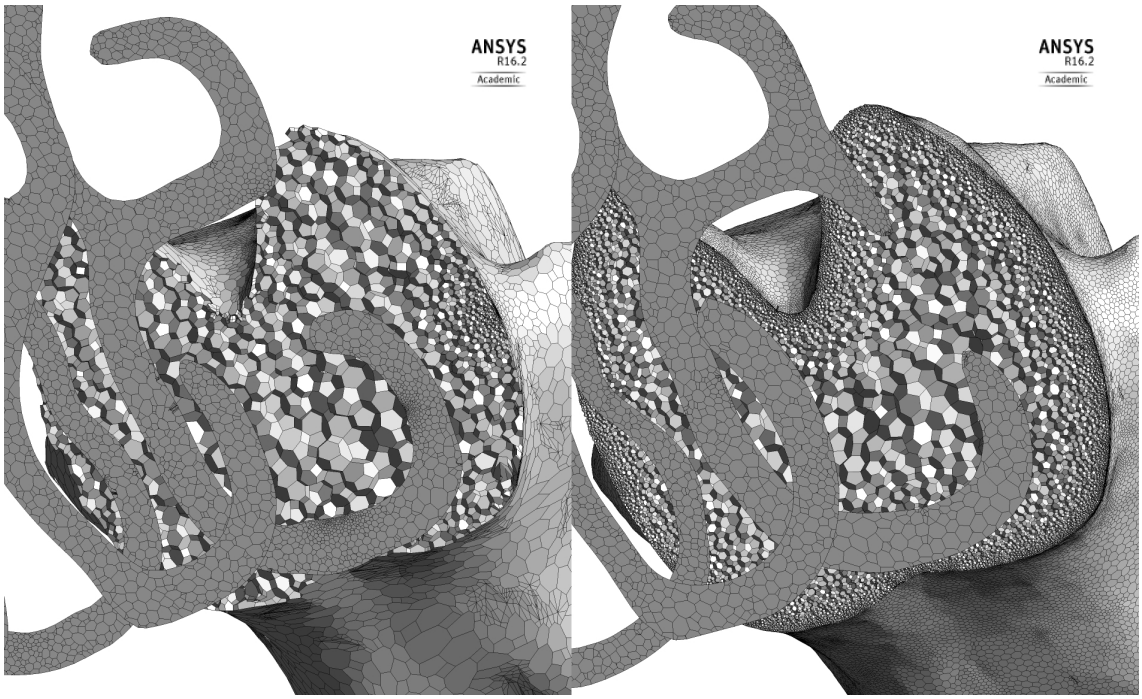

Figure 28: View of the pre(left)- and post(right)-operative grid. Parts of cross-sections from the nasal cavity, and from the nasopharynx and below.

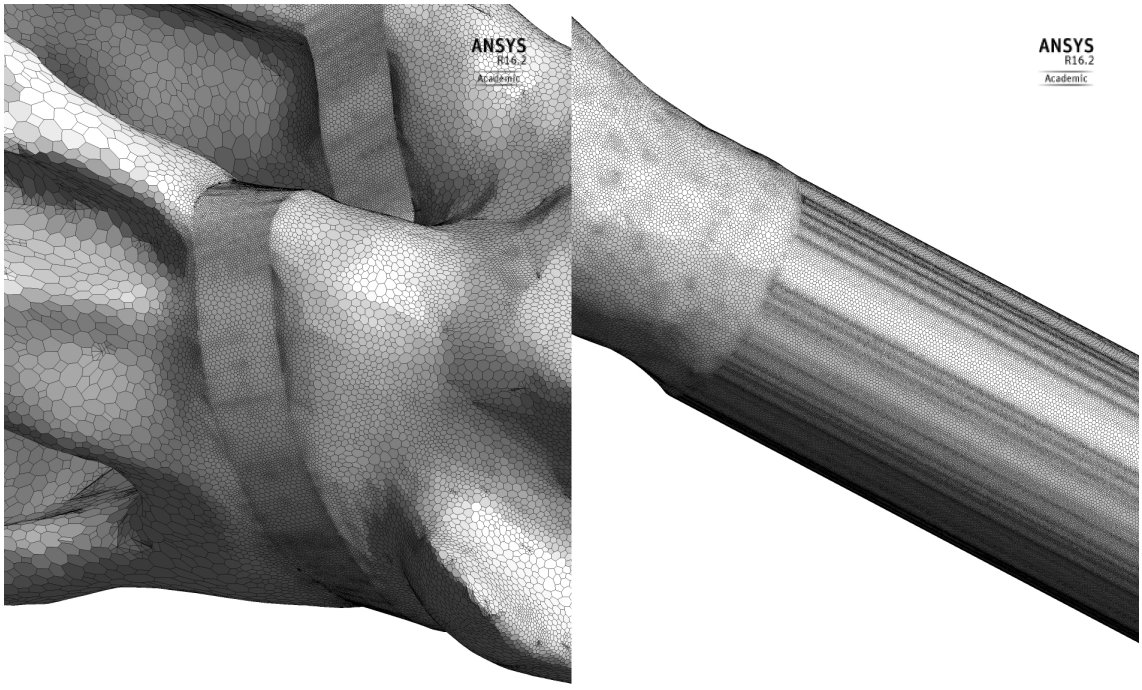

Figure 29: View of the transition zones of the post-operative model. The volume that is combining the pre-and post-operative parts is seen to the left, and the transition to the extended outlet to the right.

4.3 CFD Results

The CFD results have been post-processed in ANSYS CFD-post.

4.3.1 Velocity

The velocity distribution in the upper airways both pre- and post-operatively showed lower velocities in the nasal cavity, and an increase in velocity as the cross sectional area narrows in the pharynx. The velocity magnitudes across a sagittal cut plane can be seen in Fig.30. The plane is positioned in the middle of the pharynx and the larynx, and close to the septum on the left nasal cavity.

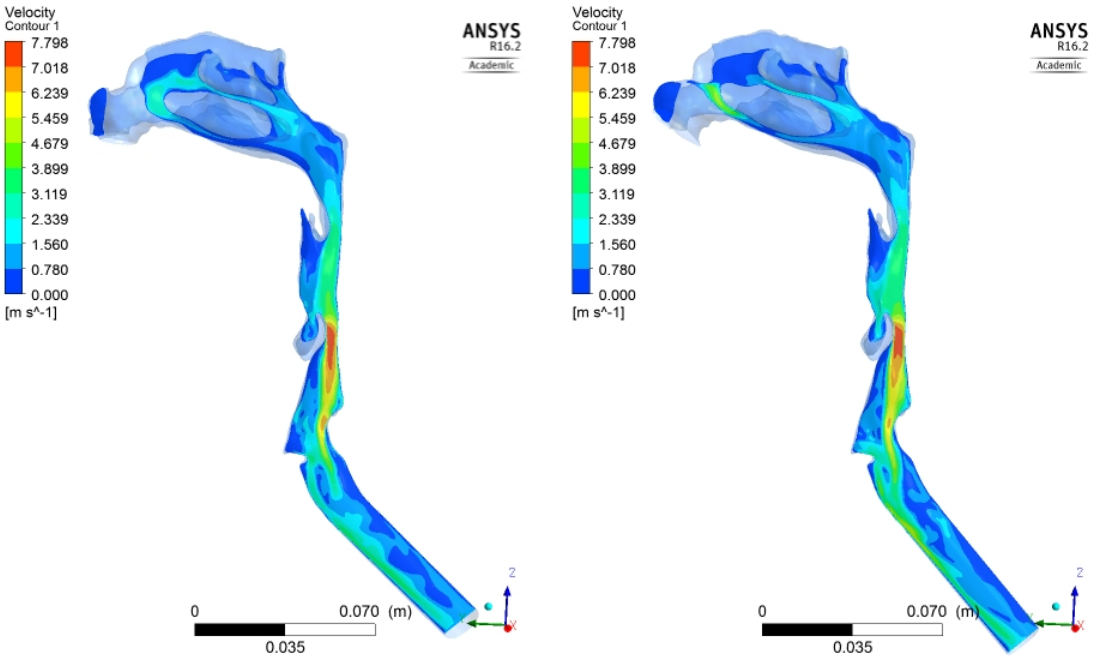

Figure 30: Contour plot of the velocity across a sagittal cut plane at the middle of pharynx and larynx, and the left nasal cavity. The pre-operative results to the left, and the post-operative on the right.

The highest velocities are found in the smallest cross sectional area which is behind the epiglottis. This narrowing creates a pharyngeal jet. A great change in the angle between the pharynx and larynx creates swirling and recirculation in the larynx. The maximum velocities are almost identical pre- and post-operative at 7.783 and 7.827 m/s, respectively. As the mass flow is constant and identical in both cases, and the pre- and post-operative geometry is the same from the nasopharynx and below, the velocity is expected to be similar. Differences in the pre- and post-operative nasal cavities can be observed as the geometry has changed (Fig. 31).

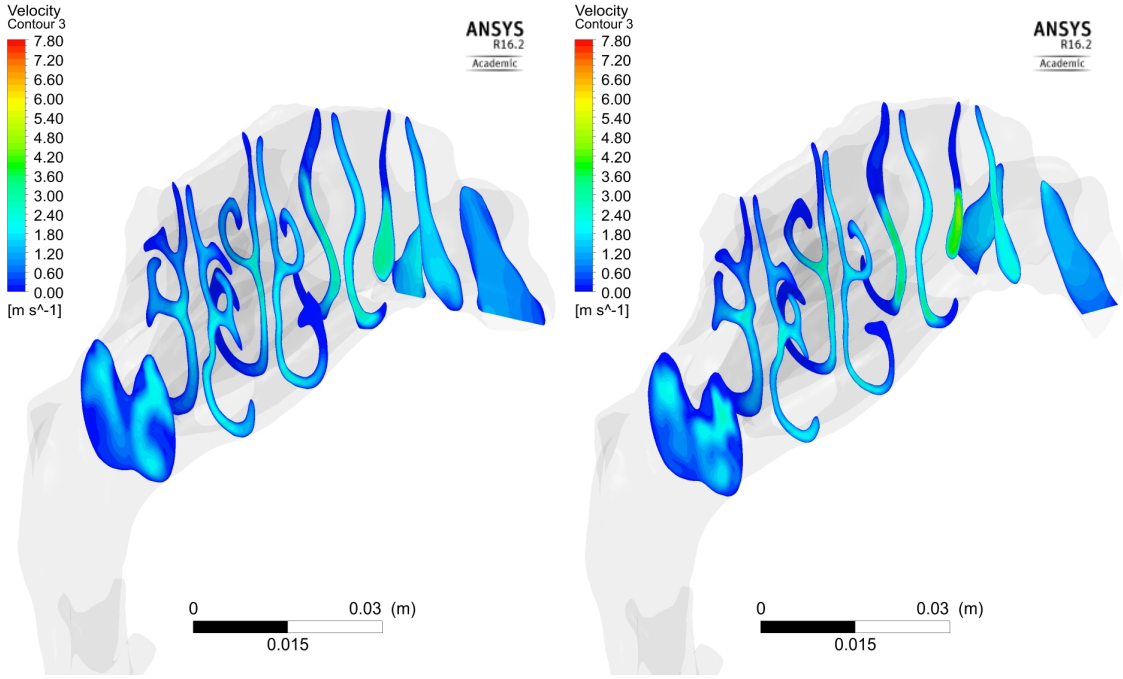

Figure 31: Contour plot of the velocity magnitude across coronal cross sections in the nasal cavity pre-operative (left) and post-operative (right). The models are viewed from the right side.

In Fig. 31 it can be seen that the velocity magnitude has increased on the left side after surgery. The highest velocities are found in the inferior nasal cavity around the inferior turbinate and close to the septum. The lowest velocities are observed in the olfactory zone and at the edges. The findings corresponds with the flow patterns described in the literature (section 2.2.). The flow is more evenly spread out in the right nasal cavity, but the same trends can be observed. The differences between the left and nasal cavity and the pre- and post-operative nasal cavities are well illustrated by the velocity streamlines, Fig. 32 and 33.

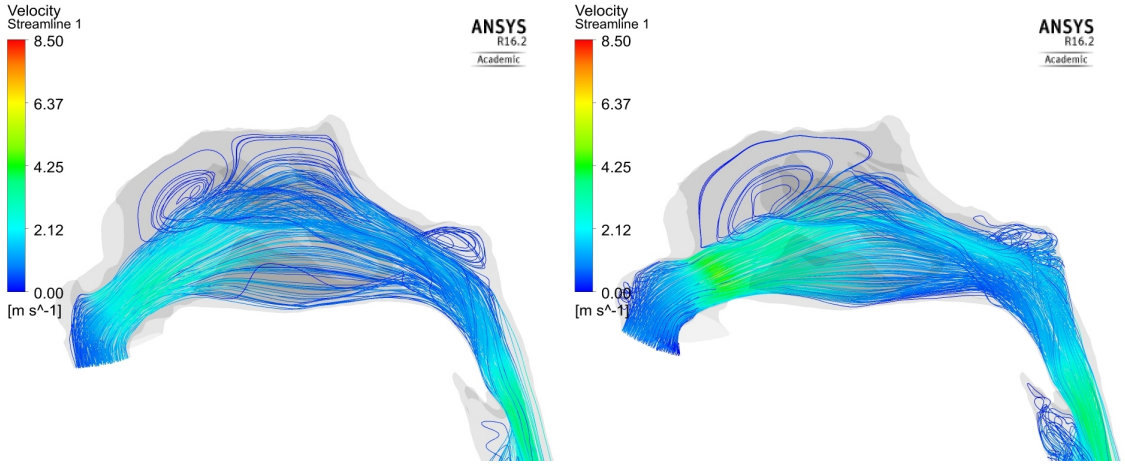

Figure 32: Velocity streamlines in the left nasal cavity pre- and post-operative, respectively.

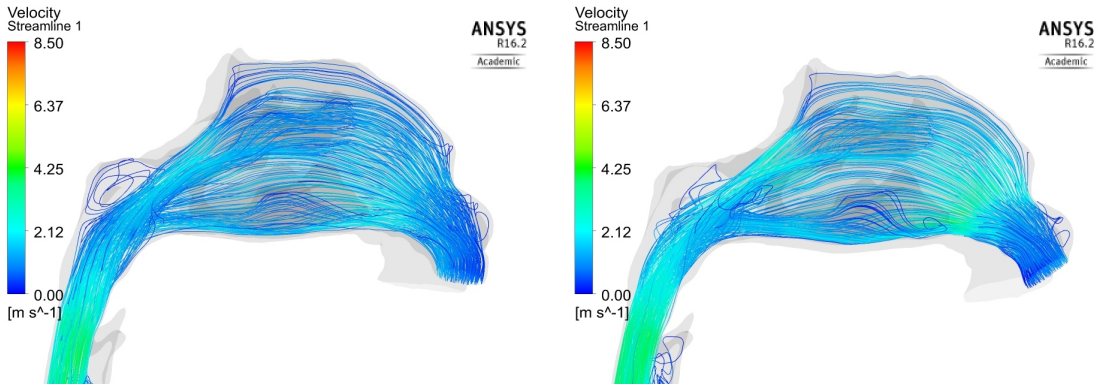

Figure 33: Velocity streamlines in the right nasal cavity pre- and post-operative, respectively.

In Fig. 32 it can be seen that the majority of the flow is in the inferior nasal cavity. After surgery, the velocities are higher in the left nasal cavity. This is a result of an increased volume in the left anterior nasal cavity allowing more air in. Before surgery 15% more of the flow went through the right nasal cavity than the left. After surgery, this difference is reduced to 8%. Even though the mass flow rate in the right nasal cavity is lower after surgery, the velocity has not decreased. However, the cross sectional area appear to have decreased (see Fig. 31). This will be discussed further in section 5.

4.3.2 Vorticity

Fig. 34 shows the vortex core regions in the pre- and post-operative models, respectively. They are identified by the lambda 2 criterion in ANSYS CFD-post.

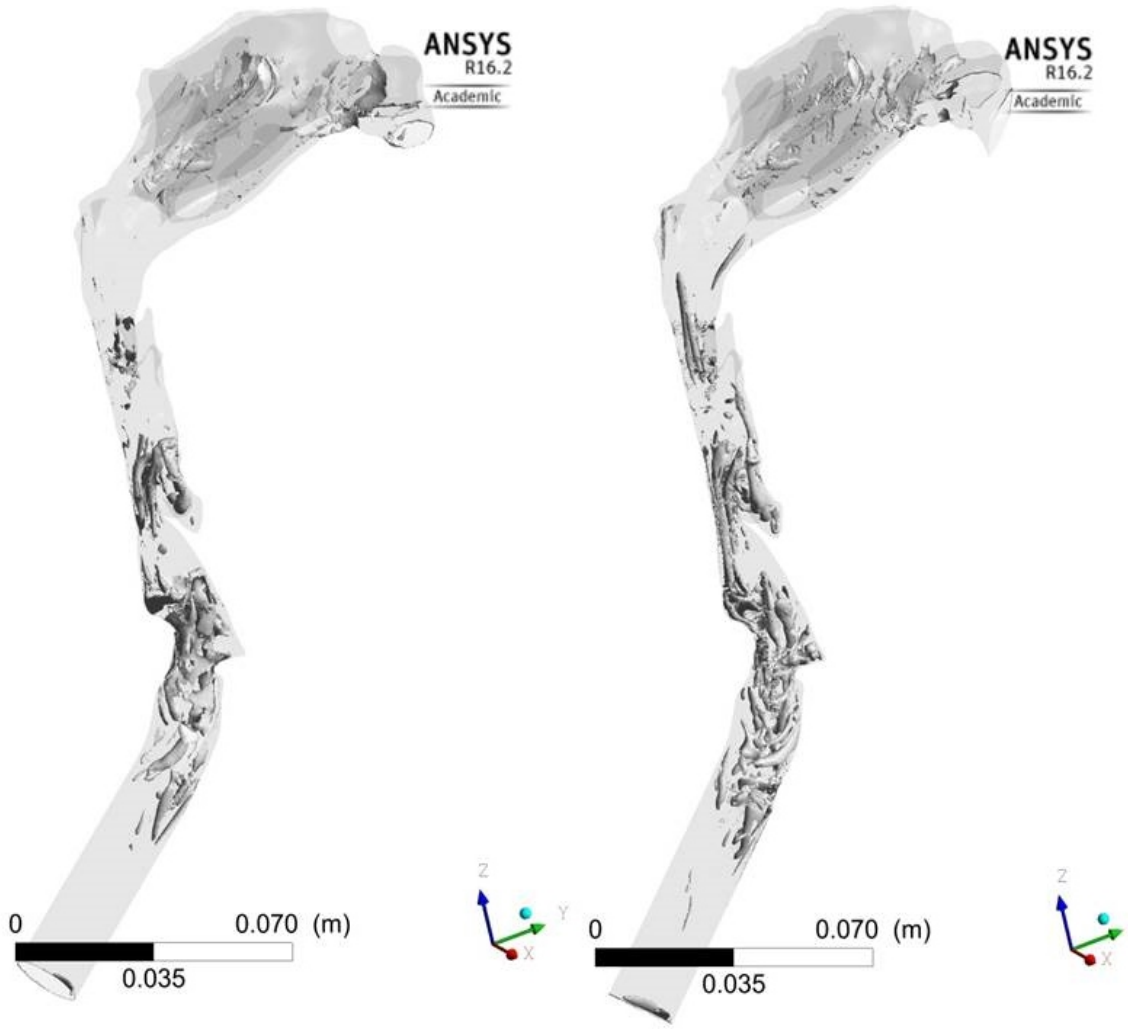

Figure 34: Vorticity regions in the pre(left)- and post-operative(right) models

More vorticity regions are detected in the pharynx of the post-operative model. These are at the regions where the velocity has increased as well, which may cause an increased amount of vorticies.

4.3.3 Pressure

At a flow rate of 250 ml/s, the pressure drop from inlet to the larynx (plane nr.11 23 is 34.46 Pa pre-operatively, and 44.56 Pa post-operatively. This means that a greater pressure difference and more effort is needed too inhale the same amount of air after surgery. The major change in pressure drop is found over the nasal cavity. This has increased with 5.41 Pa after surgery. The pressure on the wall in the nasal cavities can be seen in Fig. 35 and 36.

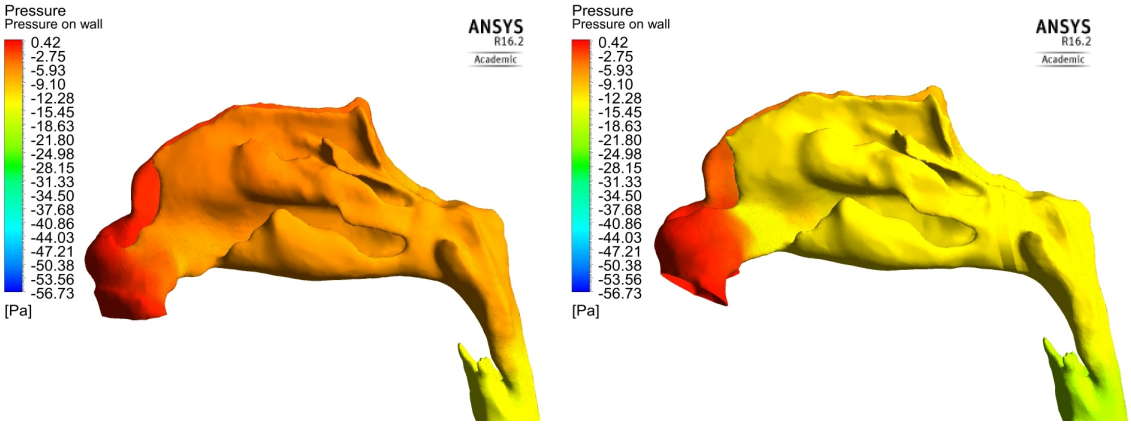

Figure 35: Contour plots of the pressure distribution at the wall in the nasal cavity pre(left)- and post(right)-operative. The nasal cavity is viewed from the left.

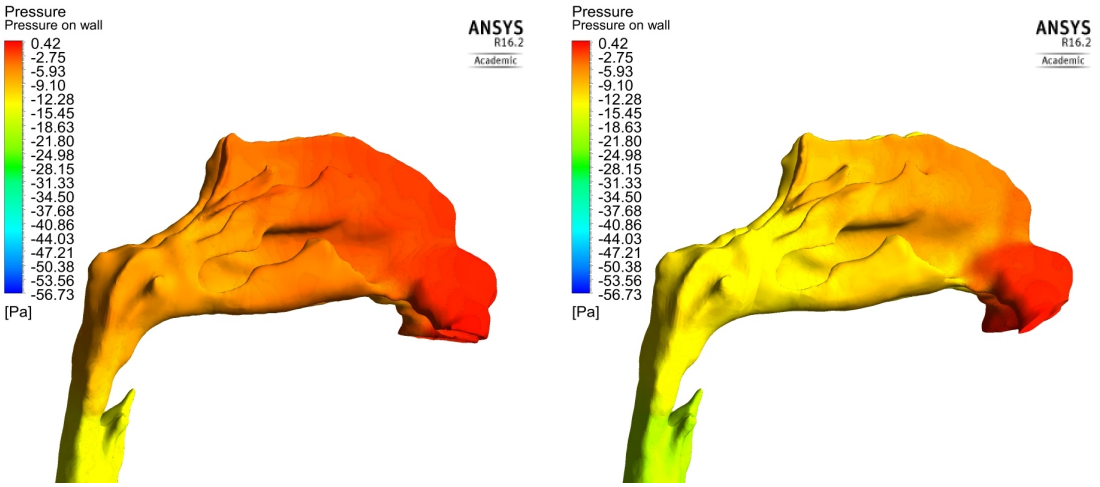

Figure 36: Contour plots of the pressure distribution at the wall in the nasal cavity pre(left)- and post(right)-operative. The nasal cavity is viewed from the right.

The major change in the pressure distribution after surgery is the high pressure gradient at the smallest cross section at the anterior nose. This rapid change can be seen on both sides post-operative, and appear to be the main reason for the total change in pressure drop over the nasal cavities after surgery. Besides this rapid change at the anterior nose, the pressure development follows the same trend pre- and post-operative, but the pressure is overall lower post-operative. Another change between the two models can be observed at the posterior laryngopharynx. The pressure drop at this region was lower before surgery, see Fig. 37 and 38.

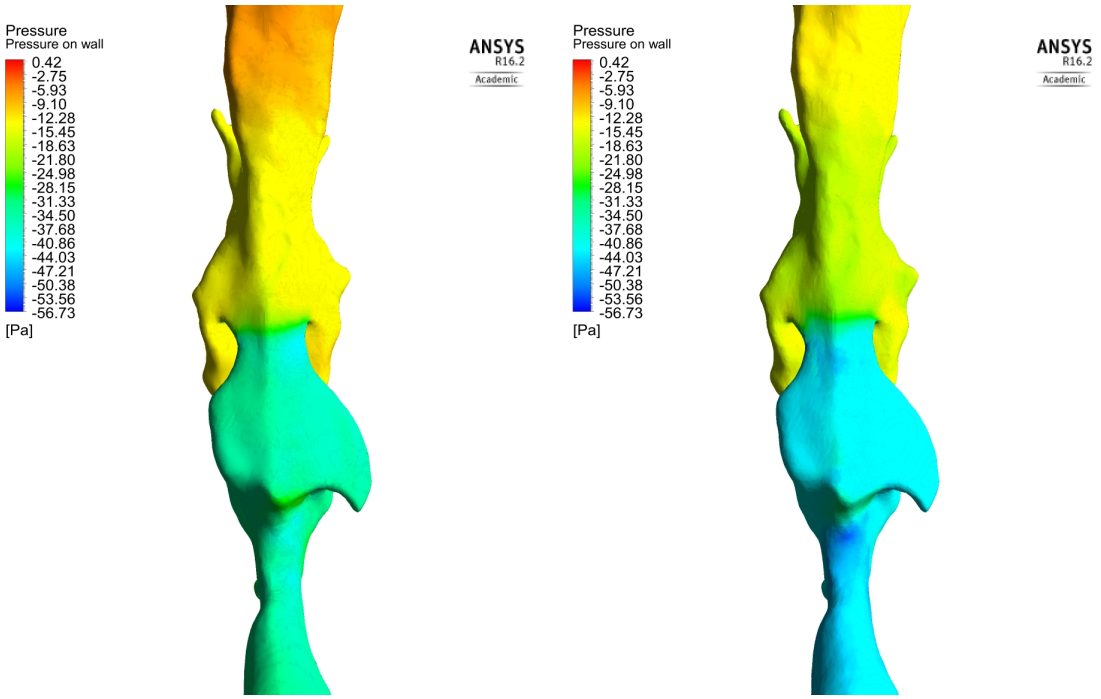

Figure 37: Contour plots of the pressure distribution at the wall in the pharynx pre(left)- and post(right)-operative.

An overview of the pressure distribution can be seen in Fig.38 where the area-averaged pressure is plotted at the sections marked in Fig. 23.

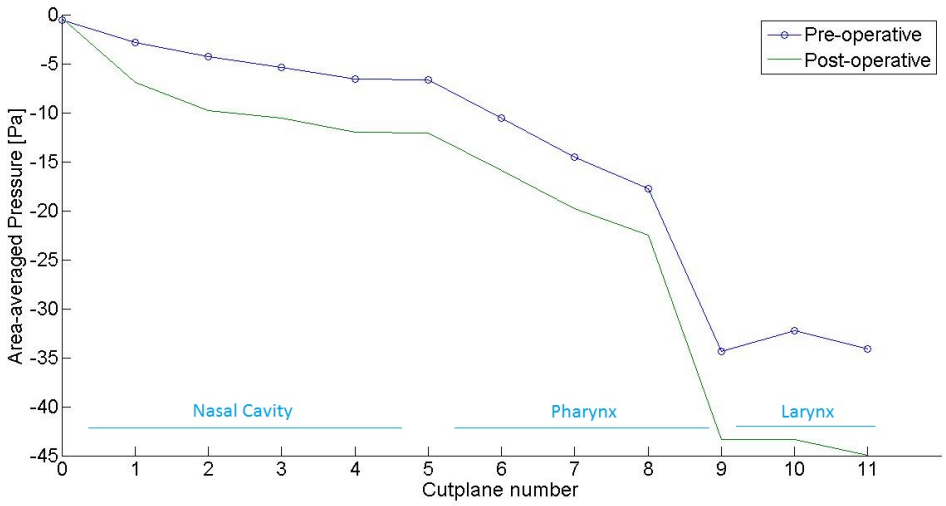

Figure 38: Plot of the area-averaged pressure at the cross-sections in Fig.23 pre- and post-operatively.

4.3.4 Wall Shear Stress

Wall shear stress is the force from the fluid on the wall, and is defined as

$$\tau_w = \mu \left(\frac{\partial u}{\partial y} \right)_{y=0} \tag{8}$$

The highest shear stress can be identified at the areas with the highest velocities - behind the epiglottis and at the laryngopharynx. Some shear stress can also be seen at the anterior left nasal cavity post-operative, see Fig.39.

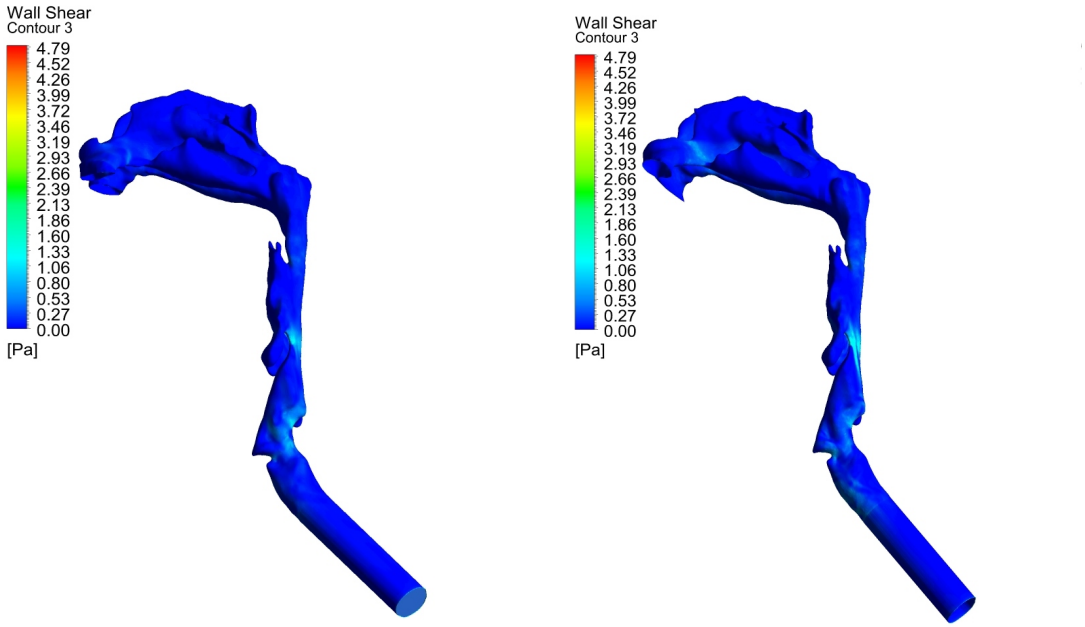

(a) Pre-operative

(b) Post-operative

Figure 39: Wall shear on the pre- and post-operative model seen from the left.

A more detailed view of the pharynx can be seen in Fig.40.

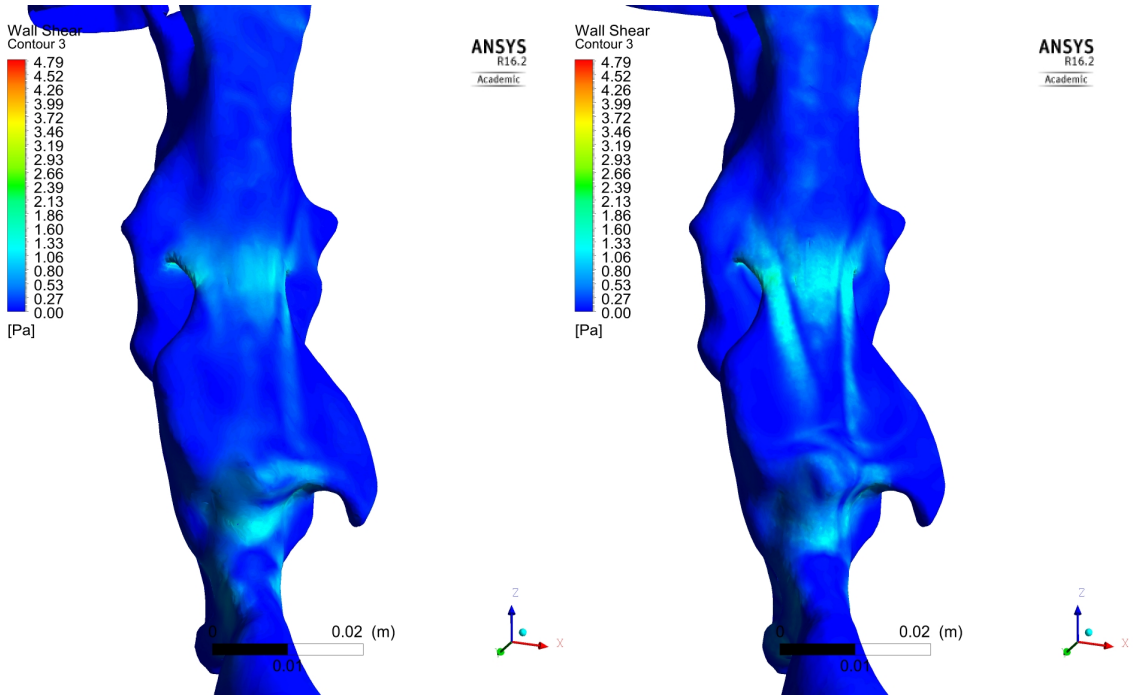

Figure 40: Wall shear at the posterior pharynx, pre-operative(left) and post-operative(right).

The greatest amount of shear stress can be seen behind the epiglottis in both models, and this has increased after surgery. At the laryngopharynx however, the shear stress is slightly reduced. This corresponds with the reduced pressure drop seen in Fig.37.

4.3.5 Comparison of CFD Results and Measured Data

4.3.5.1 Nasal Resistance

The nasal resistance was measured with rhinorestometry and rhinomanometry both pre- and post-operative. Pre-operative, measured results are only available for the right nasal cavity. This is most likely because the nasal passage was too narrow to get valuable results. Post-operative, measurements are available for both sides. However, even post-operative the results are limited and only available for measurements after decongestion. Both measured and CFD results are presented in table 2.

Table 2: Nasal resistance, measured and simulated results.

	Flow rate [ml/s]	R, RRM [Pa s/ml]	R, CFD [Pa s/ml]
Pre, right	143.787	0.1732	0.0429
Pre, left	106.201	Not Measured	0.0581
Post, right	135.127	0.1145	0.0888
Post, left	114.873	0.6167	0.1044

The measured and simulated results do not correspond well, except for the post-operative right nasal cavity. The worst correspondence is seen between the measured and simulated results after surgery on the left side.

4.3.5.2 PNIF

Simulations were done with the measured PNIF values after decongestion both pre- and post-operative. The pre-operative PNIF was 190 l/min, and the post-operative PNIF was 213.3 l/min. The pressure difference needed to produce these flow rates were 4956.98 Pa pre-operative, and 5207.89 Pa post-operative. The increase in mass flow rate and pressure drop after surgery is 12 and 5 % respectively.

5. Discussion

The aim of this master thesis and the research project it is contributing to, is to demonstrate the potential of a new patient-specific clinical tool using CFD to predict the outcome of OSAS treatment. For this to be possible, the procedure must be reproducible and give accurate results. As of now, the procedure is not fully reproducible. Part of this is related to the CT imaging, and part of it to the manual segmentation. This will be discussed in chapter 5.1. How accurate the results are as of now is also questionable, and will be discussed in chapter 5.2. The CFD results have been compared with the improvement in AHI measured in the sleep study, and with selected rhinometric measurements, but not fully validated.

5.1 Is the Procedure Repeatable?

5.1.1 CT and the Effect of the Nasal Cycle

The project work [6] addressed several issues of geometry retrieval from CT. One of the main findings was that a protocol for the image acquisition was needed as the CT datasets varied a lot. Some of the CT images for the patients had been with open mouth and some with a closed mouth. The importance of a set head position was also pointed out. The result of this was that four sets of CT were to be taken - closed and open mouth both before and after surgery - and that a head rest would be used for all four sets. Several of the patients in the study - including the patient studied in this master thesis - underwent CT before this protocol was established. For the patient in this master thesis, the head position differed remarkably as the headrest was used only for the post-operative CT. The assumption that surgery did not affect the pharynx and larynx was made, and only the nasal cavities differed in the pre- and post-operative models. A small volume was also added to the post-operative model to be able to combine the pre- and post-operative parts. This increased the volume of the nasal cavity, but are assumed to be small enough to not affect the flow much. This combination of models isolates the surgical changes in the nasal cavity, but may also exclude other differences that could have been important.

Another remark about CT is related to the nasal cycle. CT gives an instantaneous representation of the upper airway, but the geometry of the upper airway is in fact constantly changing because of the nasal cycle. The cyclic movement works in a way so that the volume of the left and the right side most of the time is asymmetric. This means that CT from the same day can look different. When comparing pre- and post-operative CT data, the differences in the geometry can be greater or smaller depending on which nasal cavity that is dominant at the time. For the patient studied in this report, a difference in the right side can be seen the geometry models. The volume seems to have slightly decreased after surgery. The same difference can be observed in the CT images. There is a more distinct difference in the left and right nasal cavity after surgery than before as seen in Fig 41 and 42. Note that the images are not taken at the same cross sections. This is because the patient was angled differently during the two CT scans.

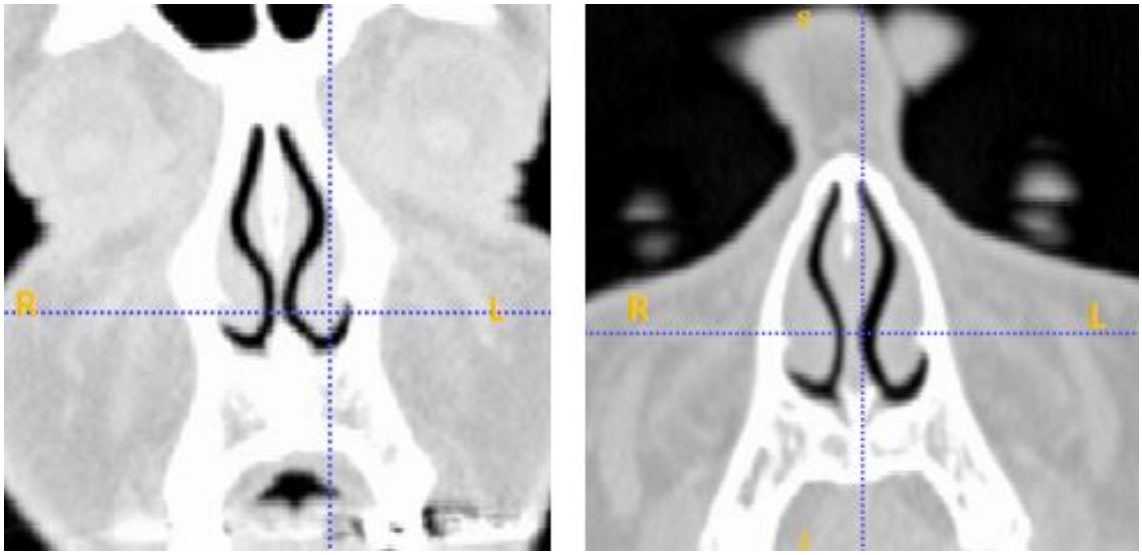

Figure 41: Coronal CT view of the nasal cavity pre(left)- and post(right)-operative

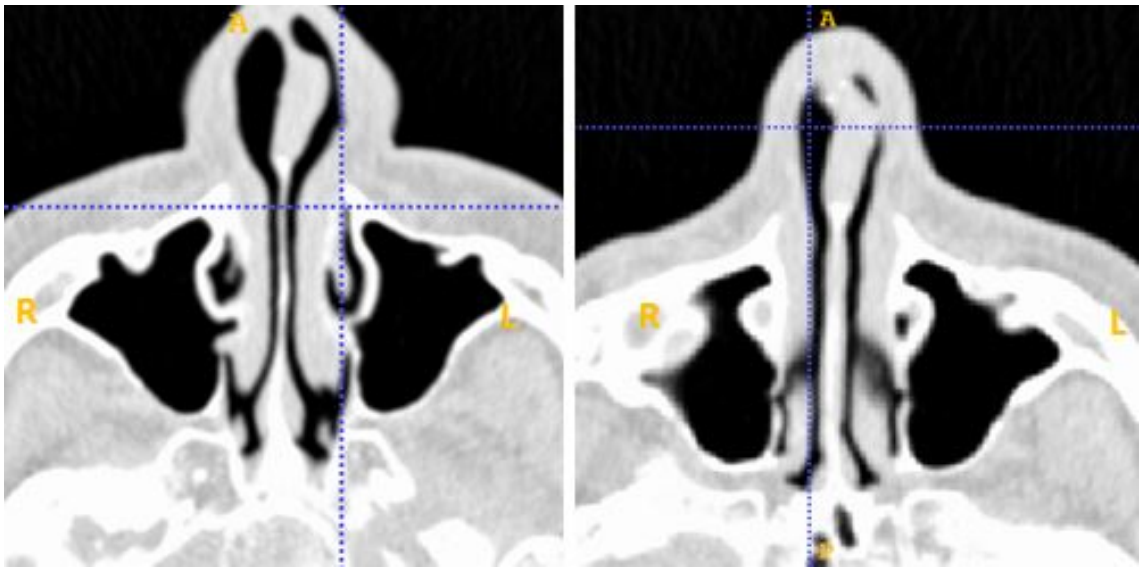

(a)

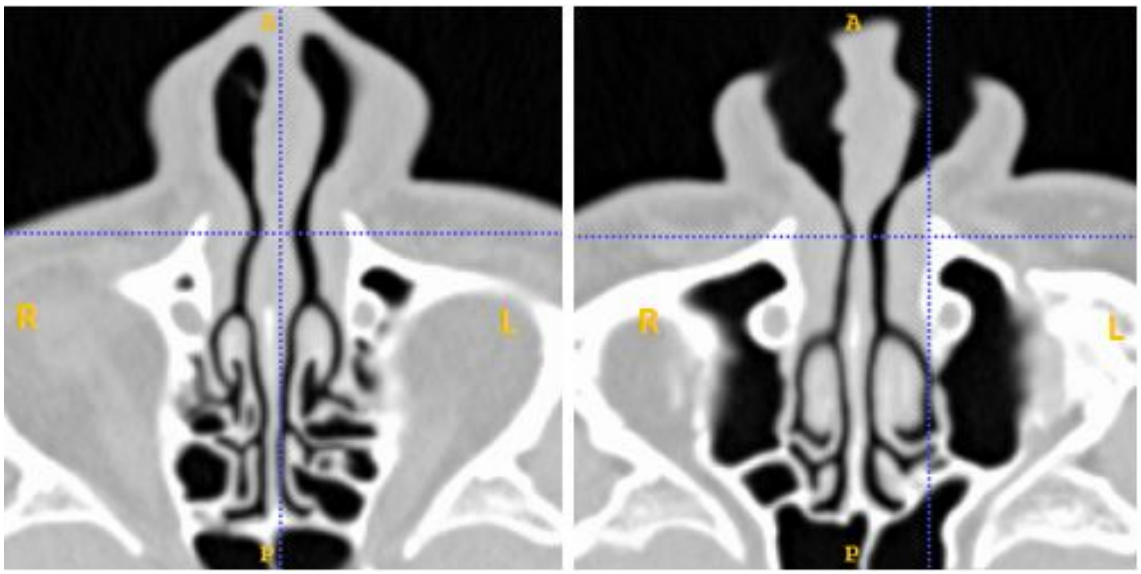

(b)

Figure 42: The figure shows two different CT axial views of Patient 12 taken pre-operative. No remarkable difference in the cross-sectional areas of the left- and right nasal cavity in the middle of the nose are observed.

The changes seen in Fig. 42 may indicate that the patient is in different nasal cycles when the CT was obtained. The need for taking the nasal cycle into account when modelling the nose have been pointed in previous studies. Patel et al [48] compared pre- and post-operative models to study nasal airway obstruction and had to limit their study subjects to those that seemed to be in the mid cycle (symmetric) of the nasal cycle both pre- and post-operative. In order to include more subjects into the study, they came up with a method for modelling the nasal cycle. By changing the thickness of the inferior and middle turbinate in addition to the septal swell body,

the nasal cycle is taken into account. Patel found that the surgical effect was more correctly simulated when the geometry has been adjusted to eliminate the influence of the nasal cycle. Another option is to simply try to avoid the nasal cycle as a source of error. This could be done by obtaining the CT after the patients nose have been decongested by nasal spray. It is however important to keep in mind that the decongested state is unnatural. When measuring the AHI during a sleep study, the nasal cycle is present, and including the nasal cycle in the model instead of eliminating it may give a more realistic result. As long as the nasal cycle is ignored, the CT scan image data can make the geometry of the nasal cavity look rather different, and make it more difficult to reproduce data.

5.1.2 The Segmentation Procedure

As pointed out in earlier chapters, the segmentation process is not fully automatic. One could try to do the manual segmentation procedure again as similar as possible, but chances are differences could occur and the geometry would vary and give different solutions for the flow. The segmentation will also be dependent on the CT resolution and the positioning of the patient as seen in this master thesis. The fact that the patient was positioned differently during CT resulted in pre- and post-operative CT slices that showed different cross-sections, and it was harder to compare the segmentation. As with all manual procedures there will be differences, and hard to redo the exact same. How big of an impact this actually will have on the results has not been looked into.

5.2 Comparison of CFD and Measured Results

5.2.1 Can the AHI Improvement be Seen in the CFD Results?

The high reduction in AHI measured clinically is not as clearly observed in the CFD results. The simulation results show a significant change in the flow patterns in the nasal cavities, but only a small change in the flow patterns in the pharynx and larynx between the pre- and post-operative models. The major differences after surgery are a more evenly distributed flow between the two nasal cavities, and an increase in the pressure drop over the nasal cavity.

The change from mouth breathing to nasal breathing can be the cause of the major

improvement in AHI. It can be hypothesized that because of the obstructions the patient had in his nose, he was breathing through his mouth during sleep. When breathing through the mouth (and opening the mouth), the volume in the pharynx decreases because the tongue and soft palate moves posterior towards the pharyngeal walls (see Fig. 4). This might even close the pharynx, and can result in both apneas and hypopneas which can explain the high AHI reported before surgery. After surgery, the simulation results shows a more symmetrical flow in the nose which might make it more desirable to breath through the nose - perhaps enough for the patient to breath only, or mostly, through his nose. If this is the case, the pharyngeal volume will be significantly larger than it is when the mouth is open, and the risk for collapse will be reduced.

It is however not known if the patient has changed from mouth- to nasal breathing after surgery as there are no available data for this, and more information about the patients sleeping habits is needed to verify this. If the case is that the patient did sleep with an open mouth, the geometry should also include the oral cavity, and a CFD study on that geometry should be included as well to relate the CFD-results with the AHI. Information from such a study could be used to predict the outcome of surgery.

However, the sleeping habits of the patient is not known, and the results should also be viewed in light of the patient sleeping with a closed mouth. Several sources of errors have to be taken into account, and the CFD-result may differ from real life. The mechanisms of OSAS is not all known either, and there can be other mechanisms causing apneas and hypopneas that are not visible by studying the flow. It has been suggested that neurological mechanisms may also influence the breathing pattern. It is currently unknown how this can be affected by nasal surgery.

A last remark is that the CT that is the base for the numerical simulations is obtained when the patient is awake, while the AHI is measured during a sleep study. During sleep, the muscles relax and the pharyngeal wall can become narrower as the muscles that is supporting it is relaxed. In addition, the muscle-relaxation may also make the tongue relax and fall posterior when sleeping on the back due to gravity.

5.2.2 Comparison with Rhinometric measurements

Comparing CFD results with clinical measurements has its difficulties. As pointed out earlier, the nasal cycle affects the geometry, and that will also affect the rhi-

nometric results. The nasal cycle affects the geometry, and the measurements and CT may be taken in different cycles and give unrealistic differences as discussed. Another difference between the clinical measurements and the CFD-results is that the clinical measurements are done when the patient is sitting, but the CT is taken while laying down. If and how this affect the results is unclear. Other difficulties will also be pointed out in the following sections.

5.2.2.1 Acoustic Rhinometry

Comparing the volume from a geometry that is based of CT with the measurements from AR is challenging. The cross sectional areas measured from AR are measured along an acoustic wave. To be able to compare the cross sectional areas from the model, the path of the acoustic wave must be know, which is not trivial.

Croce et al. [37] tried comparing AR with the geometry they had made, and pointed out that "it is nearly impossible to determine from the three-dimensional reconstruction the axis following the cross-sectional areas along the nasal cavity". However, they did determine an axis by gradually rotating cross sectional planes from horizontal at nostrils to vertical planes in the middle of the nasal cavity. The results were relatively good. Terheyden et al. [12] made a similar axis by first creating an initial guess with horizontal cross sections at the nostrils, then following a line with a 45 degree bend up to the turbinate head, where the line is bent 45 degrees again, and a straight line back to the nasopharynx where it is bent 45 degrees for the last time. This line was then adjusted by making cross sections perpendicular to the line, finding the center of gravity on those, and adjusting the line to go through all the centers of gravity. The results can be seen in Fig. 43.

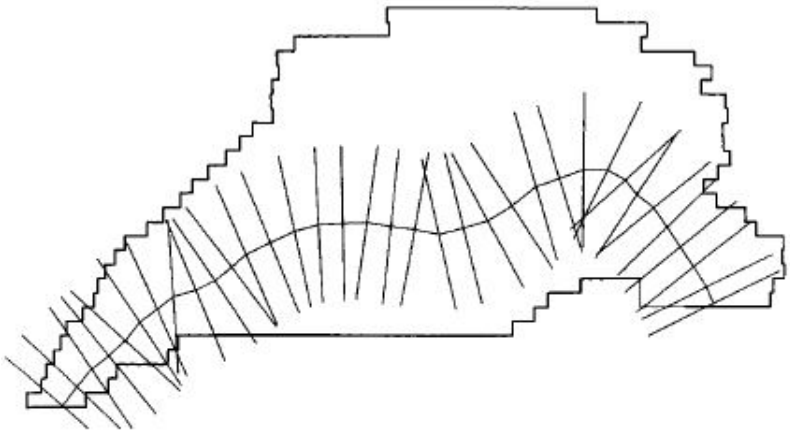

Figure 43: Placement of cross-sectional planes along the path of the soundwave suggested by Terheyden et al. [12].

Previous studies mentioned in [12] suggested that the 3D sound wave propagation causes the AR to be about 10 mm behind the actual place in the geometry. Based on this, Terheyden added 10 mm to the CT derived distances and compared with AR. This gave a good correspondence. Whether Terheydens or Croces approach is better than one another is unclear, and to correctly compare the CT derived geometry with the AR measurements, further modelling of the acoustic wave is needed.

5.2.2.2 Nasal resistance

The correspondence between the measured and computed nasal resistances was not good as stated in section 4.3.5.1. As pointed out, the result for the post-operative right nasal cavity corresponds quite well, but overall the resistances calculated are lower than those that are measured.

The pressure difference that is seen before and after surgery is unexpected. The pressure has increased over the nasal cavity, which was contrary to what was predicted as the surgery was to increase the volume of the nose, hence decrease the pressure difference. What is seen, is that the cross section at the anterior nose seem to have decreased after surgery. As discussed, this could be a result of the nasal cycle, the surgery itself, scar tissue or segmentation errors. This will however not explain the difference in the resistances. If the slightly decreased volume seen on the geometry is not in correspondence with the actual volume, and the volume is in fact larger, one would expect the pressure drop to be smaller, hence the resistance even lower. The measured resistance values are presenting a nose that is more congested

than what is seen on the simulation results.

The fact that the resistance computed is lower than the measured one, may indicate that the assumptions of a no-slip condition on the wall is too much of an idealizing of the problem. Both mucosa and nasal hairs in the nose will increase the resistance, and ignoring these may not be correct. If the flow were to be turbulent at this flow rate, the turbulent viscosity should have been taken into account, and increased the resistance. In addition, the friction coefficient would have depended on both the flow velocity and the hydraulic diameter.

Another difference worth mentioning is the measurement methods. When measuring the resistance, a mask is placed over the nose and mouth for the patient to breath normal in and out. The nasal cavity that is not being measured is physically closed, hence all air is inhaled through one side. This has not been simulated. The simulations are done for both sides at once, and the pressure drop used to calculate the resistance is from when the patient is breathing in through both nostrils. The pressure drop is therefore the same for the left and the right side, which in reality it might not be.

5.2.2.3 PNIF

From the PNIF measurements it can be seen that the patient is able to inhale a greater amount of air after surgery. Simulations were done to find the pressure drop needed to produce the two different air flows. What was found was that the pressure drop from inlet to outlet needed to achieve PNIF was higher post-surgery. However, the increase in pressure drop was much less than the increase in PNIF. It should also be noted that these simulations were done with a laminar flow model, while the flow most like is turbulent at such high flow rates.

5.2.2.4 Accuracy of the Tests

The accuracy of the clinical measurements is not known. When comparing the results from the two post-operative tests, some inaccuracy can be seen. The patient has been in for two post-operative tests as he had a cold at the first test and reported that he usually felt a more open nose. A second test was therefore taken five months later. At this test, the patient reports that there is a difference between the left and the right nasal cavity, but that it is unproblematic. A comparison of the pre(see appendix II)- and the most recent post-operative AR(see appendix IV) shows that the volume on the right side is more or less the same in both congested

and decongested state. On the left side, a great increase in volume can be seen. At the first post-operative test (appendix III), when the patient had a cold, the volume on both the left and the right side is larger than it was at the second test. This is unexpected, as one would assume that the cold would increase mucosa and make the nose more congested. However, results from RMM and RRM for the left nasal cavity were not obtained pre-operative or on the first post-operative test, but only on the second post-operative test. The lack of result from the first post-operative test was assumed to be a result of the cold and that the nose was too congested to get good results, and it is not known why this is not seen in the AR. The different sensitivities of the AR, RMM and RRM test are not known. Measurement errors may also occur such as the angle of the AR instrument that is hand held and the different AR curves that is merged to one.

6. Conclusion

In this master thesis, the air flow in the human upper airways have been simulated for an OSAS patient to study the effect of surgery using CFD. From clinical measurements it was known that the patient had a great improvement in AHI after surgery and had been almost fully alleviated from his OSAS. The aim was to see if this change in AHI could be seen in the CFD results as well, and eventually see the potential for a tool that can predict the outcome of nasal surgery. To be able to do so, a patient-specific CFD study has been done.

The protocol for geometry retrieval from CT suggested in [6] have been improved to get a more realistic model. Smoothing was needed in order to eliminate artefacts from digitalization, and more attention have been paid to the inlet and outlet geometry. As pointed out in [6], the CT has to be comparable for the geometry to be comparable. An issue with the CT from the selected patient was that a difference in the head position caused the pre- and postoperative geometry to look rather different in the pharynx and larynx. To prevent these geometric effects not caused by surgery to affect the flow field, the models have been combined. Hence, the only difference between the two models is the nasal cavity.

The CFD results showed an increase in the pressure drop over the nasal cavity after surgery, and a more evenly distributed flow between the two nasal cavities. The reason for the increase in the pressure drop is unclear, but appear to be caused by a narrower right nasal cavity. As surgery was performed in the left nasal cavity to increase the volume, it is unexpected to see such a narrowing in the right nasal cavity. However, on the CT images differences between the two sets of CT may be caused by the nasal cycle. The geometric difference caused by the nasal cycle should be taken into account, and more attention must be paid to modelling of this cyclic movement.

To be able to do the simulations, boundary conditions were set, and assumptions made. The measured nasal resistance was much higher than the one from the CFD-

results. This may indicate that the assumptions made should be reconsidered. In particular, the no-slip on the wall could be too much of an idealizing.

The great change in AHI measured clinically was not so easy to predict based on the CFD results. One suggestion is that the high AHI was a result of the patient breathing mostly through his mouth. After surgery, the air flows more easily through the nasal cavity, perhaps enough for the patient to breath mostly through his nose. This could explain the reduction in AHI. Whether or not this is the case have not been confirmed. To validate the CFD results, they were compared with clinical measurements. The correspondence between the measured and calculated resistance was not good in most cases, and more work is needed to validate the results.

From the simulations done in this master thesis, new questions and problem areas have been pointed out. The results have not been validated, but knowledge about modelling of the human upper airways have been gained. With new information, and new ideas, the patient-specific modelling can be improved and make way for a clinical tool eventually.

7. Further Work

Further work is required to gain confidence in the CFD results, and some areas of both modelling and simulating need more attention.

As one of the reasons that the AHI can decrease remarkably is changing from oral to nasal breathing, the sleeping habit of the patients should be documented. This would make it possible to verify the hypothesis. The flow results was compared with measurements of the nasal resistance. The results were not so good, but this measurement is in itself not enough to validate the simulated air flow. As done by others, experiments could be done on an in-vitro model from the same CT to validate the flow results. With the possibility to see the actual flow, turbulence models could also be tried out to see if they will model the flow more correctly. Eventually, direct numerical simulations or large eddy simulations could be tested, but requires a lot of computational time and power. New boundary conditions should be considered, and in particular the no-slip condition.

Another thing that could be included is a test of different inlets to see how sensitive the flow is to the inlet geometry. Including more of the surrounding air would be more realistic, but increases the computational time, and should therefore only be done if the inlet geometry changes the flow pattern. The nasal cycle should also be taken into account when generating the geometry. For validation of the geometry, acoustic rhinometry may be used. This does require acoustic modelling in the nasal cavity to identify the cross sections measured.

Further work for WP4 is to include more patients to see if the surgery outcome can be seen in the CFD results. If the surgery outcome is visible, it should also be possible to predict the outcome of a surgery before it is done. Fluid-structure-interaction should also be included. This could be both on the soft-palate which is already part of the project [4], but also include the pharyngeal walls that have so far been modelled as rigid walls. Eventually, as done by others, virtual surgery can

be tested out.

PATIENT SPECIFIC NUMERICAL SIMULATION OF FLOW IN THE HUMAN UPPER AIRWAYS, FOR ASSESSING THE EFFECT OF NASAL SURGERY

Maria Rolstad Jordal(1) , Sverre Gullikstad Johnsen(2), Sigrid Kaarstad Dahl(2), Balram Panjwani(2), and Bernhard Müller(1)

1. NTNU, Dept. Energy and Process Engineering, Norway; 2. SINTEF Materials and Chemistry, Norway

Introduction

Obstructive Sleep Apnea Syndrome (OSAS) is a disorder characterized by repeated collapses of the upper airways, preventing air from flowing freely, during sleep. The severity of sleep apnea is indicated by the apnea-hypopnea index (AHI), where <5 is considered normal and >30 severe. At St. Olavs Hospital, Trondheim University Hospital, Norway, intranasal surgery is being performed on patients with clinically significant nasal obstructions for alleviation of OSAS, but only one third of the surgeries are successful [1]. The goal of this study is to establish pre- and post-operative mathematical models of the air-flow in the upper airways of selected patients in order to investigate if changes in the flow pattern due to surgery can be correlated to the change in AHI. This presentation reports from the computational fluid dynamics (CFD) studies of one of these patients.

Method

Two 3D models of the upper airways were created from datasets obtained from computed tomography (CT) of an OSAS patient before, and after, intranasal surgery. The selected patient had a good response to surgery, with an improved AHI from 23 to 5.7. Segmentation of the CT images was performed in the freeware ITK-SNAP 3.2.0 [2], and the quality of the resulting 3D models was assured by clinicians. The flow field in the upper airways was studied pre- and post-operatively using the software ANSYS Fluent [3]. The study was limited to steady state, laminar, inhaling flow, with constant pressures at the inlets (nostrils) and outlet (larynx). The grid was refined until the numerical solution of the flow-field showed insignificant grid dependency. A comparison of the flow in the upper airways before and after surgery was done based on results from the CFD simulations. Selected computed results were compared with measured data to validate the CFD models.

Results and Discussion

CFD modelling results clearly show that the reduced hydrodynamic resistance in the nasal cavity after surgery affects the airflow. For identical volumetric flows, the static pressure in the upper airways is increased after surgery. This reduces the risk of collapse. However, the reduced hydrodynamic resistance may result in higher flow velocities, increasing the risk of airway collapse due to the Venturi effect where the airflow is accelerated through narrow passages (Figure 1).

Understanding how intranasal surgery changes the flow-pattern in the upper airways, and may affect the AHI in OSAS patients, is essential for improving the success-rate of current treatment options. We expect that, in the future, CFD will be used as a design tool for optimizing surgical intervention and minimizing risk for the patient. Being part of a larger set of patient-specific CFD studies, this study is a corner-stone in the ongoing work to improve our understanding of human upper airways airflow, and it is thus an important step towards computer-aided diagnostics and treatment of OSAS.

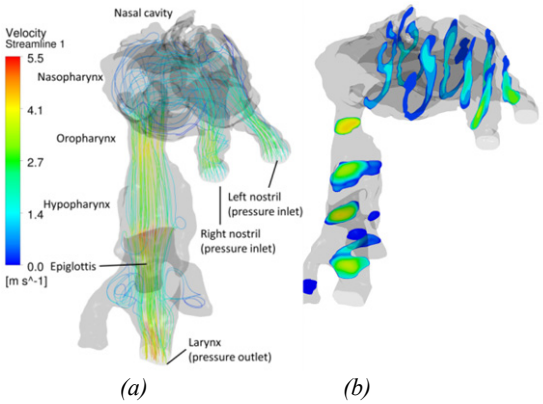

Figure 1: Velocity stream-lines (a) and contours (b) depicting the flow pattern in a patient-specific CFD model of the human upper airways.

References

1. Moxness and Nordgård, BMC Ear, Nose and Throat Disorders, 14:11, 2014.
2. Yuskevich et al, Neuroimage, 31:1116-28, 2006.
3. ANSYS Fluent, http://www.ansys.com.
4. "Modeling of Obstructive Sleep Apnea by Fluid-Structure Interaction in the Upper Airways", http://www.osas.no
5. Research Council of Norway, "Modellering av obstruktiv søvnapne ved fluid-struktur interaksjon i de øvre luftveiene",https://www.forskningsradet.no/prosjektbanken/#!/project/231741/no

Acknowledgements

This project work is part of a collaborative research project, "Modeling of Obstructive Sleep Apnea by Fluid-Structure Interaction in the Upper Airways", between NTNU, SINTEF Materials and Chemistry, and St. Olavs Hospital, Trondheim University Hospital, Norway [4, 5]. The project is funded by the Research Council of Norway, under the FRINATEK program.

Patient journal

Patient name:	J-H-L, Pas. nr. 12
Social security no.:	
Personal journal no.:	
Born:	09.04.1948
Sex:	M
Diagnosis:	

Examination journal

Title:	Examination
Created date:	29.09.2015 15:10:05
Type:	RhinoScan
Examiner:	
Software ver.:	4.0.5.0, v 3.00.Xj/v 3.0b
Probe:	

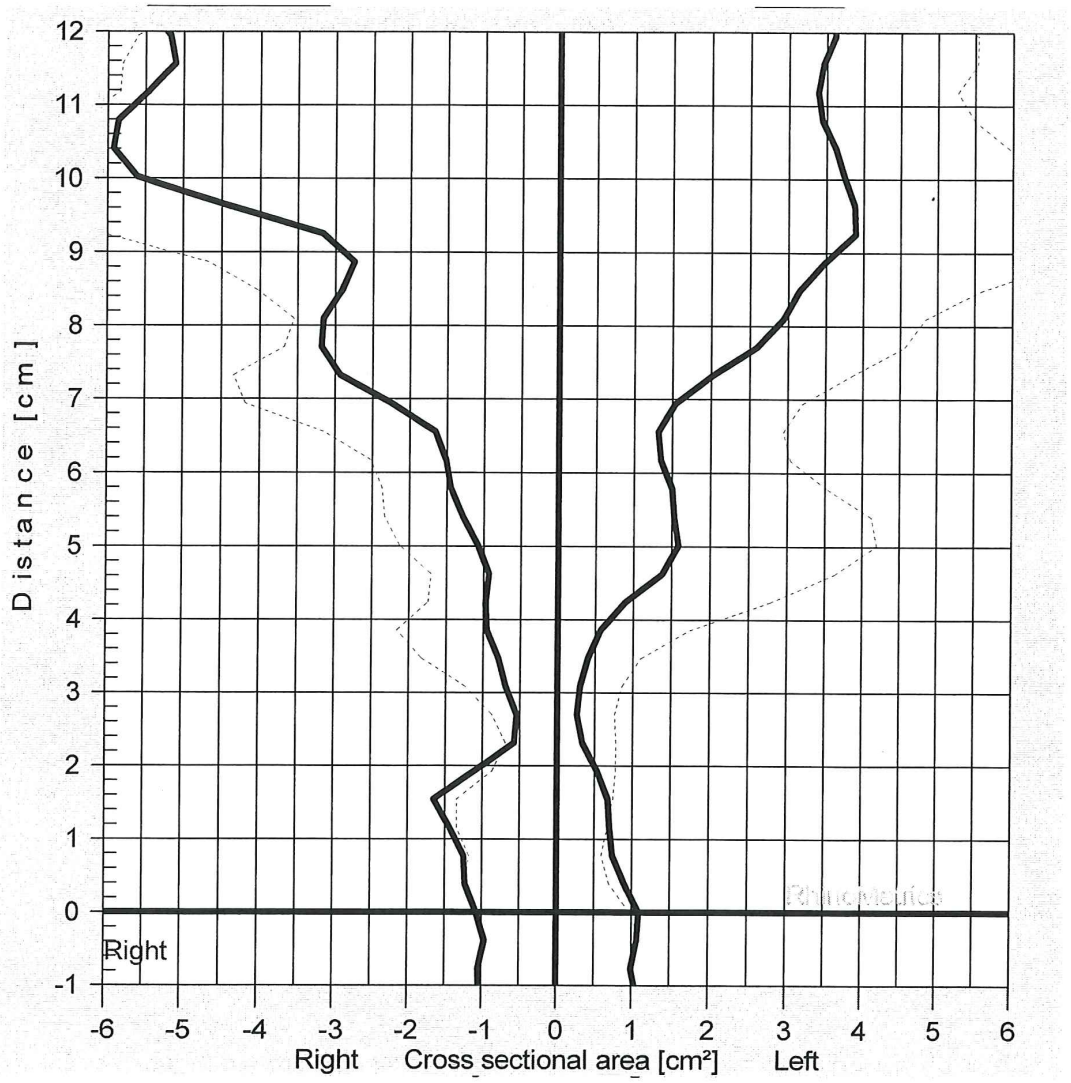

Date and time	Side	Title	Dist	MCA1	VOL1	Dist	MCA2	VOL2	Nose Piece
Distance ranges:			[0.00;3.00] cm			[3.00;5.20] cm			
Units:			[cm]	[cm²]	[cm³]	[cm]	[cm²]	[cm³]	
29.09.2015 14:42:48	L	Før avsvelling	2.70	0.26	1.84	3.00	0.29	1.93	
29.09.2015 15:09:22	L	Etter avsvelling	0.77	0.60	2.22	3.00	0.83	5.40	
29.09.2015 14:42:45	R	Før avsvelling	2.70	0.54	3.28	3.00	0.66	2.01	
29.09.2015 15:09:14	R	Etter avsvelling	2.31	0.69	3.24	3.00	1.16	4.03	

Patient journal

Patient name: J-H-L, Pas. nr. 12
Social security no.:
Personal journal no.:
Born: 09.04.1948
Sex: M
Diagnosis:

Examination journal

Title: Examination
Created date: 06.01.2016 14:39:37
Type: RhinoScan
Examiner:
Software ver.: 4.0.5.0, v 3.00.Xj/v 3.0b
Probe:

NB! Pas. er litt nesetorkjølet for tiden. Opplever seg åpnere i nesen vanligvis.

Else 6/1-16

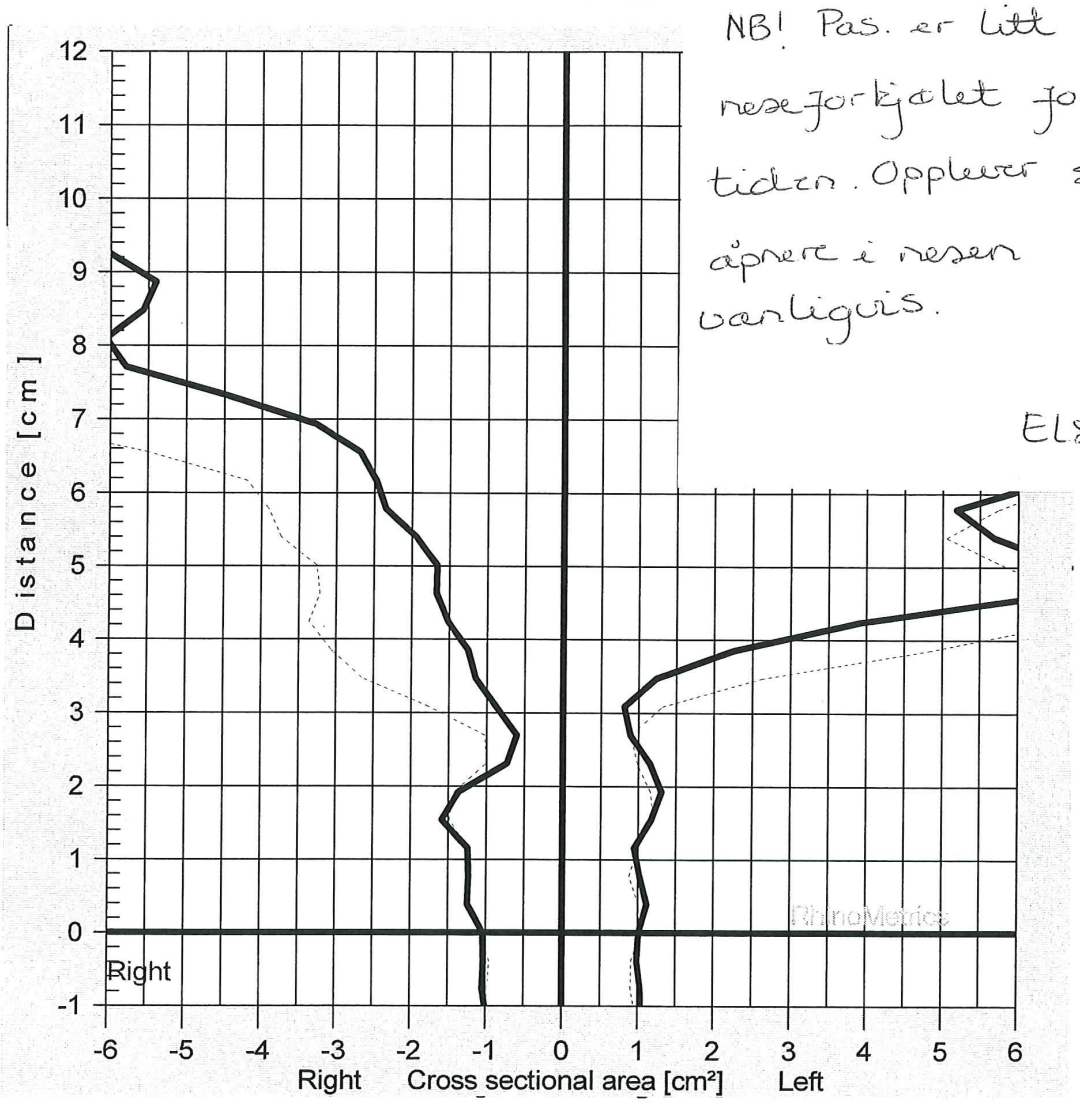

Date and time	Side	Title	Distance ranges:	Dist	MCA1	VOL1	Dist	MCA2	VOL2	Nose Piece
				[0.00;3.00] cm			[3.00;5.20] cm			
			Units:	[cm]	[cm²]	[cm³]	[cm]	[cm²]	[cm³]	
06.01.2016 14:13:29	L	Før avsvelling		3.00	0.83	3.22	3.08	0.81	8.31	
06.01.2016 14:39:02	L	Etter avsvelling		0.77	0.88	3.10	3.00	1.23	11.77	
06.01.2016 14:13:57	R	Før avsvelling		2.70	0.60	3.37	3.00	0.82	3.04	
06.01.2016 14:39:00	R	Etter avsvelling		2.31	1.00	3.71	3.00	1.61	6.49	

2. gangs postopr. tester pga. forglemt sist! APPENDIX

Patient journal

Patient name: J-H-L, Pas. nr. 12
Social security no.:
Personal journal no.:
Born: 09.04.1948
Sex: M
Diagnosis:

Examination journal

Title: Examination
Created date: 07.06.2016 16:03:06
Type: RhinoScan

3.0b

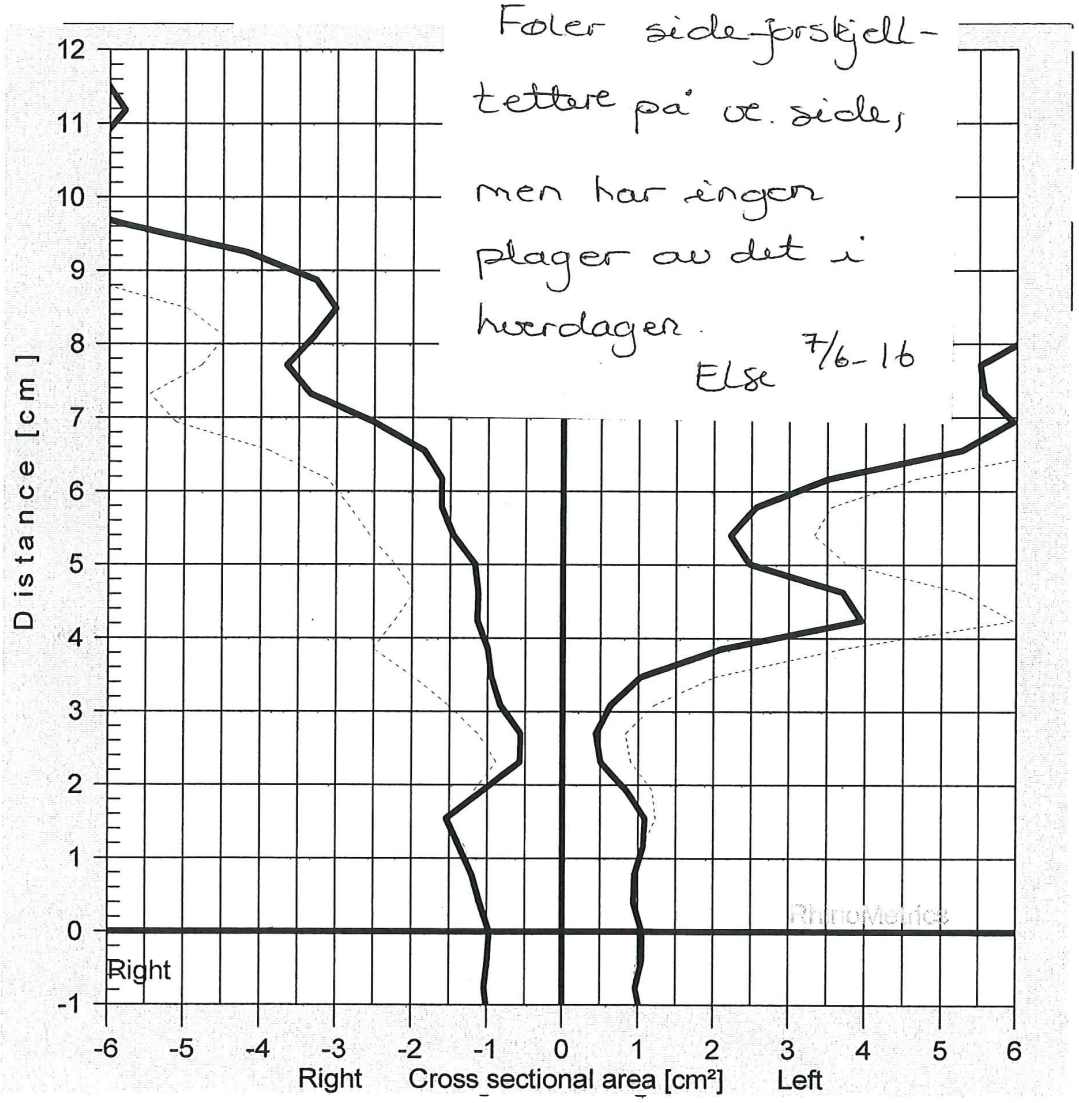

Date and time	Side	Title	Dist	MCA1	VOL1	Dist	MCA2	VOL2	Nose Piece
Distance ranges:			[0.00;3.00] cm			[3.00;5.20] cm			
Units:			[cm]	[cm²]	[cm³]	[cm]	[cm²]	[cm³]	
07.06.2016 15:37:00	L	Før avsvelling	2.70	0.44	2.52	3.00	0.59	5.27	
07.06.2016 16:02:26	L	Etter avsvelling	2.70	0.83	3.09	3.00	1.13	8.27	
07.06.2016 15:36:57	R	Før avsvelling	2.70	0.56	3.12	3.00	0.77	2.31	
07.06.2016 16:02:23	R	Etter avsvelling	2.31	0.88	3.56	3.00	1.44	4.63	

Bibliography

[1] P. A. Yushkevich, J. Piven, H. Cody Hazlett, R. Gimpel Smith, S. Ho, J. C. Gee, and G. Gerig, "User-guided 3D active contour segmentation of anatomical structures: Significantly improved efficiency and reliability," *Neuroimage*, vol. 31, no. 3, pp. 1116–1128, 2006.

[2] A. Inc., "Ansys 16.2." https://www.ansys.com.

[3] "Prosjektbanken - modellering av obstruktiv søvnapne ved fluid-strukturinteraksjon i de øvre luftveiene." https://www.forskningsradet.no/prosjektbanken/!/project/231741/en.

[4] "Modeling of Obstructive Sleep Apnea by Fluid-Structure Interaction in the Upper Airways." http://osas.no/description.

[5] M. H. Moxness and S. Nordgard, "An observational cohort study of the effects of septoplasty with or without inferior turbinate reduction in patients with obstructive sleep apnea," *BMC Ear, Nose and Throat Disorders*, vol. 14, no. 1, p. 11, 2014.

[6] M. R. Jordal, "Geometry retrieval from ct and mri of the human upper airways." The Norwegian University of Science and Technology, 12 2015.

[7] "the 22nd congress of the european society of biomechanics." https://esbiomech2016.org.

[8] Blausen.com staff, " Blausen Gallery 2014 The Respiratory System." Wikiversity Journal of Medicine https://en.wikiversity.org/wiki/Wikiversity$Journal of Medicine/Blausen gallery$2014.

[9] Beverly Hills Sinus, "Anatomy of the nose." http://www.beverlyhillssinus.com/nasal-and-sinus-disorders/nasal-polyps/.

[10] J. Tu, K. Inthavong, and G. Ahmadi, *Computational Fluid and Particle Dynamics in the Human Respiratory System*. Springer, 2013.

[11] Science-Based Medicine, "Dental management of obstructive sleep apnea." https://www.sciencebasedmedicine.org/dental-management-of-obstructive-sleep-apnea/.

[12] H. Terheyden, S. Maune, J. Mertens, and O. Hilberg, "Acoustic rhinometry: validation by three-dimensionally reconstructed computer tomographic scans," *Journal of Applied Physiology*, vol. 89, no. 3, pp. 1013–1021, 2000.

[13] "Patient specific modeling for prediction of success of osas surgery." http://osas.no/work-package/wp4.

[14] S. Standring and N. Borley, *Gray's Anatomy: The Anatomical Basis of Clinical Practice*. ClinicalKey 2012, Churchill Livingstone/Elsevier, 2008.

[15] A. Sahin-Yilmaz and R. M. Naclerio, "Anatomy and physiology of the upper airway," *Proceedings of the American Thoracic Society*, vol. 8, pp. 31–39, Mar 2011.

[16] G. J. Gibson, "Obstructive sleep apnoea syndrome: underestimated and undertreated," *British Medical Bulletin*, vol. 72, no. 1, pp. 49–64, 2004.

[17] American Academy of Sleep Medicine, "Sleep-related breathing disorders in adults: Recommendations for syndrome definition and measurement techniques in clinical research," *SLEEP*, vol. 22, no. 5, pp. 667–689, 1999.

[18] R. B. Fogel, A. Malhotra, and D. P. White, "Sleep Â· 2: Pathophysiology of obstructive sleep apnoea/hypopnoea syndrome," *Thorax*, vol. 59, no. 2, pp. 159–163, 2004.

[19] I. Ayappa and D. M. Rapoport, "The upper airway in sleep: physiology of the pharynx," *Sleep Medicine Reviews*, vol. 7, no. 1, pp. 9 – 33, 2003.

[20] N. AlGhanim, V. R. Comondore, J. Fleetham, C. A. Marra, and N. T. Ayas, "The economic impact of obstructive sleep apnea," *Lung*, vol. 186, pp. 7–12, 2008.

[21] M. Camacho, V. Certal, S. E. Brietzke, J.-E. C. Holty, C. Guillemeniault, and R. Capasso, "Tracheostomy as treatment for adult obstructive sleep apnea: A systematic review and meta-analysis," *The Laryngoscope*, vol. 124, pp. 803–811, 2014.

[22] N. B. Powell, "Contemporary surgery for obstructive sleep apnea syndrome," *Clin Exp Otorhinolaryngol*, vol. 2, pp. 107–114, Sep 2009. 19784401[pmid].

[23] M. Zhao, T. Barber, P. Cistulli, K. Sutherland, and G. Rosengarten, "Computational fluid dynamics for the assessment of upper airway response to oral appliance treatment in obstructive sleep apnea," *Journal of Biomechanics*, vol. 46, no. 1, pp. 142 – 150, 2013.

[24] N. B. Smith and A. Webb, *Introduction to Medical Imaging : Physics, Engineering and Clinical Applications*. Cambridge University Press, 2010.

[25] Materialise, "Mimics." http://biomedical.materialise.com/mimics.

[26] "3d slicer." https://www.slicer.org/.

[27] F. M. White, *Viscous Fluid Flow*. McGraw Hill Education, 3 ed., 2011.

[28] Sharcnet, "Index of/software/ansys/16.0/en-us/help/wb$_m$*sh.*"*https* : *//www.sharcnet.ca/Software/Ansys*/16.0/*en* − *us/help/wb*$_m$*sh/*.

[29] C. S. Burwell, E. D. Robin, R. D. Whaley, and A. G. Bickelmann, "Extreme obesity associated with alveolar hypoventilationâa pickwickian syndrome," *The American Journal of Medicine*, vol. 21, no. 5, pp. 811 – 818, 1956.

[30] R. Kessler, A. Chaouat, P. Schinkewitch, M. Faller, S. Casel, J. Krieger, and E. Weitzenblum, "The obesity-hypoventilation syndrome revisited*: A prospective study of 34 consecutive cases," *Chest*, vol. 120, no. 2, pp. 369–376, 2001.

[31] H. Gastaut, C. Tassinari, and B. Duron, "Polygraphic study of the episodic diurnal and nocturnal (hypnic and respiratory) manifestations of the pickwick syndrome," *Brain Research*, vol. 1, no. 2, pp. 167 – 186, 1966.

[32] M. S. Aldrich, *Sleep Medicine : Normal Sleep and Its Disorders*. Oxford University Press, USA, April 1999.

[33] C. Sullivan, M. Berthon-Jones, F. Issa, and L. Eves, "Reversal of obstructive sleep apnoea by continious positive airway pressure applied through the nares," *The Lancet*, vol. 317, no. 8225, pp. 862 – 865, 1981. Originally published as Volume 1, Issue 8225.

[34] S. Schreck, K. J. Sullivan, C. M. Ho, and H. K. Chang, "Correlations between flow resistance and geometry in a model of the human nose," *Journal of Applied Physiology*, vol. 75, no. 4, pp. 1767–1775, 1993.

[35] I. Hahn, P. W. Scherer, and M. M. Mozell, "Velocity profiles measured for airflow through a large-scale model of the human nasal cavity," *Journal of Applied Physiology*, vol. 75, no. 5, pp. 2273–2287, 1993.

[36] K. Keyhani, P. W. Scherer, and M. M. Mozell, "Numerical simulation of airflow in the human nasal cavity," *Journal of Biomechanical Engineering*, vol. 117, pp. 429–441, Nov 1995.

[37] C. Croce, R. Fodil, M. Durand, G. Sbirlea-Apiou, G. Caillibotte, J.-F. Papon, J.-R. Blondeau, A. Coste, D. Isabey, and B. Louis, "In vitro experiments and numerical simulations of airflow in realistic nasal airway geometry," *Annals of Biomedical Engineering*, vol. 34, no. 6, pp. 997–1007, 2006.

[38] D. J. Taylor, D. J. Doorly, and R. C. Schroter, "Inflow boundary profile prescription for numerical simulation of nasal airflow," *J R Soc Interface*, vol. 7, pp. 515–527, Mar 2010. 19740920[pmid].

[39] J. D. Backer, O. Vanderveken, W. Vos, A. Devolder, S. Verhulst, J. Verbraecken, P. Parizel, M. Braem, P. V. de Heyning, and W. D. Backer, "Functional imaging using computational fluid dynamics to predict treatment success of mandibular advancement devices in sleep-disordered breathing," *Journal of Biomechanics*, vol. 40, no. 16, pp. 3708 – 3714, 2007.

[40] L. K. Fan, Y an Cheung, M. M. Chong, H. D. Chua, K. W. Chow, and C. H. Liu, "Computational fluid dynamics analysis on the upper airways of obstructive sleep apnea using patient-specific models," *IAENG International Journal of Computer Science*, vol. 38, no. 4, 2011.

[41] J. S. Rhee, S. S. Pawar, G. J. Garcia, and J. S. Kimbell, "Towards personalized nasal surgery using computational fluid dynamics," *Arch Facial Plast Surg*, vol. 13, pp. 305–310, Apr 2011. 21502467[pmid].

[42] G. Mylavarapu, M. Mihaescu, L. Fuchs, G. Papatziamos, and E. Gutmark, "Planning human upper airway surgery using computational fluid dynamics," *Journal of Biomechanics*, vol. 46, no. 12, pp. 1979 – 1986, 2013.

[43] A. Weissheimer, L. M. de Menezes, G. T. Sameshima, R. Enciso, J. Pham, and D. Grauer, "Imaging software accuracy for 3-dimensional analysis of the upper airway," *American Journal of Orthodontics and Dentofacial Orthopedics*, vol. 142, no. 6, pp. 801 – 813, 2012.

[44] Y. Ito, G. C. Cheng, A. M. Shih, R. P. Koomullil, B. K. Soni, S. Sittitavornwong, and P. D. Waite, "Patient-specific geometry modeling and mesh generation for simulating obstructive sleep apnea syndrome cases by maxillomandibular advancement," *Mathematics and Computers in Simulation*, vol. 81, pp. 1876–1891, May 2011.

[45] H. Nakano, K. Mishima, Y. Ueda, A. Matsushita, H. Suga, Y. Miyawaki, T. Mano, Y. Mori, and Y. Ueyama, "A new method for determining the optimal ct threshold for extracting the upper airway," *Dentomaxillofacial Radiology*, vol. 42, no. 3, 2013.

[46] A. Inc., "netfabb basic 7.3." https://www.netfabb.com/products/netfabb-basic.

[47] A. inc., "Meshlab v1.3.3." http://meshlab.sourceforge.net/.

[48] R. G. Patel, G. J. M. Garcia, D. O. Frank-Ito, J. S. Kimbell, and J. S. Rhee, "Simulating the nasal cycle with computational fluid dynamics," *Otolaryngology – Head and Neck Surgery*, vol. 152, no. 2, pp. 353–360, 2015.